Lancaster University

3D Modelling by Computational Fluid Dynamics of Local Interactions of Momentum, Mass and Heat Transfers with Catalyst Deactivation in Gas-Solid Catalytic Reactors of Low Aspect Ratios

By

Faris Abdullah Alzahrani

A thesis submitted to Lancaster University in partial fulfilment

of the requirements for the degree of Doctor of Philosophy

in Chemical Engineering

October 2016

Engineering Department

Faculty of Science and Technology

Lancaster University

Declaration

I declare that this thesis consists of original work undertaken solely by myself at Lancaster University between the years 2013 and 2016. In case where contributions by other authors are referred to, they have been properly referenced.

October 2016

Acknowledgement

This project could not have been finished without the support of many people. I would like to extend my sincerest thanks to my supervisor, Dr. Farid Aiouache, for his guidance throughout the course of this work. His advices, comments and support during this research work were fundamental for its development. I appreciate greatly his time, continuous patience, priceless help and encouragement, enthusiasm and truly motivating introduction to the world of chemical engineering research. It has been a great pleasure and an honour to work for him. I would not have been contemplated such an undertaking without him. The support from the Chemical engineering Department of Lancaster University is gratefully acknowledged. Besides the academics, there were many people who defined my life during my work, I am very grateful to them. A huge thank you goes to my wife who has tolerated me while undertaking this academic and research life. At last, but not least, I would like to thank my mother and my brothers and my sisters for their support in my choices; they made me who I am today.

Thanks everybody

Abstract

Packed beds of gas-solid systems are extensively used as reactors, separators, dryers, filters, heat exchangers and combustors. The design of packed beds requires a detailed knowledge of local dynamics of flow, composition and temperature. Unfortunately, investigations for the development of 3D modelling codes by computational fluid dynamics are still not sufficiently mature compared with those relying on 2D modelling or simplified pseudo-homogenous models. This project investigates non-uniform catalyst deactivation in packed bed reactors of low aspect ratios under steady-state and dynamic operations. Low aspect ratio packed beds were selected as they are known to generate non-uniform distribution of local flow. Detailed knowledge of flow dynamics in terms of local structure of the packed bed, pressure drops, interstitial flow, heat and mass rate distributions was examined. The discrete element method was used to generate various packing configurations and the results of profiles of porosity were in a good agreement with the semi-analytical models, especially, in the vicinity of the wall. Similar oscillation trends with damping profiles towards the centre of the packed beds were observed. Flow heterogeneity was assessed by tests of mass transfer dispersion through a Lagrangian approach. Interactions of fluid flow, mass and heat transfers, and local deactivation of alumina catalyst Al_2O_3 of CO oxidation were investigated under design and operating conditions. An increase in the activation energy of deactivation promoted the deactivation by accelerating the reaction rate and releasing additional thermal energy, which in turn accelerated the deactivation. The 3D modelling allowed observation of local catalyst deactivation at packing pore level which is typically not accessible by the 2D modelling or pseudo-homogeneous models. In addition, the deactivation was quite asymmetrical along axial and radial directions, leading to uneven rates of thermal expansion and contraction and causing local deactivation associated with temperature runaways.

Contents

Lists of Figures

List of Tables

Abbreviations

AR: tube-to-particle diameter Aspect Ratio

CFD: Computational Fluid Dynamics

DEM: Discrete Element Method

FD: Finite Differences

FE: Finite Elements

FV: Finite Volumes

GCI: Grid Convergence Index

GMRES: Generalized Minimal Residual Solver

I.D: Internal Diameter

LDV: Laser Doppler Velocimetry

MRI: Magnetic Resonance Imaging

PBR: Packed Bed Reactor

PFC^{3D}: Particle -Flow Code of Three –Dimensional

PT: Particle Tracking

PTM: Patrick Tracking Method

Nomenclature

A_w = non-dimensional pressure drops model constant(-)

B_w = non-dimensional pressure drops model constant(-)

C = concentration (mol m^{-3})

C_0 inlet concentration of reactant (mol m^{-3})

D = tube diameter (m)

DI = domain index (-)

D_m = molecular diffusion coefficient (m^2 s^{-1})

d_p = particle diameter (m)

$D_{ax/rad}$ = axial or radial dispersion coefficient (m^2 s^{-1})

$\boldsymbol{e_a^{21}}$ = relative error (-)

F = drag force per unit of volume (N m^{-3})

K = permeability of the packed bed (m^2)

h = grid size (-)

m = apparent order (-)

L = length of bed (m)

n = particle index

NP = number of Lagrangian tracer particles (-)

N = number of cells (-)

p = pressure drops (Pa)

Pe_1 Peclet number for mass dispersion (-)

Pe_2 Peclet number for heat dispersion (-)

r = radial coordinate (m)

$\bar{r}$ = averaged displacements of all particles along the radial coordinates (m)

r_{21} = refinement factor (-)

Re = Reynolds number (-)

t = time (s)

u = fluid flow velocity (m s^{-1})

$\bar{x}$ = averaged displacements of all particles along the axial coordinates (m)

$\bar{r}$ = averaged displacements of all particles along the radial coordinates (m)

a catalyst activity coefficient (-)

A pre-exponential constant of the main reaction (s^{-1})

A_D pre-exponential constant of the deactivation reaction (s^{-1})

Cp_g heat capacity of gas (J g^{-1} K^{-1})

Cp_s heat capacity of solid (J g^{-1} K^{-1})

D diffusion coefficient (m^2s^{-1})

D_a Damkoehler number of the main reaction (-)

Da_D Damkoehler number of the deactivation reaction (-)

D_{eff} or D_{ie} effective diffusion coefficient (m^2s^{-1})

E activation energy (J mol K^{-1})

E_D activation energy of deactivation (J mol^{-1})

ΔH heat of reaction (J mol^{-1})

k effective axial conductivity (Wm^{-1} K^{-1})

Δp pressure drop (Pa)

r radial variable (m)

r_e effective radius (m)

r_r radial position parameter (m)

r_s sphere center radial position (m)

r_{se} effective sphere center radial position (m)

r' normalized radial position, (Rc−r)/d (-)

R_c cylinder radius (m)

R_s sphere radius (m)

R_{se} effective sphere radius (m)

R_s* normalized sphere radius, R_s/d_p (-)

R gas constant (J mol^{-1} K^{-1})

T temperature (K)

T_0 inlet temperature (K)

T_s soild temperature (K)

T_b bulk temperature (K)

T_w wall temperature (K)

h heat transfer coefficient ($Wm^{-2}K^{-1}$)

q heat flux ($W\ m^{-2}$)

Nu Nusslt number (-)

R_i reaction rate ($mol\ s^{-1}\ kg^{-1}$)

N_i molar flux ($mol\ m^{-2}\ s^{-1}$)

k reaction rate constant ($m^3\ s^{-1}\ kg^{-1}$)

x coordinate (m)

y coordinate (m)

z coordinate (m)

Greek letters

θ angular coordinate (-)

Θ pressure difference between two discretizations (-)

ρ density ($kg\ m^{-3}$)

ρ_g density of gas phase ($kg\ m^{-3}$)

ρ_s density of solid phase (kg m^{-3})

ε = bed porosity (-)

μ = dynamic viscosity (kg m^{-1} s^{-1})

σ = standard deviation (-)

β = non-Darcy coefficient (m^{-1})

Δ = V the cell volume

ψ dimensionless pressure drop (-)

ψ_{inf} = dimensionless pressure drop of an infinite size packed bed (-)

Υ dimensionless activation energy (-)

Υ_D dimensionless activation energy of deactivation (-)

ζ dimensionless axial position (-)

τ dimensionless time (-)

Chapter 1

1. Introduction

1.1 Problem statement

Packed beds are used in various industrial applications such as heat exchangers, filtration, separation and particularly catalytic reactors owing to their simple arrangement and high surface area-to-volume ratios leading to integrated heat and mass exchanges. Catalytic reactors are those among the packed beds which are widely used in chemical, petrochemical and petroleum industries or in pollution abatement, where they are designed for steady-state applications. Catalytic packed bed reactors use catalyst particles of different shapes (generally spherical, cylindrical and etc.).These catalyst particles are usually porous and arranged in random or ordered fashions to form a packed bed. Such packed bed reactors are used either for single or multi-phase systems.

For the design of packed bed reactors, application of different models is required to be able to describe the different physical and chemical phenomena which occur inside the reactor. The main disadvantage is the lack of universality of the used models, resulting in the development of a multitude of models and modelling parameters for specific reactors used in specific processes. Flow hydrodynamics can play a basic role in evaluating the performance of such devices. The flow behaviour in such systems is complex due to interactions between fluid and packed particles, particles and column wall and fluid and column wall.

The relative importance of these interactions depends on the operating conditions such as the ratios of the column diameter to packed particle size and configuration of the flow system. This will influence the results of flow behaviour at both microscopic and macroscopic scales throughout the packed bed. In spite of interesting developments in applications of structured packings over the last years, the randomly ones are still the state-of-the-art based reactor types. At low aspect ratios (ARs) of tube –to-particle diameters of packed bed reactors (PBRs), where the wall effects dominate, the packing structure follows inhomogeneous patterns. Spheres locations in packed columns are influenced by AR because the confining nature of the wall of the column and are especially influenced in regions close to the wall. At low AR, the knowledge of fluid flow in packed bed is still however scarce, while the confining walls lead to more local heterogeneity, less fluid mixing and uneven structural porosity, making fluid flow and dispersion profiles unexpected. Moreover, these

reactors are subject to transient conditions such as accidental upstream disturbances in feed temperature, concentration or flow rates. Under such circumstances, catalytic systems can reach dynamic instabilities amplifying transient perturbations rather than attenuating. These instabilities, which originate from different flow of matter and heat through the bed, the so-called differential flow instability, have been observed more pronounced in reactors with local changes of the catalytic activity.

1.2 Research motivation

The analysis of fluid flow, heat and mass transfer processes, and also chemical reaction inside packed bed reactors is an area that has received a major deal of attention from reaction engineers. For several decades, engineers have striven to achieve better insights into the reactor system. Computational fluid dynamics (CFD) was a good approach to obtain this goal, although the use of CFD to simulate geometrically complex flows in packed tubes is a quite expensive. The actual motivation of CFD in this area is to provide more fundamental understanding of the transport and reaction phenomena at local levels inside these reactors.

Investigations and information of fluid behaviour in a low AR packed bed are still rare especially for AR values less than 3, where packed beds show more local heterogeneity in fluid flow and unexpected behaviour of the whole system. The lack of research into local events of fluid flow inside the PBRs is still significant, making description of overall performance of the catalytic reactor incomplete.

The challenge therefore, will be in finding a procedure to achieve a comprehensive understanding of the local interactions through flow patterns, species diffusion/dispersion, thermal gradients, catalytic reaction and specific attention to local deactivation of catalyst during the life time of the process, particularly when these data are not available by experiments. Works based on 1D modelling allowed understanding of physical phenomena inside packed bed reactors but were not be able to reflect local information in terms of velocity, mass and heat transfers and catalyst deactivation.

In addition, catalytic systems under some severe conditions can reach to non-uniform local catalyst deactivation during the reaction. Computational fluid dynamics methods have been extended to show local details of deactivation behaviour. Previous works have been carried out on modelling catalyst deactivation in packed bed reactors using 1D approach. [56, 66 and 151] However, to our

knowledge only two works have investigated the deactivation by using a 3D approach which were published by Dixon's group (2010) and Wehinger's group (2015) and both work were carried out for AR 4 under steady-state operations. [24 and 158]

This project aims to address issues identified in previous research but also to extend the 3D CFD modelling to obtain better understanding of the effects of non-uniform local flow, heat and mass transfers at low AR. CFD was used to capture detailed three-dimensional flow, species and temperature fields that are still often inaccessible by experiments. Local changes across the reactors have a crucial role to understand and thus improve the overall efficiency of the process. Finally, the CFD was extended to analysis of local catalyst deactivation for different ARs, where the previous works were limited by operations under stead-state operations. In this research, 2D and 3D models were investigated in order to get a comprehensive investigation of detailed catalyst deactivation in packed bed reactors.

1.3 Objectives

The 3D CFD modelling is used to:

- Achieve an insight into the complex behaviour of both non-uniform local fluid flow and spatial distributions of species in gas−solid packed beds of randomly distributed particles at low (AR). The approach is extended to packed beds of ARs ranging from 1.5 to 5 and to flow regime ranging from laminar to transitional flow limit (Re ~ 400). Explore effects of the confining wall under the knowledge of flow dynamics (i.e., local structure of the packed bed, pressure drop and interstitial flow in the void space). The results are validated by those obtained by global pressure drops and literature models. In order to ease the computation requirements of 3D modelling, the results are subsequently compared with those obtained by 2D modelling, where the structural porosity maps are obtained from actual 3D porosity distributions.
- Obtain the global kinetics of CO oxidation over alumina supported under wide range of conditions and understand the behaviour of mass and heat transfers throughout the packed bed reactor, where deactivation reactions were omitted. The results are validated by published works.
- Screen local non-uniform catalyst deactivation under steady state and transient conditions. The results are compared with 2D pseudo-homogenous modelling and literature data.

The detailed goals in this work can be divided as below:

- **Analysis of 3D fluid flow in low AR packed bed including:**
  - ✓ Porosity profiles.
  - ✓ Pressure drops based on CFD and experiments.
  - ✓ Distribution of local velocity fields.
  - ✓ Developed 2D model based on 3D porosity data.
  - ✓ Comparison of the results by the 3D model with the 2D model.
  - ✓ Radial and axial dispersion coefficient using the particle tracking method.

- **Mass and heat transfer in low AR packed bed reactor :**
  - ✓ Influence of the temperature, Reynolds numbers Re and size of particles on the total conversion profiles.
  - ✓ Distributions of conversion profiles through the bed.
  - ✓ Investigation of temperature profiles through the packed bed at different axial positions and heat transfer at various flow regimes and AR of the packed bed.

- **Local catalyst deactivation inside low packed bed reactors.**
  - ✓ Investigation of local catalyst deactivation by 3D and 2D models.
  - ✓ Comparison of dimensionless activation energy of deactivation γ_D and Damköhler number of the deactivation reaction, $Da_{D,}$ profiles obtained by 2D and 3D modelling.
  - ✓ Investigation of the wrong way behaviour (i.e., temperature disturbances) in packed bed reactors (i.e., CO oxidation at different axial positions for different AR).
  - ✓ Investigation of local deactivation under various mass and heat dispersions

1.4 Thesis outline

This thesis is organized as follows:

Chapter 2 provides a comprehensive literature review on previous research in this field. In this chapter we discuss the importance of PBRs and introduce carious aspects of catalyst deactivation. In addition, some challenges of CFD modelling of PBRs for low AR and general background on fluid flow and hydrodynamics are discussed.

Chapter 3 introduces the experimental methods and simulation procedures developed in this work. Since any CFD work requires experimental validation, pressure drop was selected as one parameter to be investigated at various scales of ARs. The 3D simulation relies on a porous structure of the PBR. The DEM method for packing generation is introduced. It is then followed by the procedure of volume element method of domain meshing and then 3D CFD modelling by coupling momentum, heat and mass transports and chemical reaction.

Chapter 4 shows simulation results of structure of generated packed beds in terms of average porosity, spatial distribution of porosity by 2D map and radial porosity profiles at various (ARs). Also, flow dynamics in terms of pressure drops and local velocity at various ARs by (2D and 3D) is investigated and compared with experimental data and literature models. Radial and axial dispersion coefficient are investigated using the particle tracking method (PTM), and then results are compared with literature models. Moreover, the 2D model results are compared with 3D ones to assess efficiency of the commonly used 2D pseudo-homogeneous approach.

Chapter 5 investigates mass and heat transfers in the generated packed beds in terms of the effect of flow regime and temperature on the overall conversion rate of CO oxidation. It provides predictions of heat transfer inside the packed bed and across the gas/solid phases without consideration the chemical reaction. The model results are then validated with literature data operated at similar conditions.

Chapter 6 extends investigation of non-uniformity inside the low AR packed beds to local catalyst deactivation at different ARs of the PBR by 2D and 3D modelling. Effects of phenomena associated with the deactivation such as the wrong way behaviour, mass dispersion and heat dispersion on deactivation are analysed and then compared with those developed by different authors. The results of 3D modelling are compared with the 2D pseudo-homogeneous approach.

Finally, chapter 7 summarizes the relevant conclusions achieved in this work and suggests some recommendations for future works.

1.5 Methodology (work plan)

The work aimed to study non-uniform local flow inside randomly porous media of gas−solid packed beds of low aspect ratios (AR) by using three-dimensional modelling (3D) via CFD to achieve the aforementioned objectives.

Initially, a granular packing of densely spherical particles will be built by means of DEM in order to mimic experimental samples. The 3D DEM code will be written in the built-in FISH programming language of particle flow code 3D (PFC3D) and will be used to generate realistic packing samples of random structures with varied ARs. The packing geometry, which will be defined by the 3D coordinates of particle centres, will be then embedded into the commercial CFD package COMSOL Multiphysics 4.4 via 3D AutoCAD (Autodesk) processing, allowing a dedicated meshing to take place by using a computer of 128 GB RAM.

The generated geometries will then be validated by comparison of the bed structure properties, such as average porosity and spatial distribution of porosity, with literature models. Also, pressure drops and local velocity distributions will be assessed by comparison of the 3D modelling as well as relevant 2D literature modelling with literature models. CFD model will be extended to predict mass transfer phenomena inside the generated packed beds in terms of dispersions and conversion profiles as well as the heat transfer trends inside the reactor (i.e., temperature behaviour at different axial positions and also heat distribution profiles through the bed). Finally, local deactivation under steady state and dynamic operations will be presented by 2D and 3D modelling and validated by published works.

1.6 Contribution of the thesis

The present work provides a comprehensive information about gas-solid catalytic systems of randomly packed beds of low AR ranging from 1.5 to 5 using a numerical CFD approach. The actual contribution of CFD in this area is the achievement of more fundamental understanding of fluid flow, transport and reaction phenomena inside reactor tubes under steady-state and dynamic operations. Works based on 1D modelling allowed understanding of physical phenomena inside packed bed reactors but were not be able to reflect local information in terms of velocity, mass and heat transfers and catalyst deactivation which are not easily accessible by experiments. Some of relevant contributions achieved in this thesis are summarized as follows:

- 3D modelling was successfully used to obtain a reasonable insight into interaction of gas with solid phases in terms of non-uniform local flow, species and heat distributions and

understand the effects of the confining wall at low AR under knowledge of flow dynamics (e.g. local structure of the packed bed, pressure drop, and interstitial flow in the void space).

- 2D modelling approach was successfully developed based on structural porosity maps which were obtained from 3D porosity distributions in order to minimize the computation requirements of 3D modelling and was in a good agreement with the 3D modelling, confirming the benefit of using the porosity distribution from 3D maps to access insights into industrial packed beds of large computation time and hardware power.

- 3D modelling was successfully applied to describe the strong interactions between chemical kinetics and transport of momentum, mass and heat and described well distribution of mass and heat through the PBRs in terms of species concentration, temperature distribution, transport and conversion.

- 3D modelling was successfully used to Investigate non-uniform (local) catalyst deactivation in packed bed reactors of low ARs under steady-state and transients operations and was extended to local catalyst deactivation at packing pore level which is difficult to reach experimentally. The relevant instability of the reactor owing to catalyst deactivation was well addressed by the wrong way behaviour of temperature under transient operations.

1.7 Publications & Presentations & training related to this work

Publications

1- **Faris Alzahrani**, Mohammed Aldehani, Hao Rusi, Michael McMaster, Daniel Luis Abreu Fernandes, Suttichai Assabumrungrat, Meabh Nic An tSaoir, and Farid Aiouache,''Gas Flow Visualisation in Low Aspect Ratio Packed Beds by Three-Dimensional Modelling and Near–Infrared Tomography''. Industrial & Engineering Chemistry Research. **2015**, 54, pp. 12714-12729.[18]

2- Mohammed Aldehani, **Faris Alzahrani,** Meabh Nic An tSaoir, Daniel Luis Abreu Fernandes, Suttichai Assabumrungrat and Farid Aiouache,'' Kinetics and reactive stripping modelling of hydrogen isotopic exchange of deuterated waters. Chemical Engineering and Processing: Process Intensification. **2016**, 108, pp. 58-73.

Presentations

A. Posters

1- Simulation of 3D modelling flow dynamics in packed beds of low aspect ratio, ChemEngDayUK at University of Manchester, 7-8 April 2014.
2- 3D modelling of flow dynamics in packed beds of low aspect ratio at Comsol Conference, Cambridge, 17-19 September 2014.
3- European Symposium on Chemical Reaction Engineering (ESCRE) Conference, Germany on 27-30 October 2015.

B- **Oral**

1- CAMURE conference for chemical engineering, Screening local deactivation in packed beds, Lyon (France), 07- 09 December 2014,

Trainings

1- COMSOL workshop under title "introduction to COMSOL Multiphysics", University of Cumbria, 15 January 2014.
2- End Note course in Lancaster University, 04 February 2014.
3- COMSOL workshop under title "introduction to COMSOL Multiphysics", Lancaster University, 28 January 2015.
4- A webinar under title "Reaction Engineering with Advanced simulation", London, 24 September 2015.
5- The role of hydrogen in the carbon-catalyst reaction: the example of amorphous carbon conversion to grapheme, Lancaster University, 16 March, (Seminar).
6- High performance computing-based computational fluid dynamics for offshore renewable energy, Lancaster University, 7-8 April 2016, (workshop).

7- Photoconductivity methods in the study of semiconductors, Lancaster University, Lancaster University, 13 April 2016, (Seminar).

8- Teaching bachelor students for one week on (introduction for using Comsol software) in Lancaster University.

Chapter 2

2. Literature Survey

2.1 Engineering reactors for catalytic reactions

Majority of chemical transformations during industrial practice often involve use of different types of catalysts to achieve the desired products. The application of catalysts at industrial scale, particularly in the early years of the 20th century, led to a breakthrough of the chemical manufacturing. In chemical engineering processes, packed beds are frequently used as catalytic systems. Nowadays, majority of commercial gas-phase catalytic processes are taking place in these types of reactors and some of the major catalytic processes which occur in PBRs are listed in Table 2.1. [1]

Table 2.1 Main packed bed catalytic processes

Basic chemical industry	Petrochemical industry	Petroleum refining
Steam reforming	Ethylene oxide	Catalytic reforming
CO conversion	Vinylacetate	Isomerization
Ammonia synthesis	Maleic anhydride	Polymerization
Sulfuric acid synthesis	Phthalic anhydride	Hydrocracking
Methanol synthesis	Styrene	(Hydro) desulphurization

Besides the suitable catalyst, it is substantial to design the right reactor type and develop strategies for efficient translation of laboratory process to industrial practise. Reaction and reactor engineering play a considerable role in chemical and process industries. In fact, the engineering of reactors focuses on all the necessary actions to obtain best possible hardware and operating conditions of reactors to carry out the desired conversion of raw materials or reactants to value added products. Various functions occur through the catalytic reaction, such as reactants will be adsorbed on catalyst surface then will contact with active sites to allow chemical reactions to take place, providing an appropriate environment such as temperature and concentration fields for adequate time and allowing for removal of products from catalyst surfaces.

Actually, ideal reactor engineering requires better chemistry, for instance thermodynamics and catalysis, and suitable engineering operations (fluid dynamics, mixing, heat and mass transfers, computational models and real-time process monitoring and control) during the reaction process. A catalyst is a substance which supplies an alternative path of reaction where the activation energy is lower to reach the products in a short period without affecting chemical equilibrium associated with a reaction as shown in Figure 2.1. Catalysts have a positive impact in many different applications. Using these catalysts however may lead to issues associated with deactivation, rendering the catalyst less efficient. [2]

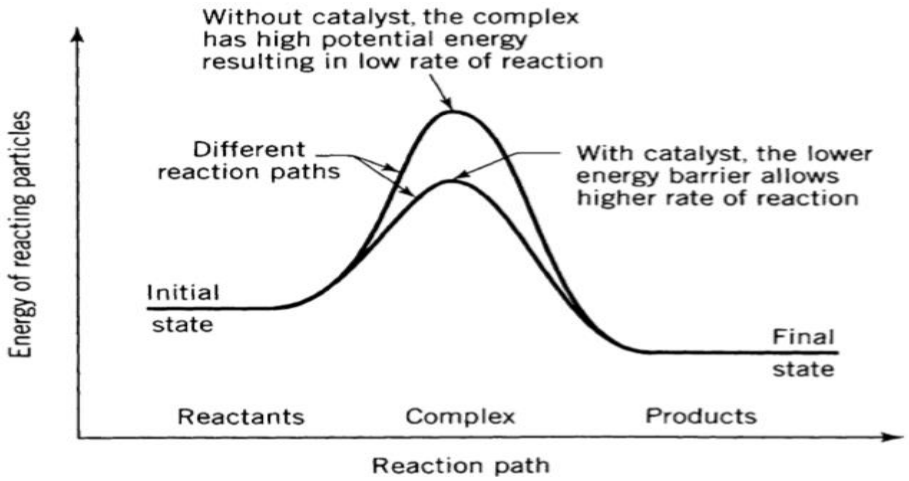

Figure 2.1. Effect of catalyst during chemical reaction [2]

2.2 Packed bed reactors (PBRs)

2.2.1 Introduction

Packed bed reactors (PBRs) are extensively used in the chemical, environmental and technological processes. In the chemical field, packed beds might be found in varied applications such as filtration, reaction, separation and purification units. Flow hydrodynamics can play a basic role in evaluating the performance of such devices. Packed bed reactors are preferred due to their simple technology and ease of operation. The flow behaviour in such systems is complex due to interactions between the fluid and the packed particles, the particles and the column wall, and the

fluid and the column wall. The relative importance of these interactions depends on the operating conditions, the internal design and the overall geometry (i.e., configuration of the flow, shape and size of the packing and relevant size of these to container size (bed to particle ratios)). These will affect the results of behaviour of the flow, mass and heat transports at various time and space scales during a process operation. Among various configurations of catalytic reactors, packed bed reactors are still popular in carrying out catalytic processes owing to their flexibility to hold many types of chemical reactions under convenient design and control of fluid flow, mass and heat phenomena taking place. In spite of interesting developments of packed bed reactors holding structured packings, those containing randomly packed beads are still the state-of-the art of reactor types, particularly in gaseous-solid packed reactors. [3] The solid phase, represented by catalyst particles, can be varied in shapes such as sphere, cylinder, pellet, etc. [4]The catalyst particles have a significant role in processes of adsorption, chemical reaction and other separations processes. [5] The fluid dynamics plays a considerable role in the overall performance of PBRs, particularly PBRs of low AR owing to local heterogeneity. A comprehensive knowledge of the packing structure such as chemical nature, particle size, geometry, porosity and particle distribution, is of essential importance when evaluating reaction rates throughout packed beds. Also, local flow conditions, mass and heat transport phenomena are intrinsically related to overall performance of the PBR. Geometrical characteristics of the reactor, for example, the length and diameter will affect radial and axial flow behaviour, as well as the mechanisms of heat and mass transports inside the PBRs. [6]

2.2.2 Modelling and design of packed bed reactors (PBRs)

Modelling of a packed bed is a complicated task because of the large amount of factors which should be taken into account in order to achieve a realistic model. For the design of a packed bed, application of several models is required to be able to describe the different physical and chemical processes occurring inside the bed. In order to achieve a good understanding of local events, it is important to obtain accurate data from inside the packed bed, however, it is very difficult to capture these data experimentally, particularly near the packing surface or the wall, making empirical correlations popular to describe species transport and heat transfer in PBRs. [6]

Fluid dynamics plays a significant role during the design of these equipment since the transport of chemical species, mixing or contacting catalytic surfaces is entirely described by the fluid dynamical conservation laws. The essential considerations in design of packed bed reactors include heat exchange, pressure drop, safe operating temperature extent and catalyst packing. In PBRs,

reactions occur on the catalyst particles which are placed in the reactor tubes either randomly or structurally. The feed is given from one side and products will be taken from another side of the reactor. Based on the nature of the reaction system, also the heat is supplied to the tube wall or taken out by using cooling jackets .The PBRs schematic illustration is shown in Figure 2.2.

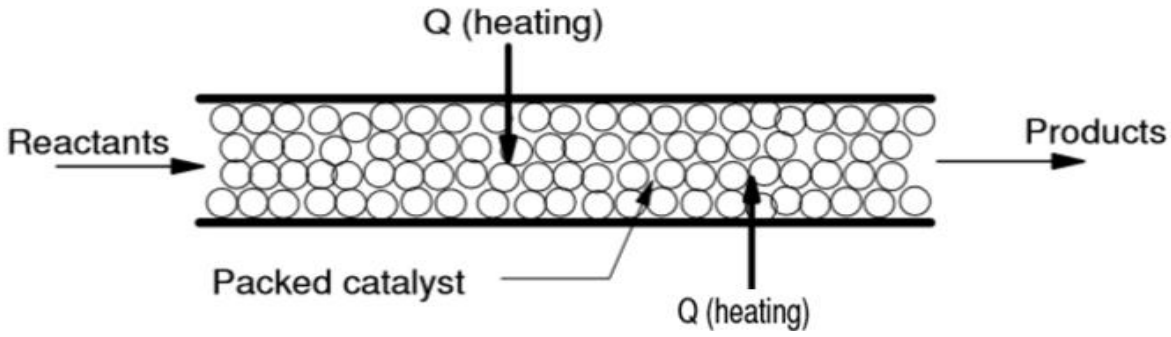

Figure 2.2. Schematic illustration of a packed bed reactor. [7]

An efficient modelling of flow and heat transfer through the reactor has considerable importance in the chemical industry. In order to model a PBR, transport phenomena taking place inside the bulk fluid, the catalyst particles and at their interfaces have to be considered utilizing the convenient reaction rate expressions. These phenomena which occur in PBRs can be classified as below:

- Convection of the fluid
- Heat transfer by the tube wall
- mass and heat dispersion in the fluid phase
- mass and heat transfer between bulk fluid and catalyst
- Conduction in the solid phase (catalyst)
- Intra-particle diffusion of heat and mass

The transport phenomena that have been dealt in the conventional packed bed modelling approaches depend on fairly radially simplifying assumptions such as pseudo-homogeneity, use of correlation-based effective transport parameters, velocity field, uniform catalyst particle surroundings and reaction source terms by using effectiveness factors. [7] In general, the design of packed bed reactor requires a significant knowledge of heat transfer characteristics inside the bed.

For example, within a packed bed reactor, the evaluation of temperature profile as well as the heat transfer rates is basic for assessing performance of the reactor. [8] The design of catalyst particles for packed bed reactors is governed by various competing considerations , e.g. smaller particles have less internal resistance to diffusion (better effectiveness factor) ,while the large particles have lower pressure drop. Using large catalyst particles is necessary, particularly when the fluid flow rate is high to mitigate the pressure drop. [9]

2.2.3 Aspect ratio (AR)

Aspect ratio (AR) is a significant feature in PBRs which means the ratio between tubes to particles diameter (D/d_p). In general, packed beds are considered to be at a low aspect ratio if the wall effects dominate the packing structure and the bed is packed in heterogeneous pattern. [10] PBRs can be classified into two types depending upon (AR); low AR packed beds (AR<13) and large size packed beds (AR>13). At low AR, usually the system includes a relatively small number of particles. [11] Figure 2.3 shows different sizes of reactors based on AR.

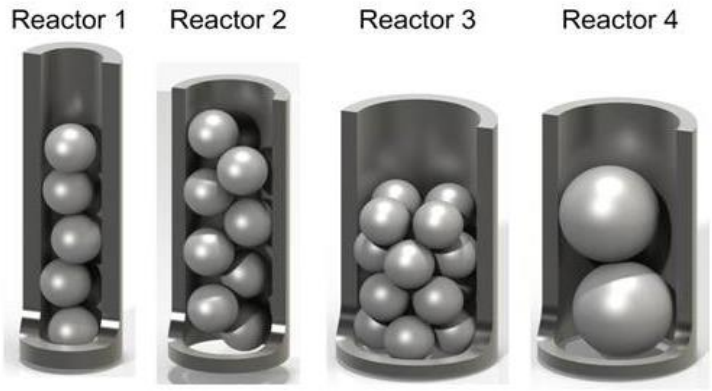

Figure 2.3. Different sizes of packed bed reactors. [4]

2.2.3.1 Low aspect ratios (ARs) of Packed bed reactors

Packed beds of low aspect ratios (ARs) of tube to particle diameter are commonly used in various industrial applications, owing to their simple arrangement and high surface-area-to-volume ratios, leading to integrated heat and mass exchanges. Driven by reduced pressure drops and improved heat exchange, innovative designs of these low AR packed beds have been demonstrated for applications including catalytic reactors (i.e., steam reforming, composite structured packing, nuclear reactors, meso- and micro-chemical reactors), separators (i.e., dehumidification adsorbers

for energy storage, chromatographic columns, filters, and CO2 sequestration) and thermal exchangers (compact heat exchangers). [12-16 and 17] These growing applications have attracted interest into understanding local phenomena taking place using both advanced experimental tools and advanced modelling. Unfortunately, these tools were not sufficiently dedicated toward very low AR packed beds (i.e., AR less than 5), owing to disperse phenomena taking place, requiring spatially resolved observations. This applies even more to gas flow dynamics where phenomena of mixing and dispersions are strongly affected by density and temperature changes. [18]

In large packed bed reactors at high (AR), the wall effects can generally be neglected, due to the small size of the region in the vicinity of the wall compared with the bulk region of the reactor. [19-22] Low AR PBRs are particularly used for extremely exothermic or endothermic systems e.g., oxidation and reforming systems. Heat must be sharply transferred into or out of a narrow reactor tube where the tube wall has a significant effect on heat transfer and flow of reactants around the catalyst particles. These in turn affect some properties during catalytic reactions process such as catalyst activity, selectivity and deactivation. [23] In this type of reactors, the particles close to the wall zone will behave differently to those in centre of the bed. The challenge will be in how to achieve a comprehensive understanding of the local interactions through flow patterns, species pellet diffusion, thermal gradients, catalytic reaction and specific attention to the deactivation of catalyst. [24] The understanding of local flow structures is important in determining the global behaviour of a flow or transport system, in several cases the hydrodynamic modelling of reactors is still depending on unidirectional axial plug flow approach .[23]

The main drawback of low AR PBRs is when the number of particles increase, then in this case, the system will be complicated for computations. A comprehensive understanding and an accurate description of fluid flow and heat transfer inside packed beds are necessary for the modelling of these reactors. Accuracy of modelling of low AR PBRs is complex because the presence of wall impacts across the entire radius of the bed. Computational fluid dynamics (CFD) has been adopted as a suitable tool by many studies, as illustrated in the following section, to achieve a better insight into reactor systems.

2.2.3.2 Some previous studies on low aspect ratios (AR) of PBRs

McGreavy et al., (1984) used Laser Doppler Velocimetry (LDV) to obtain access to the fluid flow of a packed bed of AR of 6.5 arrangement. [25] Further works from the same group (1986) investigated flow distribution and confirmed that the flow would be distributed differently from top to the exit of the bed. This indicates that measurement of flow profiles at (above or below) the bed is unsuitable. [26] Other authors investigated the radial profiles to obtain a general velocity distribution at AR ranging from 3 to 11. The results were extrapolated by using Brinkman equation to radial flow profiles inside the bed. [27]

Thompson and Fogler (1997) examined the fluid flow in a packed bed by using a network-model. The various randomly beds were generated by computational fluid dynamics (CFD) and were compared to experimental data of PBR of AR of 12, and 7500 particles. [28] Cheng and Yuan (1997) showed that at low AR, the wall influence on the packed bed is significant and must be taken in account. They used a modified Ergun equation to calculate the velocity distribution by introducing an effective tube diameter to ensure that the pressure loss would be predicted from the free flow space. [29]

De Klerk (2003) showed that there was oscillatory variation in packed beds at close wall region. He also noted that multiple stable packing arrangements exist through the same packing mode, which complicates modelling of low AR PBRs. [30] The main consensus in literature is that wall impacts are clear up to 5 particle diameters from the wall. [31] Winterberg and Tsotsas (2000) found that the operating conditions such as Reynolds number (Re), AR and wall friction would release an uneven flow, leading to pressure drops trends far from those following classical Ergun model. [32]

Freund et al., (2003) stated that the symmetry would not be fulfilled at low (AR) of PBRs when considering the cross-section of bed column of only a limited number of particles. Even the semi-empirical correlations which are extended to take into account axial and radial porosity, flow and transport parameter variations, cannot describe the local phenomena in detail. [33] Di Felice and Gibilaro (2004) showed that the assumption of homogeneous fluid velocity and void fraction distributions inside a bed cannot be true close the tube wall, where particles tend to arrange themselves differently. In case the wall zone represents a tiny fraction of the whole, it is possible then to neglect the inhomogeneity. [34]

Bai et al., (2009) used the discrete element method (DEM) and a CFD package to model a PBR of AR less than 4. Simulations were carried out by using spherical and cylindrical particles packed randomly and structurally in cylindrical and square ducts. Numerical data were validated by comparison with laboratory and pilot-scale experiments. [35] Baker et al., (2011) used 3D Magnetic Resonance Imaging (MRI) scans of packed beds of cylindrical shape and image results were used as templates for CFD modelling. Their results revealed that the Finite Volume method (FV) is applicable as an alternative tool for fluid flow visualization and agreement were found with those obtained by the Lattice Boltzmann method technique. [36]

Eppinger et al., (2011) investigated the fluid flow by 3D CFD modelling under laminar, transitional and turbulent flow regimes for AR ranging from 3 to 10 .The packing was generated via DEM method and a new meshing method that uses a minimum number of cells per particle ($\sim 10^4$) was validated. [37] Rong et al., (2013) examined the impact of porosity on flow over packed beds of uniform distribution of spheres by using the Lattice Boltzmann method. They concluded that the porosity would affect velocity distribution, particularly for low follow regimes. [38]

2.3 Catalyst deactivation in packed bed reactors

Catalyst deactivation can be defined as the loss of activity or selectivity of the catalyst over time and which is a significant problem in the catalytic process for industrial applications. Total costs in the industry for catalyst replacement and process shutdown is about billions of dollars per year. [39] The loss of activity in a well-controlled process occurs slowly. However, process upsets or poorly designed hardware can lead to a significant failure. For instance, in steam reforming of methane or naphtha, major attention should be taken to protect reactor operation at extremely high temperatures to avoid the formation of large quantities of carbon filaments which plug catalyst pores, leading to process shutdown for periods ranging from a few hours to several days. [39]

Research into catalyst deactivation receives less attention in the open literature than the discovery of new catalysts. The study of process catalyst deactivation is more complex than new catalyst discovery and it requires multidisciplinary skills, appropriate equipment, comprehensive knowledge of process conditions, and in some situations time and patience. [40] Certainly, a good catalyst gives high activity. A high activity permits the use of relatively small reactors and operation through mild conditions. However, the activity is not the only important feature for the catalyst but

the high selectivity for the desired products is often a significant property as well. In addition, it is very important that a catalyst retains its activity and selectivity for some time. [41]

The reaction conditions can be oxidising (exothermic fuel catalytic cracking (FCC)) or reducing (endothermic steam reforming), the temperature and pressure can vary from mild to severe. The timescale for industrial catalyst deactivation can vary from fractions of a second, in between the regeneration cycles of fluidized catalytic cracking, to several years for catalysts in fixed beds. The scope of catalyst deactivation is therefore very wide and detailed description of its kinetics is necessary under variable operating conditions.

Deactivation of catalyst presents many challenges in catalysis applications and relevant studies of catalyst deactivation are concerned with selection of the most convenient catalyst for the plant operations, including prediction of the life for the plant operation at large scale production. [41] Real life prediction and optimization need monitoring the catalyst performance inside an industrial scale operation which is indeed often missing in the laboratories or pilot scale studies. [40] Moreover, the environmental costs of increased by-product waste and waste catalyst disposals must be taken into account. In order to make progress, to meet deadlines and to prevent reactor instability, laborious work on approximate descriptions of the deactivation tendencies of several alternative catalysts and followed by a detailed study of the best catalyst, is often to be followed. [40]

2.3.1 Mechanisms (Types) of catalyst deactivation

There are several paths for heterogeneous catalyst deactivation. For instance, a catalyst can be poisoned by contaminants in the feed, pores and voids of catalyst surfaces might be fouled by various ways such as carbon or coke deposits (i.e., cracking reactions) or condensation reactions of hydrocarbon reactants, intermediates and products (i.e., oligomerisation reactions). In the treatment of a power plant flue gas, the catalyst may be dusted, plugged or corroded by fly ashes. Catalytic converters used to decrease emissions from petrol or diesel engines can be poisoned or fouled by fuel or lubricant additives and engine corrosion products. In some cases, when the catalytic reaction is conducted at high temperatures, thermal degradation can take place in the form of active phase crystallite growth and collapse of the carrier (support) pore structure. [39] Furthermore, the presence of oxygen or chlorine in the feed gas may cause formation of volatile oxides or chlorides of the active phase, followed by gas-phase transport from the reactor. Similarly, changes within the

oxidation state of the active catalytic phase might be produced by the presence of reactive gases in the feed. [39] Deactivation of catalyst may occur via different mechanisms of chemical or physical nature. These are usually divided into five types namely poisoning, fouling (coking), thermal degradation, mechanical failure of catalyst and finally corrosion (leaching). [42]

Poisoning

Poisoning can be defined as deactivation by strong adsorption of impurities inside the feed while reactants and products adsorb on catalyst surface. The difference between temporary and permanent poisoning is not usually clear, and sometimes the strong poisons at low temperature are less harmful during high-temperature applications. In general, high temperatures help remove these deposits by depolymerisation or volatilization. In some process such as catalytic combustion, because of the high temperatures >1270 K, poisoning by effects of sulphur and halogens is less problematic than in catalytic processes occurring at low temperatures, due to weak adsorption of these poisons at this high temperatures. [41]

In oxidation processes, generally air is used as reactant. The purity of the ambient air may be disappointing and air pollution components may carry undesired products that lead to poisoning. On the anther hand, poisoning sometimes may be useful because it gives the option to improve the selectivity. [41] Poisoning can be reversible or irreversible and strongly adsorbed of poisons might lead to the restructuring of the surface or some significant changes in catalytic properties, particularly for reactions which are sensitive to surface structure. In addition, the adsorbed poison might inhibit the surface diffusion of adsorbed reactants. [39] Under a poisoning process, the overall catalyst activity can decrease without affecting the selectivity, however often the selectivity is affected, since some of the active sites are completely deactivated while other sites are still practically unaffected. [42] Figure 2.4 shows the deactivation phenomena inside a catalyst particles.

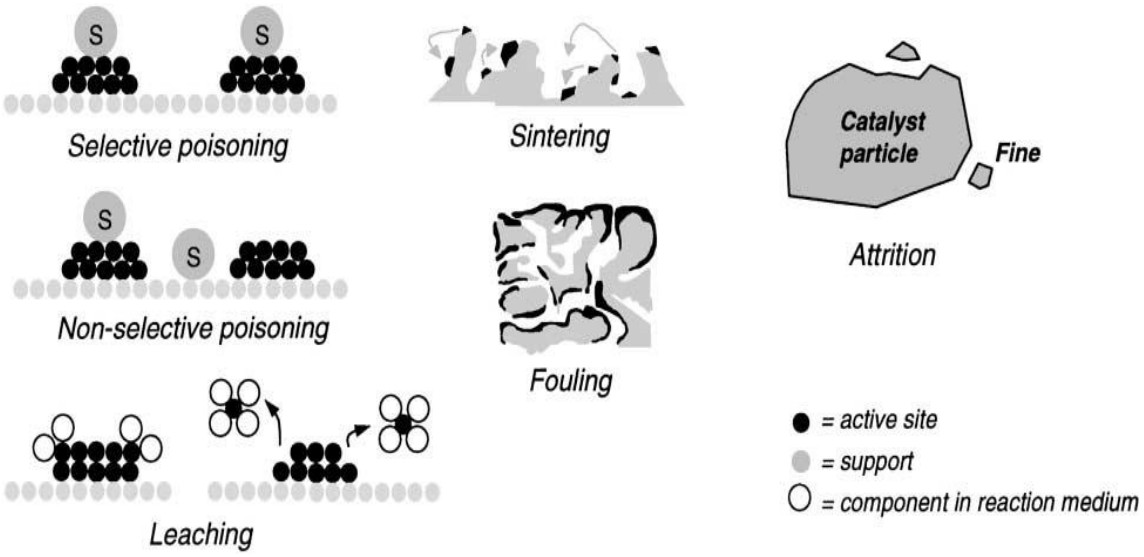

Figure 2.4. Major types of deactivation in heterogeneous catalysis. Moulijn et al. 2001. [41]

Fouling

The fouling is defined as the physical (mechanical) deposition of species from the fluid phase onto catalyst surface, which results in loss of activity of catalyst and blockage of surface sites or pores. In the advanced stages of fouling, it may lead to crashed catalyst particles and plugged reactor voids. Important examples are the mechanical deposits of carbon and coke in the porous catalyst particles, although carbon- and coke-forming processes include chemisorption of various types of carbons or condensed hydrocarbons, which can act as catalyst poisons. In fact, carbon is a product of CO disproportionation but coke is produced via decomposition or condensation of hydrocarbons on catalyst surfaces and often consists of polymerized heavy hydrocarbons. [39] However, coke forms can vary from large molecular weight hydrocarbons to primarily carbons, for instance graphite structures depend on the conditions under which the coke was formed and aged. The chemical structures of cokes and carbons vary with some properties of the system (i.e., reaction type, catalyst type and reaction conditions). [39] In the petroleum refinery fouling by the deposition of ‘coke’ can play an essential role. Based on the process conditions (temperature, partial pressure of steam, hydrogen, etc.), many reactions might occur which cause coke or carbonaceous materials, leading to formation of a layer of carbonaceous material on catalyst surface and to inaccessible active sites. [41] Deactivation of supported metals by carbon or coke can take place chemically, due to chemisorption, physically or mechanically, because blockage of surface sites, plugging of pores and destruction of catalyst particles by carbon filaments may occur independently or simultaneously. [39]

Thermal degradation (Sintering)

Thermal degradation is a physical feature causing the catalyst deactivation due to sintering and chemical transformations. Sintering is the loss of catalyst active surface because of the crystalline growth. Figure 2.5 shows this kind of deactivation.

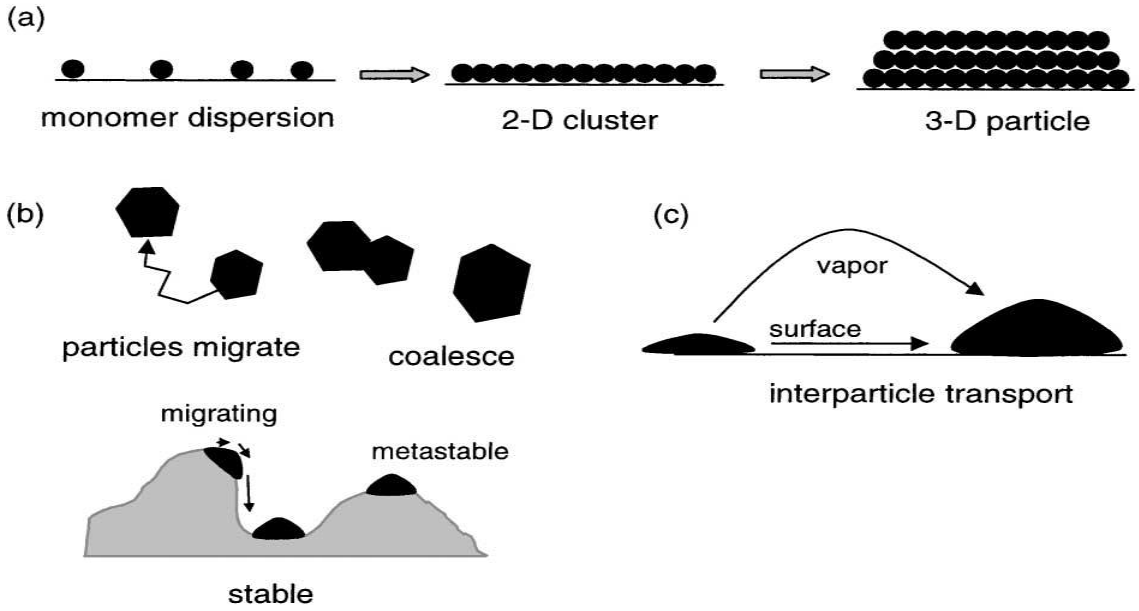

Figure 2.5. Schematic of the different stages in the formation and growth of particles from a monomer dispersion. Moulijn et al., 2001. [41]

Firstly, the atoms are assumed to be present as small clusters of atoms or small metal particles (a monomer dispersion). Surface diffusion of the atoms will cause formation of two-dimensional clusters and further three-dimensional particles (Figure 2.5a). These particles might grow into larger ones over different mechanisms. Particles can move and coalesce (Figure2.5b) or also atoms move from one particle to another by two ways such as volatilisation or surface migration (Figure2.5c).The most important mechanism for sintering of small particles usually is the movement of atoms rather than particles by a hopping mechanism or surface diffusion, depending on the operated conditions (e.g., temperature, pressure and type of surface atoms). In fact, during the sintering process, the large particles grow at the expense of small ones and the position of the particle can contributes to sintering as well. In another path, thermal degradation may occur in all steps of the life cycle of the catalyst. It can occur because of the local heating through preparation (calcination), reaction (hot spots, mal-distribution) and regeneration (coke burn-off). A prediction of a tendency to sintering might help in reasonable catalyst selection and design. [41] Baker et al., (1991) have reviewed the influences of sintering on the activity of catalyst. Specific activity (based

on catalytic surface area) might increase or decrease with increasing metal crystallite size through sintering. [43]

Mechanical failure of catalyst

Mechanical failure of catalysts is usually observed in many different forms which depend on the kind of reactor, including (1) the crushing of granular, pellet and monolithic catalyst forms because of a load in the packed beds, (2) the attrition, size reduction and breakup of catalyst granules. [39] Mechanical strength is very crucial feature to give the catalyst resistance against crushing such as during transport and loading of the catalyst inside the reactor. Catalyst particles of packed bed face strong stresses during its life cycle (i.e., expansion by heating during the start-up and contraction by cooling during the shut-down of the process) and this cycle is even more pronounced when multiple regenerations of catalyst are necessary by the process.

The shape of the catalyst particles affects the mechanical strength. The spherical particles are in fact the most suitable. The mechanical strength is related to porosity as well, for example, macro-pores will lead to reduce strength. [41] Commercial catalysts are usually vulnerable to mechanical failure in large part due to the way of formation. Two major mechanisms are involved in mechanical failure of catalyst agglomerates. First, is fracture of agglomerates into smaller ones and the second is erosion of particles which have diameters under range between 0.1 to 10 μm from the surface of the agglomerate. [39]

Mechanical stresses cause fracture or corrosion in fluidized or slurry beds which might result from (1) collisions of particles with each other or with walls of reactor, (2) shear forces which are created by turbulent eddies or collapsing bubbles at high flow rates. [39] Thermal stresses take place as catalyst particles are heated or cooled sharply. In fact, they are magnified by temperature gradients across particles and also by differences in thermal expansion coefficients at the interface of two different phases. Chemically driven stresses can occur as phases of different density are formed during the chemical reaction. [39]

Corrosion / Leaching

The reaction medium might be completely corrosive. By considering alumina, for instance during high or low pH extent, alumina will dissolve at pH higher than 12. Therefore, at pH values close to 12 both corrosion and leaching will take place. On the other hand, the same concept might occur at pH value less than 3. For significantly high or low pH, carbon can be affected as well. For example, the sulphiding process of oxides when H_2S is present in a reaction medium. Oxygen–sulphur exchange will occur and lead to a sulphide phase. Another example in the hydro-purification of petroleum fractions, a molybdenum oxide phase will be changed in a molybdenum sulphide phase. Especially in liquid-phase catalysis, leaching usually is substantial. For instance in the solid-catalysed fat hydrogenation, Nickel is the catalyst of choice. It is clear however that traces will appear in the product, and this would not happen with noble palladium catalyst, which is not cost-effective though. [41]

2.3.2 Kinetics of catalyst deactivation

The kinetics of catalyst deactivation might be studied via three levels, fundamental, semi-empirical and empirical. In the first type, the deactivation kinetics is related directly to changes in the active sites of the catalyst. In the second type, a semi-empirical study, the actual deactivation kinetics will be related by an empirical expression to the rate of any measurable change on the catalyst e.g. an increase in carbon deposit. The last one, in an empirical level the deactivation kinetics will be defined by empirical power – law expressions including any influencing parameters. Majority of industrial studies of catalyst deactivation are semi-empirical or empirical .[40] The concept of separability which was introduced by Szépe and Levenspiel is frequently assumed in studies of catalyst deactivation by expression shown in Equation (1) to solve both the main chemical reaction and the kinetics of the deactivation. According to this concept, the rate *r* of the main reaction at time *t* is the product of two separable terms. [44]

$$r = f_1(C,T)f_2(a) \qquad (1)$$

Function f_1 shows the kinetics of the catalytic reaction while function f_2 describes the current activity a. The physical basis of this concept is that there is negligible effective linkage between f_1 and f_2, the deactivation reaction decreases the number of active sites of the main reaction however, leads to no other change to its kinetics. [44] Based on Levenspiel's approach, the deactivation kinetics of solid catalysts can be defined by the simple power-law form in equation (2):

$$\frac{da}{dt} = k_d(C_1^{n_1}C_2^{n_2} \ldots . C_i^{n_i})a^m \qquad (2)$$

Where, k_d is the deactivation rate constant, a is activity of catalyst at time t relative to fresh catalyst, m is the order of the deactivation, C_1– C_i the concentrations of components for the fluid phase, n_1–n_i represent the orders of the concentration dependencies. [40] In fact, the deactivation of a porous catalyst particles depends on some factors such as the actual deactivation reactions, existence or absence of pore diffusion slowdown and the way of poisoning on the surface, etc. The deactivation may take place in four different ways.

Firstly, the reactant can produce a side product which deposits on and deactivates the surface (parallel deactivation).

$$A \rightarrow R + P\downarrow \qquad OR$$

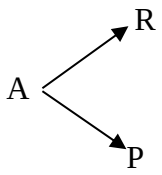

Secondly, when the reaction product might react to produce a material which then deposits on and deactivates the surface, (series deactivation).

$$A \rightarrow R \rightarrow P\downarrow$$

Thirdly, the impurities in the feed can deposit on and deactivate the surface (side-by-side deactivation.)

$$A \rightarrow R$$

$$P \rightarrow R\downarrow$$

Where, P is the material that deposits on and deactivates the catalyst surface.

The main difference between these three kinds of deactivation reactions is that the deposition depends on the concentration of reactant, product and some other materials in the feed respectively. A fourth way of catalyst deactivation, which includes the structural modification or sintering of surface of the catalyst is caused by exposure of the catalyst to severe conditions. This type depends on the time which the catalyst spends under high temperature system and it is unaffected by

materials in the gas flow (independent deactivation). [44] This type has no concentration dependency. More complicated cases can have mixed concentration dependency (reactants, products and/or impurities) for instance, deactivation reactions in reaction networks. [45]

Power-law expressions have been found to be appropriate for a wide diversity of deactivation reactions. They are usually applied to a single mechanism for the activity deactivation despite in few cases different deactivation processes can predominate simultaneously in different parts of the catalyst bed. Also, more complex expressions will be necessary when different deactivation processes are interdependent in some way. Certainly, when the concept of 'separability' is not enough approximated, then the above expressions will not be applied and more complex expressions will be necessary to fit observed deactivation data such as depending on quantity of accumulated coke or changing the order of deactivation with degree of deactivation for single site poisoning and multiple site adsorption. [46 and 47] Also, if the function $f_1(C,T)$ changes significantly through deactivation, then additional terms will be added to the previous deactivation equations. In some cases of deactivations, the activity does not drop to zero. A deactivation expression which sounds adequate for deactivation along short periods might need to be modified when test data extend through a longer timescale.

One example is the sintering of supported metals but the phenomenon of a residual or steady-state activity is reported to take place more usually. In generalized power-law expressions, the activity a is changed with $a–a`$ where $a`$ is a limiting steady-state value. It is significant to point that the deactivation is investigated for a sufficiently long period to justify the additional parameter $a`$. [48] Furthermore, there is the risk that the parameter $a`$ may simply compensate for poor experimental data, an unsuitable power-law expression or non-separable kinetics. But, the lack of a term for the steady-state value might be compensated by uncommon characteristic of the power law. In some situations, using the generalized power-law expressions has been found to lead to a reduction in the deactivation order m, which means simpler, and consequently more reasonable deactivation kinetics. In the sintering mechanism, the $a`$ might be defined in terms of the surface equilibrium particle size distribution. [48]

On the other hand, the activity by power-law expression gives a simpler and more direct statement of deactivation than the combination of coking kinetics with an activity-coke relationship. The

additional mistake from the measurement of the content of coke will increase the overall doubt in the deactivation model as compared to the activity power-law approach. Knowledge of coking kinetics can be important step for different reasons, for instance, when feed stock conversion to coke is considerable, if detailed information on (location and content) of coke is required for design purposes (such as regeneration or reactor pressure drop) and for catalyst improvements. [49]

During the process of catalyst development, the coking kinetics might provide helpful mechanistic vision into the effect of catalyst composition on the stability of catalyst. In some situations, selectivity can be related to the quantity of coke. Activity power-law expressions are unsuitable if the influence of changes in pore diffusion is considerable, in this case, when the deactivation is caused by fouling, it is necessary to study the fouling (coking) kinetics in relation to the pore structure to model the deactivation kinetics in realistic way. [49]

2.3.3 Influence of composition and temperature gradients on deactivation

2.3.3.1 Internal heat and mass resistances

When the pore resistance to diffusion is significant compared to the reaction rate then concentration gradients for reactants and products will take place during catalyst pellets. Deactivation types (parallel, series and side-by-side) are affected in different ways by pore diffusion resistance. Parallel deactivation tends to take place near the pellet exterior where most of the main reaction occurs. The deactivation front might occupy a thin shell at the outside of the pellet, then moves inwards as the catalyst deactivates. However, series deactivation, takes place more in the pellet interior ,where concentration of the product is higher, leading to evolution of a deactivation front from the inside of the pellet outwards. [40] In side-by-side deactivation, feedstock poisoning, the effect of pore resistance is potentially more complicated. The main reaction or the deactivation reaction can be affected by the pore resistance or both might be influenced to similar or different extents, based on their respective reaction and diffusion rates inside the pellet. For a quick poisoning reaction with high diffusion resistance the deactivation takes place mostly at the pellet exterior such as pore-mouth deactivation.

The main reaction might experience increasing diffusion limitation as an increasing proportion of the remaining active sites are situated deeper in the pellets. Pore-plugging is severe case of pore-mouth deactivation in which access into the pores for the reactants becomes totally blocked, leading

to a serious loss of activity. [40] On the other hand, for a slow poisoning reaction, the effect of pore diffusion resistance will be low and the deactivation will take place uniformly through the pellet. Deactivation processes with more complex fluid composition dependence might also vary during the pellet, but independent deactivation, being independent of fluid composition, has to be invariant during the pellet except if there are temperature gradients as well. The optimal pellet design for catalyst life depends on the deactivation kinetics. For example, in series deactivation, low pore resistance can be desirable to reduce the internal concentration of reaction product. Strong pore-resistance to a reactive feedstock poison will help to protect the activity of the pellet interior for the main reaction. Once again, the optimum design might need a more subtle balance between the reaction rates and diffusion rates inside the pellet for the main reaction and a poisoning reaction. [40]

In fact, the empirical power-law expressions described earlier are frequently applied to catalyst pellets without allowance for any impact of pore-resistance on deactivation rate. The parameters determined by fitting these expressions to observed deactivation data may be affected by these influences and, in this case, the values determined for crushed catalyst pellets will not be valid for all pellets without some further allowance for the influence of intra-pellet gradients. Moreover, the parameters determined from accelerated deactivation tests may also be affected by changes to the composition gradients inside pellets. [40] Usually, deactivation kinetics is more complex if pore diffusion is a crucial factor. The impact of an intra-pellet concentration gradient may lead to a non-uniform intra-pellet deactivation profile. The pore structure of the pellet and the dispersion of a supported active phase might change because varied reasons such as sintering processes and these changes can affect the selectivity as well. [49]

2.3.3.2 Mass and heat dispersions

Concentration and temperature gradients during the catalyst bed affect deactivation types differently. Parallel deactivation is significant in regions of the bed particularly where the concentration of reactants or the rate of the main reaction is high such as at the front of isothermal beds. In fact, during catalyst deactivation, the zone of peak activity and the deactivation front both move down the bed, occasionally leading to a sudden drop in conversion when the active catalyst is exhausted. The change in the overall catalyst performance through time is a combination of integral reaction kinetics with mean-bed and integral deactivation kinetics.

However, in non-isothermal cases, where a peak temperature zone moves through the bed, the fall-off in conversion at end-of-life is even more sudden. Series deactivation increases towards the end

of isothermal and adiabatic reactor beds where the concentration of product is greatest and in adiabatic beds, the temperature is greatest as well. For non-isothermal beds it might be most serious in the peak-temperature zone. The profile of side-by-side (feed poison) deactivation over the bed will reveal a peak at the front of the bed for very reactive poisons or will be more uniform along the bed, based on the kinetics of the deactivation reaction. [40]

2.3.3.3 Process design and reaction engineering

Practically, industrial process are designed to obtain the target process capacity over the design catalyst life such as the time between planned shutdowns. The reactor design e.g. (type, size and number of tubes) has to permit for appropriate reaction conditions for both the target capacity and the target catalyst life. This means a control of temperature and composition gradients. Usually, better knowledge of catalyst deactivation leads to a better reaction engineering and to a longer catalyst life. There is however a general compromise to be made between the detailed kinetics, detailed description of insights into the reactor, the time to meet deadlines and relevant costs. The catalysis and the reaction engineering have been integrated in various ways to reduce catalyst deactivation under steady-state operations. The reaction kinetics and the deactivation kinetics are frequently known only approximately. [40]

The objective always is to obtain a proper combination of reaction conditions and catalyst formulation. The reaction temperature may be controlled for catalyst life as well as for reaction control by selection of an isothermal reactor and also, the temperature rise might be limited by using several adiabatic reactors in series with inter-cooling or intermediate injection of cold feedstocks. The reactant concentrations may be controlled also by using intermediate injection points for reactors in series way. A well-known example is a non-uniform distribution of catalyst in packed beds. If the deactivation process is particularly severe in one zone of the bed then it might be better to use a specific deactivation-resistant catalyst formulation in that zone, and a different formulation in the rest of the bed. This approach has been adopted for the steam reforming of hydrocarbons such as an alkalized Ni/Al_2O_3 catalyst is used in the top of the bed to provide better resistance to carbon lay-down and a non-alkalized formulation is used within the rest of the bed. [40] Multi-layered PBRs with zones of catalyst activity and other reduced or non-activity have been popular with exothermic reactions with improved catalyst life, reaction yield and product selectivity.

2.3.4 Process dynamics and catalyst monitoring

The ultimate test of a catalyst is its performance during the process. Usually, more information may be derived from the study of plant catalysts than is possible in a research study. Ideally, monitoring has to start with sample-testing of fresh catalyst for uniformity. The charging procedure for the plant reactor must be monitored to ensure careful handling and also safe loading. Clumsy loading may lead to break the pellets, dust formation and uneven packing; all of these factors can cause uneven flow patterns and therefore, uneven catalyst deactivation. [40]

Process data must be available from plant log-sheets such as flow rates, compositions, temperature profiles of reactor and analyses (*in-situ* or remote) of the crude product stream and any inter-reactor streams, potential even of *in-situ* analyses of the intra-reactor fluid composition. It is important to design the plant reactor instrumentation so that catalyst deactivation might be monitored. Adequate provision should be made for measurement devices e.g. temperature sensors, catalyst (powders) sampling devices, etc. For simple cases, the plant catalyst may be monitored directly via plant data. However in some more complicated and non-isothermal cases may need the periodic return to standard operating conditions or use of a reactor model.

These studies may provide worthy background information, based on the available data such as change in activity with location inside the bed. The deactivation may not become clear until the catalyst is almost spent, and again causes an unplanned plant shut-down. It is very important during monitoring of the deactivation to remove samples of the catalyst periodically throughout its life for ex-reactor measurements of activity. Alternatively, an *in-situ* and spatially resolved probe can be set up to detect the first signs of reaction limitation. [40]

2.3.4.1 Packed bed reactors with spatially variable activity

Reactors with axial variation of catalyst activity might be common. Variation of catalyst spatial activity may be arranged by some ways such as via temperature control, by changing the loading of active metal on the support or during on-stream deactivation. Yakhnin and Menzinger (1999) showed in case of catalyst deactivation under kinetically controlled conditions and the primary reaction which exhibits ignition behaviour that it can form a zone of deactivated catalyst downstream of the entrance to the packed bed. [50] Therefore, a zone of active catalyst followed by a zone of fully deactivated catalyst, followed in turn by active catalyst, was formed. Usually, deactivation will be more noticeable in case of spatially variable (heterogeneous) activity in PBRs.

A good example is the segregated catalyst bed into alternate layers of active and inactive material. Layers of various catalysts have been common for improving selectivity for some types of complicated reactions under non-isothermal conditions to obtain higher conversion with reactors exposed to composition modulation or also to extend the region of stability especially, with highly exothermic reactions. [51, 52, 53, 54 and 55] Due to concentration change and temperature differences, catalyst deactivation in these packed beds will be non-uniform. It has been shown that sudden variations in activity of the catalyst resulted in temperature excursions that are much bigger than those in beds of uniform activity when temperature disturbances take place upstream of a reactor. Under convenient circumstances, disturbances introduced at the inlet of a reactor could be amplified in the zone of a reaction front.

2.3.4.2 Dynamic instability of PBR in presence of spatially variable activity

Catalytic systems can reach dynamic instabilities under some transient conditions such as disturbances in feed temperature, concentration or flow rates. These instabilities, which originate from different flow of mass and heat through the bed. These differences have been observed more pronounced in reactors during non- uniform or local catalytic activity. PBRs running exothermic reactions are dynamically unstable, in other words, they tend to amplify transient perturbations of input temperature rather than attenuating them. This dynamic or thermal instability due to the inherently different rates of matter and heat flow throughout the reactor bed. The instability of the PBR is commonly the differential flow instability (DIFI). [56 - 58] Rate difference between the flow of heat and matter is a general feature of packed beds since heat gets absorbed by the high capacity of packing and its rate of propagation is consequently, slowed down relative to the more rapidly flowing reacting fluid. This differential flow which unleashes the inherent tendency of exothermic reactions towards thermal runaway or explosion. As a result of this, packed bed reactors tend to amplify, rather than attenuate, perturbations of inflow temperature, concentration and fluid flow. [57] However, the tendency to amplify temperature-transients is almost common during exothermic of PBRs, therefore the consequence of this will be the dynamical instability often, but not always, turns out to be not very dramatic. [56 and 59]

In general, during transient conditions, the dynamic response of the reactor can have some unexpected characteristics that lead to control failures, deactivation of the catalyst and wrong-way behaviour. This behaviour was first predicted by Crider and Foss (1966). [60] McGreavy and Naim (1977) and Windes et al., (1989) investigated the wrong-way behaviour by using 1D and 2D dimensional mathematical models. [61 and 62] The wrong-way behaviour may take place when a

sudden drop of the inlet temperature is introduced to a steady-state operated PBR. The decrease in the rate of reactant consumption causes a concentration wave prior to the reaction region. This wave travels with the mean speed of the flow stream whereas the thermal wave lags behind, because it gets "caught" in the packing due to the thermal inertia of the latter. When the fast wave of reactant concentration overtakes the slow-moving hot spot, the resulting increased rate of reaction may lead to large temperature excursions before the new steady-state is established .[63]

The thermal behaviour of PBR through its transient operation is influenced by the deactivation of catalyst as well. Since the heat is released by the surface reaction, the rate at which the catalytic activity is lost is conceivably one of the factors leading to the thermal instability of the system. Jaree et al., (2003) showed experimentally that the reversible self-poisoning of the Pt/Al_2O_3 catalyst by CO triggered a dramatic temperature excursion when the system changed from ignited state to a complete extinction. [64] For irreversible deactivation, Yakhnin and Menzinger (1999) numerically investigated the effect on the thermal instability of PBR. This simulation study used a one dimensional and pseudo-homogeneous model and showed that a localized deactivation can entail a travelling thermal front with a much higher temperature compared to a catalyst bed with uniform activity. [50]

2.4 Challenges and limitations of modelling PBRs of low aspect ratio AR

Models of fluid flow in these packed beds have been historically based on simplified one-dimensional (1D) pseudo-homogenous models or heterogeneous two-phase models. Improvements of these models contained introduction of the two-dimensional (2D) models with inclusion of concepts of axial or longitudinal dispersion and radial or transversal dispersion, relying on the average structure of porosity. The 2D models of heat and mass configurations rely on lumping the local structure and the local flow velocity inside the packing and between the packing and the containing wall, and their key parameters (i.e., porosity, permeability, viscosity, and dispersion constants) are estimated by experimental data and regression analysis of appropriate models. [65]

These 1D and 2D models are as well driven by empirical solutions, yielding disagreements between the data of various literature works obtained inside the packing as well as those in regions in the vicinity of the confining walls, and thus rational understanding of crucial underlying phenomena is still challenging. [12 - 15] Furthermore, these models raise issues of arbitrary combinations of the non-Darcy (grain) and the nonporous Darcy scales and provide challenging representations of the nonslip/slip assumptions or actual viscosity at the surface of the grain. [66] This is particularly the

case for low AR packing, where the tube wall effects and the local phenomena strongly dominate. [13 - 15 and 67] Owing to the limitation in space resolution of the detailed flow picture inside these beds, these models give few insights into the local mechanisms and possible methods of controlling the rates of chemical or transport events. [68] In reality, thermal energy is transported by radial convective flows as fluid is displaced around the packing elements, while features of the flow in regions of stagnant and reverse exits have been identified by a number of spatially resolved experiments. [30, 69 and 70]

Local insights are known to be linked to performances of flow dynamics as well as heat and mass transfers, leading to requirements of more realistic levels of knowledge of transport processes by three-dimensional (3D) modelling. The 3D modelling of the flow field and transport using actual or computer-generated bed shapes has been growing through the past few years, as it offers comparable spatiotemporal resolution with 3D experimental methods such as tomographic techniques (i.e., X-ray computer tomography, magnetic resonance imaging (MRI), laser Doppler anemometry, etc.). [13 and 14] From the 3D simulation results, profiles of radial porosity, velocity, temperature, and dispersion are becoming accessible from a sufficient amount of data, while a limited number of experiments are used.

Laboratory experiments on local velocity profiles were visualized for liquid flow by Giese et al., (1998) using the refractive index matching technique and by Gladden et al., (2006) using MRI, ascertaining many simulation works on fluid flow in porous media of different structures (spheres, cylinders, ordered, disordered, monodisperse and polydisperse, and so on). [68 and 71] The approaches using 3D modelling are still, however, limited by requirements of large memories and computational power. [14] Current simulations, consisting of hundreds to over a thousand packed particles, still require large computation time, leading to simulations being carried out for small or laboratory scales. [12 and 72]

2.4.1 Modelling transport properties

Literature is equally replete with a variety of mathematical models to solve the velocity and concentration domains inside the column, obviating to some degree the necessity of using empirical correlations in the model governing equations. But, it is fair to say that a number of approximations generally known as 1D, 2D, or quasi-homogenous approximations underlie the basic postulates of

the governing equations, which are far away from providing a realistic image for velocity and associated concentration profiles prevalent through the packed column. At 1D transport models, the approximations are usually related with the averaging of radial porosity, velocity profiles, and dispersion coefficients. While, in 2D models, the approximation involves decoupling of flow fields from those of concentrations by assuming prescribed velocity profiles, which are radially or angularly symmetric. As a result, these models are not available to describe, especially, the influences of flow or circulation through the voids between the particles, those of the stagnant zones around the particles or the zones which are close to the wall of the reactor. [1, 73-76]

Likewise, the spatial variations in porosity and dispersion coefficients in 2D models are incorporated by different empirical correlations reported in literature. There is another limitation of the existing 1D and 2D models for packed beds which have low AR in predicting concentration profiles within the voids. In principal, when the dimensionless groups e.g. Reynolds number (Re) or Peclet (Pe) number in different sets of equations for the conservation of species, momentum and the corresponding dimensionless boundary conditions are identical, the solutions must be the same as well, although actual solutions of the velocity and concentration fields will be different because of scaling impact. The situation, however, becomes non-trivial in PBRs because different packing arrangements possible for the same AR, in this case the overall bed porosity can be the same but the local porosity vary from one arrangement to the other. As a result of this, the concentration profiles are different. This is one of the causes why the existing literature correlations cannot be realistic for calculating effective Peclet numbers for packed beds at low AR (particularly AR<10), since concentration profiles will be considerably influenced by the packing arrangements. In such case, it will be more realistic to solve fully 3D profiles without using existing correlations. [73-76]

With the advent of fast computational machines through the past decade, computational fluid dynamic (CFD) models have gained tremendous potential in solving a wide range of fluid flow issues with significant numerical accuracy without having to depend on some of those approximations which were mentioned above. More strict simulation approach based on a new type of simulation procedures, e.g. the direct 3D simulation of the flow inside the actual 3D geometry of the bed which consist of discrete individual particles instead of a pseudo-homogeneous porous medium have been developed. Of course, the availability of refined mathematical models and the perpetually increasing performance of computers make detailed 3D simulations more feasible.

However, in spite of it is possible to simulate the fluid flow inside a packing consisting of a few hundred particles, it is still not possible to implement a 3D simulation of a complete full-scale industrial packed bed reactor with an adequate resolution in a reasonable amount of time. [13] Indeed, we should rather regard this approach as a tool for the analysis of the complicated processes on a formerly unreachable level of detail, draw consequences and to establish cross-links between the detailed simulation and the traditional modelling approaches via combination the gained knowledge from the first to the latter. Therefore, the challenge is to analyse and to take advantage of the great deal of detailed local information achieved from 3D simulations. Main advantage of using 3D is to improve the physical insight into the local processes, which allows for a more fundamental understanding of how global characteristics are affected. [12] These insights may be used for critical evaluations and convenient modifications of traditional modelling approaches.

2.4.2 Computational fluid dynamics (CFD) simulation and PBRs of low AR

The relatively young field of CFD is quick growing because of increasing computer capacities and growing field of applications. It is an established research tool in mechanical and civil engineering where it is used to calculate stress within solid structures. Also, it has been used for instance, in the automobile and airplane industry to replace expensive wind tunnel testing of new designs. Recently CFD has been introduced in chemical engineering field with the introduction of specific fluid mixing programs and the option to solve for chemical reactions. [73 and 77] CFD investigations of low (AR) of PBRs date back to the early twentieth century. Due to the difficulties in measuring fluid flow, mass and heat transfer inside the bed by conventional means without disturbing the packing arrangement, modelling by using CFD have been developed and improved. In general, 2D and 3D CFD models have been applied to several fields to simulate fluid flow profiles and heat transfer, etc. [73 and 77]

The earliest CFD packed bed simulations used 2D models. Dalman et al., (1986) used an axisymmetric model as a first insight into flow patterns over the beds. The effect of particle size on heat transfer of the bed has been investigated by numerical method via two-dimensional model. [78] At 3D models, in which eight spheres are located into two layers with four ones without solid–solid contact points however, the hydrodynamics and heat transfer phenomena could appear reasonably through a packed bed with sphere particles. [50, 79 and 80] Mass and heat transfer characteristics of PBRs at low AR has been studied by Romkes et al., (2003) and their aim was to evaluate whether CFD software can be used to predict the rate of mass and heat transfers from the catalyst particles to the fluid and also to develop simple engineering correlations for composite structured reactors. [81] The hydrodynamics and heat transfer features of a randomly packed bed for cylindrical particles of

AR (2) have been studied by Ahmadi and Hashemabadi (2008). [82] Mirhashemi et al., (2011) have investigated numerically and experimentally the heat transfer of a single cylindrical particle which is influenced by wall. They have investigated effect of the wall on heat transfer of particles in seven various ARs and concluded that with increasing value of AR over 12, the wall would have no considerable impact on Nusselt number (Nu). [83]

Other research groups have used commercial CFD packages to simulate the behaviour inside packed beds. Calis et al., (2001) applied the commercial code CFX-5.3 to a structured bed of spheres and validated the values for pressure drops which were obtained from the simulations against the experimental ones. [84] Other authors used Lattice Boltzmann (LB) technique for simulation of fluid flow and reactions through a packed bed of spheres. This method used another approach where packing topology is divided into cubic LB grids and individual elements are labelled as solid or fluid zones. At a high resolution of the grid, it was found possible to achieve more accuracy for flow profiles. [85] Freund et al., (2003) added simple reactions to the simulation and highlighted the problems regarding non-isothermal operations. [33]

2.4.3 Derivative framework for CFD modelling of PBRs

Experimental methods are the foundation of any theoretical analysis however, are sometimes replaced by modelling methods if experiments are limited by data size and range, field disturbance, personal safety, measurement accuracy and off course costs. Realizing a specific CFD and showing the results on screen will give insights into the packed bed reactor which may not be accessible by physical probes. The general method for approaching a simulation problem of fluid flow associated with mass and heat exchanges and also a chemical reaction inside a packed bed reactor is summarized in Figure 2.6.

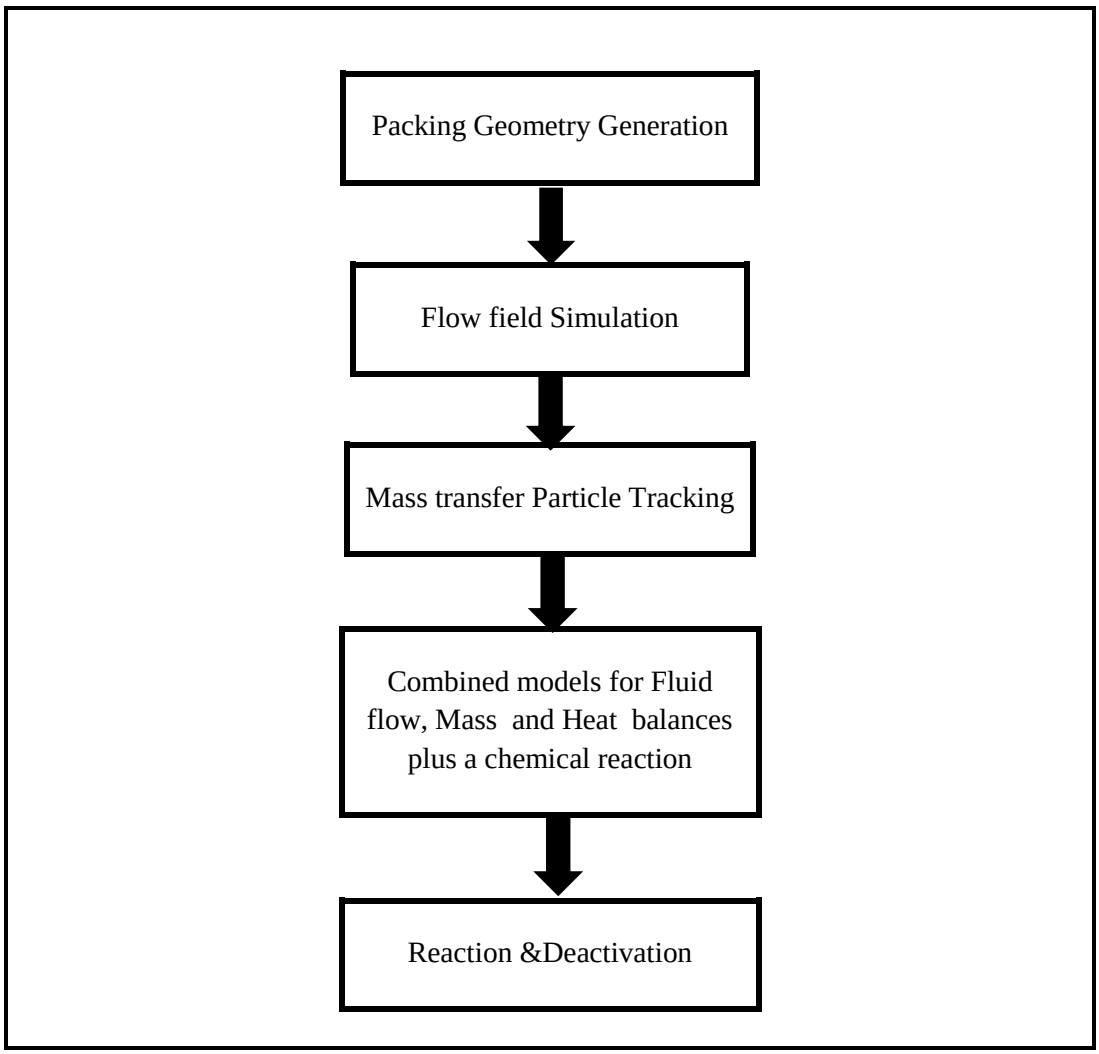

Figure 2.6. Derivative framework for CFD modelling of a PBR

First step is the generation of packing geometry. In general, random or ordered packing could be generated from experimental data by using spatially resolved techniques, for instance, tomography based on MRI, X-ray, neutron radiation, gamma radiation, etc. Alternatively, packing is also generated by simulation of particle assemblies by using statistical methods, e.g. Monte Carlo or discrete element methods (DEM). Once created, the data of packing are transferred to the flow solver where packing volumes are discretized by defined meshes and then integrated with flow, heat and mass modules. Comparison of the relevant features of the generated random packing (i.e., average porosity and radial porosity profiles) with experimental data shows that the applied simulation approach produces realistic packing that matches experimental data well. [86]

Validation of the global flow behaviour uses pressure drop, local velocity, relevant axial and radial dispersion profiles which are compared with experimental data or established models. Lagrangian,

Eulerian, Hamiltonian and Newtonian particle tracking methods are used to assess mass and heat dispersion profiles, indicating the mixing efficiency of the packing structure. A combination of momentum, mass and heat balances along with the kinetic model of reaction and catalyst deactivation are used for screening local catalyst activity. The program code numerically solves the Navier-Stokes equations and associated differential equations for energy and mass balances over a number of approximate differential 'Δ' control spaces, surfaces or volumes. These control elements are small within the flow domain that as a whole would describe the domain geometry. There are four differential equations, which a CFD code needs to use in a packed bed reactor, defined as follows: [86]

- Equation of motion for momentum conservation
- Continuity equation for conservation of mass
- Thermal energy equation for conservation of energy
- Mass balance for conservation of chemical species

The size and number of control elements or "meshes" is determined by the user in the geometry creation step, where once the geometry has been defined. Potential errors can occasionally be caused by the mesh being too large to allow accurate approximation of solution in the mesh volume used. When the mesh is made smaller, the solution is more accurate until a certain size of mesh where the solution becomes mesh independent, which means that any further refinement of mesh will not cause further convergence in the solution. [86]

Commercially available CFD codes use one of three discretization techniques for creating meshes. These are known as finite differences (FD), finite volumes (FV) or finite elements (FE). The main drawback of the FD method is the limitation to uniform structured meshes, which makes it difficult to use for complex geometries. FD is mostly used in civil engineering for calculation of stresses in beams and the result is a 2D or 3D grid of rectangular (or square) elements. FV and FE methods can support both structured and unstructured grids or meshes and because of this they are appropriate for complex geometries, such as packed bed geometry. [87]

An unstructured mesh is either a 2D structure of triangular or rectangular cells or a 3D structure of tetrahedrons, and other irregular polyhedrons. FV methods are more convenient for flow situations as the mass balance is satisfied for each volume elements, making it more accurate (see Figure 2.7).

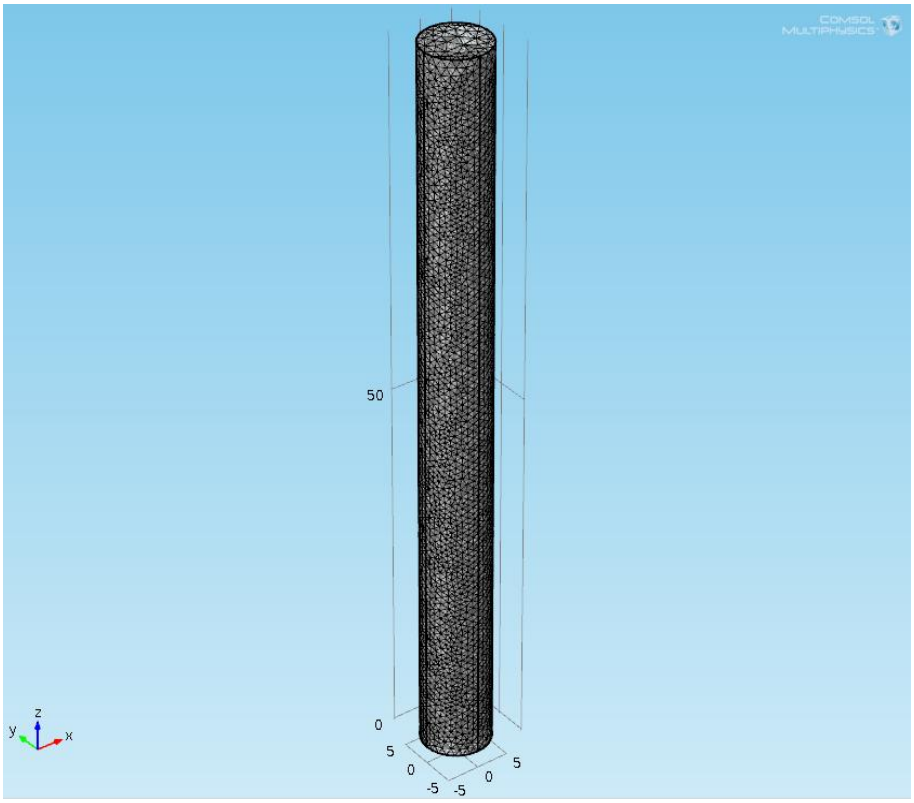

Figure 2.7. Example of unstructured 3D mesh applied to a cylindrical tube

2.4.4 Characteristics of computational fluid dynamic (CFD)

CFD has some kind of certain limitation. Firstly, the numerical solution is a kind of discrete approximate calculation method which depends on the reasonable physics and applied mathematics and relies on calculation based on the discrete finite mathematics models. The final results cannot provide any form of analytic expression, it is only the numerical solution on limited discrete points which has certain calculation errors. Secondly, it is not like a physical model that gives flow phenomenon and qualitative description. CFD often requires the original body observation or physical model tests to provide some flow parameters and needs to establish the validation of mathematical model. Thirdly, programming and data collection, sorting and correcting, to a great extent, depends on experience and skills of users. Numerical processing methods may lead to a fake result e.g. producing pseudo-physical influences like numerical viscosity and dispersion. However, some other shortcomings, by somehow, can be overcome by using 3D modelling and high computer configurations. [86]

2.4.5 Packing geometry

The most common style of a packed-bed is the random configuration of particles in a confining cylindrical tube. In several cases, the catalyst particles are spherical serving as representative model geometry. Simple sphere geometries allow for a relatively easy and well- defined generation of the packing as spheres are defined by their centre positions as degree of freedom. Moreover, packings of spheres reflect the influence of the packing structure stronger (e.g., wall effect features stronger oscillations in the radial porosity profile) than packings of other particle shapes and, consequently enable to study more clearly its effect on the transport processes. [12]

A quick and an effective way to generate and to discretize the 3D structure of a packed bed is an essential prerequisite for a systematic investigation of local transport phenomena. Since the structure of a random packing is theoretically unpredictable in all details in advance, synthetic generation methods such as the DEM is used. Briefly, imitating the technical filling method, spherical particles are initial randomly placed into a cylindrical tube as shown in (Figure 2.8, a). After this raining method, the packing is compressed by rearranging the spheres with an increased probability into gravity direction. The process stops after meeting the convergence criteria which accounts for the change in potential energy and the plausibility of the sphere positions (e.g., mechanical stability), (see Figure 2.8, b). [12]

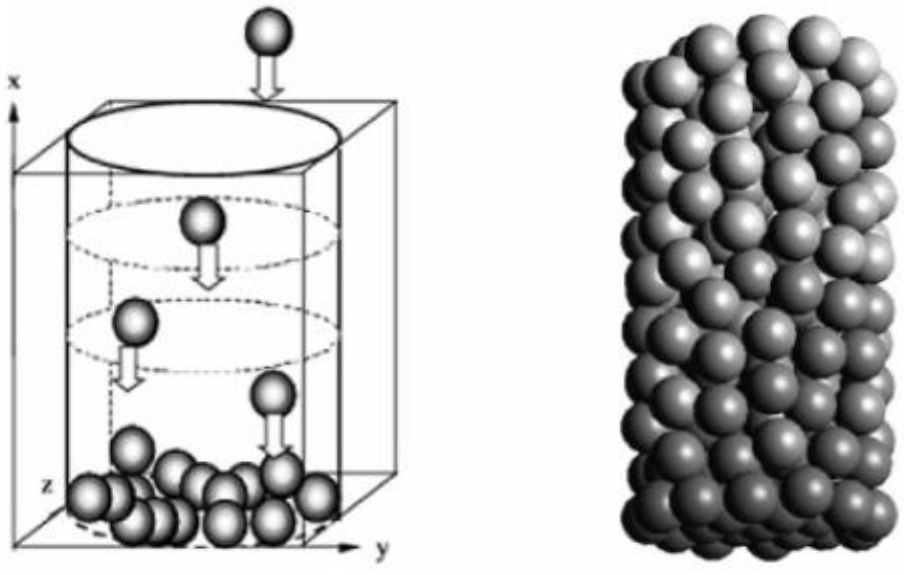

(a) (b)

Figure 2.8. Generation of the random packing: raining process (a) and (b) the resulting sphere packing [12]

2.4.5.1 Discrete element method (DEM)

DEM can be defined as a numerical model capable of describing the mechanical behaviour of assemblies of spheres. DEM depends on the use of an explicit numerical scheme in which the interaction of the particles is monitored by contact and the motion of the particles modelled particle by particle. [88] This method, which is pioneered by Cundall (1979), is a powerful numerical tool that is widely used in several scientific and engineering issues. [88] The relevant algorithm calculates behaviour of a large number of particles together in confined space via accounting the spatial velocity of these particles along with linear, rolling and radial frictions from associated collision-handling algorithms. [89]

The fundamental idea of DEM is the use of discrete time-steps during the simulation and to assume that the velocity and acceleration between these steps are constant. In case, choosing a small enough time-step, this assumption leads to a negligible error in the results. Usually if two particles collide in the real world, they deform by exerting a force in the direction of the contact. This deformation is simulated by letting the particles overlap. When the collision between two particles can be sufficiently simulated (meaning that it is within the error tolerances), a domain with many concurrent collisions could be simulated via handling these collisions sequentially. More mathematical details on how to calculate the forces resulting from a collision, at Radeke (2006). [90] The solution scheme is similar to that used by the explicit finite-difference method for continuum analysis. The use of an explicit, as opposed to an implicit, numerical scheme will make it possible to simulate the nonlinear interaction of a huge number of particles without large memory requirements or the need to an iterative procedure.

2.4.5.2 Particle-flow code of three-dimensional (*PFC^{3D}*)

The PFC^{3D} has been developed by ITASCA Consulting Group Inc., to simulate movement and interaction of stress in assemblies of rigid spheres. It relies on the Discrete Element Code by Cundall et al., (1979), allows finite displacement and rotations of discrete bodies. [88] PFC^{3D} algorithm was used in our simulations. General particle-flow model simulates the mechanical behaviour of a system comprised of a collection of particles. The model is composed of distinct particles that displace independently and interact only at contacts or interfaces between the particles. If the particles are assumed to be rigid and the behaviour of the contacts is characterized

using a soft contact approach in which a finite normal stiffness is taken to represent the measurable stiffness that exists at a contact, then the mechanical behaviour of such a system can be described in terms of the movement of each particle and the inter-particle forces acting at each contact point. [91]

Newton's laws of motion provide the essential relationship between particle motions. PFC^{3D} models the movement and interaction of stressed assemblies of rigid spherical particles using the DEM. The calculations performed in the DEM alternate between the application of Newton's second law to the particles and a force-displacement law at the contacts. Newton's second law is used to determine the motion of each particle arising from the contact and body forces acting upon it, while the force-displacement law is used to update the contact forces arising from the relative motion at each contact. The presence of walls in PFC^{3D} requires only that the force-displacement law accounts for particle-wall contacts. Newton's second law is not applied to walls, due to the wall motion is specified by the user. [91]

The calculation cycle in *PFC^{3D}* is a time stepping algorithm which needs the repeated application of the law of motion to each particle, a force-displacement law to each contact and also, a constant updating for wall positions. Contacts that may exist between two particles or between a particle and a wall are formed and broken automatically through the course of a simulation. The calculation cycle is illustrated in figure 2.9. At the binging for each time step, the set of contacts is updated from the known particle and wall positions. Then, the force-displacement law will be applied to each contact to update the contact forces based on the relative motion between the two entities at the contact and the contact constitutive model. After that, the law of motion is applied for each particle to update its velocity and position based on the resultant force and moment arising from the contact forces or any other forces affecting on the particle. Also, the wall positions are updated depending on the specified wall velocities. The calculations performed in the two boxes as shown in Figure 2.9, which can be done efficiently in parallel. [92]

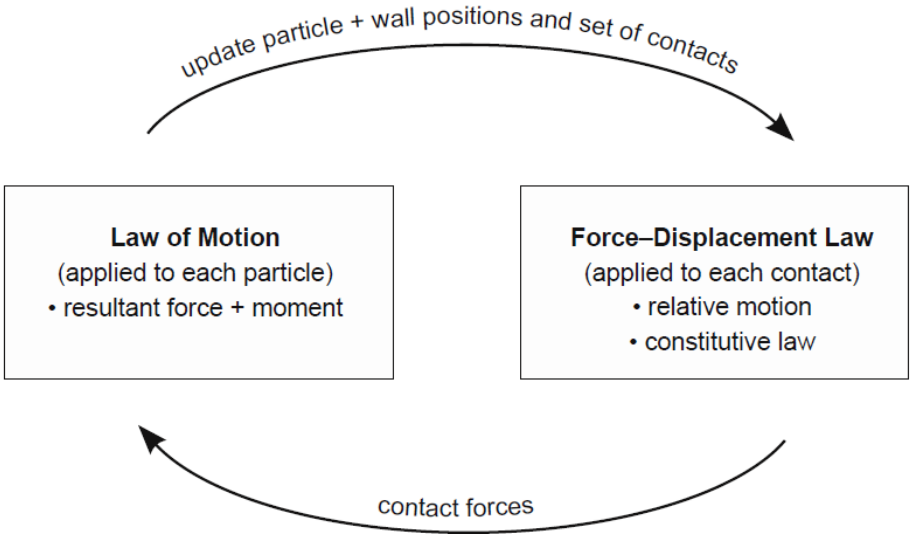

Figure 2.9. Calculation cycle in PFC^{3D,} ITASCA, 2008. [92]

2.4.6 Commonly used CFD codes

2.4.6.1 PHOENICS

PHOENICS that is short for Parabolic Hyperbolic or Elliptic Numerical Integration Code Series is the first set of CFD and heat transfer commercial software in the world. PHOENICS runs on PC's, workstations, supercomputers and parallel processors and is able to solve steady-state or transient problems involving laminar, turbulent and chemically reactive flows. PHOENICS is supplied with a wide range of models for heat transfer, turbulence, physical properties, and combustion and reaction kinetics. Application specific versions are available. PHOENICS can be used for a wide variety of fluid flow simulations which include fluid of (gases or liquids), multi-phase flows, particle tracking, non-Newtonian flows, and also, reacting flows. Complicated geometries can be established by using menu-driven or visual reality interfaces. Interfaces exist to ALGOR, PATRAN, IDEAS, IGES and other CAD or graphical display tools. Usually users can combine their own calculations into a model. The simulation results can be displayed by 3D in coloured plots for any selected variable. [93]

2.4.6.2 ANSYS Fluent

ANSYS Fluent® is a commercial CFD package from ANSYS Inc. It is the relatively popular CFD package, which shares 60% market. Every relevant industry related to fluid, heat transfer and chemical reaction can use it. It has a wealth of physical model, advanced numerical method and strong before and after processing functions in the aerospace, automobile design, oil and gas turbine design. [94]

Fluent is used to simulate complex flows within the scope from incompressible to highly compressible fluids. As a result of using the many kinds of solving methods and multiple grids accelerating convergence technology, Fluent can achieve the best convergence speed and the precision of solutions. Flexible unstructured grid, adaptive grid technology based on the solution and mature physical models, all make Fluent has a wide application in aspects of transformation and turbulence, heat transfer and phase change, chemical reaction and combustion, multiphase flow, rotating machinery, moving/deformation meshes, noise, materials processing and fuel cell. Fluent has some advantages as below:

- Good stability: it has a lot of examples of assessment which are in good accordance with the experiments.
- Wide range of applications: it contains a variety of phenomena (i.e., heat transfer, combustion, flow models of chemical reaction and moreover, fluid-solid mixing with domains from low speed to hypersonic and from single phase flow to multiphase flow). [86]

2.4.6.3 COMSOL Multiphysics®

COMSOL Multiphysics® is the fastest growing CFD code making it a major part of science and engineering. COMSOL was developed by graduate students of Germund Dahlquist at the Royal Institute of Technology in Sweden in 1997. The computer simulation environment in COMSOL needs simple implementation of data and models (linear and nonlinear), allows open access to popular Matlab programs (Mathworks) and uses extensive post-processing tools. [86]

The properties of COMSOL become apparent with use. COMSOL requires that every type of simulation involved in the package has the ability to be combined with any other. Another noticeable characteristic of the COMSOL platform is adaptability. In addition, any change or add-on of the model can be made and any formula could be edited during the study. COMSOL

Multiphysics has several problem-solving benefits as well. When starting a new project, using COMSOL helps to understand the problem. It is possible to examine the different geometrical and physical characteristics of the model. From beginning to the end, COMSOL is a complete problem-solving tool. COMSOL is applied in this research as it was found the only one to our knowledge that allows implementation of reaction rates in every single domain of the packed bed. This flexibility of using reaction rates for every single particle, group of particles or layers of particles will lead to possibility to design of packed beds of non-uniform catalytic activity. [86]

2.5 Packed bed structure and flow dynamics

2.5.1 Packing structure and porosity distribution

Property constants of the packed bed (i.e., porosity, tortuosity or permeability) may change from macroscopic point of view, even if the bed was repacked with the same batch of particles. Rumpf and Gupte (1971) have analysed the influence of various distributions of spherical particles through a relatively extensive range of porosity ($0.35<\varepsilon<0.70$) and suggested a different dependence upon porosity. [95] For the zone of packed bed porosity within (0.35 to 0.55), the proposed porosity function did not differ significantly from the conventional capillary model (an average difference of ~10%). Ergun also made an interesting point that when a transformation of his equation was carried out by employing the fundamental expressions for the shear stress, hydraulic radius and interstitial velocity, it would cause complete elimination of porosity. In fact, any variation in these parameters shear stress, hydraulic radius and interstitial velocity is the result of the effect of the confined walls on average porosity and local porosity, especially for low AR packed beds. Generated packed beds are therefore characterised by both (average) porosity and local porosity profiles. [96]

2.5.1.1 Average porosity (Bed porosity), ε

According to Klerk the average porosity can be influenced by some factors such as the tube to particle diameter ratio (D/d_p) or aspect ratio (AR), confining wall, particle size distribution, particle shape, roughness of the particle surface and the bed height. [30] Among the numerous the relationship between the average porosity and (AR), the one established by Zou and Yu (1995) has the most cited and therefore was used in our simulations. [97]

$$\varepsilon = 0.372 + 0.002(e^{\frac{15.306 d_p}{D}} - 1) \ , \quad D/d_p > 3.95 \qquad (3)$$

$$\varepsilon = 0.681 - 1.363\frac{d_p}{D} + 2.241(\frac{d_p}{D})^2 \ , \quad 1.89 \leq D/d_p \leq 3.95 \qquad (4)$$

$$\varepsilon = 1 - \frac{2}{3}\frac{(d_p/D)^3}{\sqrt{2(d_p/D)-1}} \ , \quad D/d_p < 1.89 \qquad (5)$$

2.5.1.2 Locally radial porosity

Radial distribution of porosity is a structural characteristic of packed beds and presents a significant importance for beds with low ARs of tube-to-particle diameters owing to the influence of the confining wall. The spheres near these walls form more ordered structures than spheres in the internal regions, leading to oscillatory trends of porosity and to damping behaviours in the near-wall regions. This damping profile has been demonstrated by Roblee et al., (1958) who used cork spheres within molten wax, as well as by Sederman et al., (2001) who used the MRI technique to observe the flow of water through a packing of ballotini spheres. [98 and 99] The damping profile could be computed by combining the angularly averaged data from a limited number of cross-sectional projections of porosity and then expressed in terms of empirical, semi-empirical, or analytical models. [73, 75, 76, 81 and 82]

The accuracies of these models were good in regions either near the wall or near the centre of the packed bed, but they were rarely good for both regions. For instance, Mueller et al.,(1991,1992) who described the oscillations with a Bessel function of the first kind of order zero and the radial damping with an exponential function, developed a model that over-predicts the radial porosity near the wall but describes the radial porosity accurately when the radial distance increases from the wall. [100 and 101] Govindarao et al., (1990) developed analytical expressions using concentric cylindrical channels of good accuracies in the near wall regions, particularly for packed beds of large AR. [15] Dixon et al., (1988) improved the semi-empirical models by computing the effect of the shape of beads (i.e., spheres, cylinders, or hollow cylinders). [102] Theuerkauf et al, (2006) used the discrete element method (DEM) which accounts for particle−particle and particle−wall mechanical interactions to measure particle-scale structure and porosity in a series of beds with AR in the range 3−20. [72]

Mariani et al., (1998) improved analytical expressions to estimate the radial porosity profiles and the distribution of spherical particle centres. The comprehensive expressions relate the intersection of a sphere and cylindrical surface in terms of natural functions which arise from integral calculus. The link between the distribution of spherical particle centres and radial properties inside randomly packed beds were addressed as well, and consequently, the results have considerably improved the understanding of this relationship. [103] In fact, characteristics of our generated packing in terms of radial porosity profiles will be compared with the most representative empirical model developed by Muller (2010) ,as showed in equation 6 for various AR .[104]

$$\varepsilon(r') = 1 - S_e(r'), \qquad (6)$$

Where,

$$S_e(r') = \pi[R_{se}^2 - \alpha(r_e - r_{se})^2] \qquad (6a)$$

And,

$$R_{se} = R_s^* - \frac{ar'^2}{r'^2+2} \quad with\ a = 0.045 - 0.55e^{-D/d_p}, \qquad (6b)$$

$$r_e = \frac{(r_{se}+r)^2 - R_s^{*2}}{4r_{se}}, \qquad (6c)$$

$$r_{se} = \lfloor r_r + R_s^* \rfloor, \qquad (6d)$$

$$r_r = br'^2 + r' + R_s^*, with\ b = 0.037 - 2.0e^{-D/d_p}, \quad (6e)$$

$$\alpha = \frac{1}{cr'^{1.4}+1},\ with\ \ c = 1.83 - \frac{19.2}{D/d_p} + \frac{40.5\ln(D/d_p)}{(D/d_p)^2}, \quad (6f)$$

With,

$$R_s^* = \frac{1}{2}, \qquad d^* = 1.0, 0 \le r' \le \frac{R_c}{d}, \qquad R_c = \frac{D}{2}, \qquad and\ D/d_p \ge 2.0.$$

2.5.1.3 Effect of confining wall of low (AR) of PBRs

The confining wall of low AR packed beds affects not only the porosity distribution but also the fluid flow in terms of velocity and pressure drops. Early investigations by Kozeny (1927) and Carman (1997) and Ergun (1953) essentially used Darcy and Forchheimer approaches for randomly distributed particles. [105,106 and 96] However, Happel, (1958), Bertil Anderson (1961), Molerus (1977) and Eisfeld and Schnitzlein (2001) used knowledge of the local flow behaviour near the solid surface inside the packing. [107-110]

The distribution of the local velocity in the intergranular space, the pressure drop and the permeability were found to be affected by the flow regime, the internal structure of the packed bed, the dimensions and the shapes of both the particles and the packed bed. [111] The flow behaviour was a function of interactions between the fluid, the particles and the column wall. [112] In addition to the flow, the confining walls have effects on the dispersion of species and heat in packed beds of low AR. Influenced by the structural porosity of the packing, the interaction of convective and diffusive transports presents trends of residence time distribution and dispersions of different trends than those observed in large AR packed beds.[13]

2.5.2 Pressure drop in low aspect ratio (AR) of PBRs

Flow dynamics in terms of pressure drops and velocity provide a perfect representation on wall effects and subsequent influences on catalytic deactivation profiles in low AR packed beds. Mehta and Hawley (1969) and Brauer (1971) described the wall impact by considering the hydraulic diameter which includes the surface area of the tube. [113 and 114] Tsotsas and Schlünder (1988) showed that the fundamental effect of the spatial constraints was an increase in the average bed porosity with respect to the porosity of the infinitely extended bed packed bed. However, a small error in the predicted void fraction may translate to a major error in pressure drop prediction. Due to this inherent error, many packed beds are oversized with a capacity safety factor. [115]

An alternative method to address the expected error is to conduct specific pilot plant tests with representative particles. Given the packing material and the correct tube diameter, the Ergun equation is fitted to the test data via varying the Ergun equation constants and also, the effective particle diameter and void fraction. If the actual AR is used in the test rig, the predicted pressure drop from the modified Ergun equation may be adequate but these tests are expensive and need

significant pre-work to investigate .Typical packing supports could break and degrade after pouring. To reduce the impacts of broken particles, the tests need to be completed with fresh particles, which can require drums of catalyst to be examined. For this reason, there is a considerable limitation on the variations of packing shapes and sizes which can be reviewed for reactor design and catalyst deactivation screening. [35]

The empirical correlation of Ergun model is based on homogeneous assumptions and averaged characteristics therefore, it is not applied to the packed beds of low AR, where the tube wall local phenomena dominate. The local changes in porosity can cause large variations in the predicted velocity profile. Because of this, 3D flow simulations have been used to reflect the local effects. The advent high power computing technology has contributed in advancements fundamental modelling which provide an alternative approach, by coupling the DEM and CFD technologies to handle this issue. The flow within the space between particles inside the packed bed was achieved by solving the transport equations and resulted a very detailed solution containing local values of all related variables for instance, pressure, velocity, and shear stress and turbulence properties. [35]

2.5.3 Local velocity distribution in low aspect ratio (AR) of PBRs

The local flow distribution is validated and discussed by means of radial component profiles of velocity. At low AR of packed beds, the assumptions most often found in the literature on uniformity of the component of the velocity vector makes no sense, as several authors such as Froment and Bischoff (1979), Vortmeyer and Schuster (1983). They were able to observe a significant radial and angular dependence of velocity. [1 and 14]

A variety of analytical and empirical models to calculate radial velocity distributions have been developed. For example, Vortmeyer and Schuster (1983) developed a model by solving the modified Brinkman equation for flow motion where a wall-effect term was taken into account. [14] This equation, is written as follows:

$$V = B\left\{1 - exp\left[\beta\gamma\left(1 - \frac{r}{R}\right)\right][1 - m\gamma\left(1 - \frac{r}{R}\right)]\right\} \qquad (7)$$

Where, V is the ratio of superficial velocity to average superficial velocity (v);

$$\gamma = \frac{R}{d_p}\ ,\ \beta = \frac{4m}{4-m}\ ,\ C = ln(Re+4)\ ,\ R{:}\,radius\ of\ bed,\ r{:}\,radial\ position \quad (7a)$$

$$B = \frac{\gamma^2}{2}\{\frac{\gamma^2}{2} - \frac{(m\gamma-1)(\beta\gamma+1)}{\beta^2} + m\left[\frac{\gamma^2}{\beta} + \frac{2\gamma}{\beta^2} + \frac{2}{\beta^3}\right] - \frac{e^{\beta\gamma}}{\beta^2}\left[1 - m\gamma + \frac{2m}{\beta}\right]\}^{-1} \quad (7b)$$

$$m = \begin{cases} 112.5 - 26.31Re + 10.97Re^2 + 0.1804Re^3\ , & for\ 0.1 \le Re \le 1 \\ -1803 + 201.62C - 3737C^{0.5} + 5399C^{\frac{1}{3}}\ , & for\ 1 \le Re \le 1000 \\ 27\ , & for\ Re > 1000 \end{cases}$$

2.5.4 Particle tracking of mass dispersion (PTM) in PBRs

In addition to the flow, dispersion of species inside packed bed reactors has a strong influence on the progress of a chemical reaction. The interaction of convective and diffusive transports, which in packed beds is mainly affected by the random structure (porosity) of the packing, determines the residence time distribution, the degree of conversion and especially, local catalyst deactivation. [116] The mass dispersion of species inside 3D-packed beds is recurrently validated by means of the averaged radial component (D_{rad}) and the averaged axial component (D_{ax}) of dispersion.

These components are computed by mass dispersion experiments which use either a continuous approach of chemical concentration tracing or a discontinuous approach of particle tracing to fit dispersion constants at dynamic operations. The later approach, which uses the DEM, follows a Lagrangian method where movement of concentration equivalent particles is tracked instead of fluid species. The convective motion along streamlines and by a diffusive motion between different streamlines allows distribution of the particles to be reconstructed and the underlying models of axial and radial dispersions as a function of the dimensionless Peclet number (Pe) to be developed. [12]

In fact, the basic concept of the particle tracking method (PTM) is to move a large number of non-interacting tracer particles, which represent concentration equivalents, by a convective motion along streamlines and also by a random diffusive motion which allows particles of fluid to jump between different streamlines. Based on the spatial distribution of the particle ensemble, one can reconstruct common Euler concentration profiles and also residence time curves. The corresponding equation

of motion for the convective coordinates of the Lagrangian particles is illustrated by a stochastic differential equation as below. [117]

$$d\overrightarrow{x_L}(\overrightarrow{x_0},t) = \overrightarrow{u_L}(\overrightarrow{x_L}(\overrightarrow{x_0},t),t)dt + \sqrt{2D_m dt}\vec{\xi}(t) \qquad (8)$$

Where $\overrightarrow{u_L}(\overrightarrow{x_L}(\overrightarrow{x_0},t)$ is velocity of particle (m s^{-1}) which is the local velocity of the carrier that can be achieved by an arbitrary CFD solver. [118] D_m represents the molecular diffusion coefficient (m^2 s^{-1}) and $\vec{\xi}(t)$ is an array of normal distributed random numbers with zero mean and unit variance. The feature of this equation is the scaling of the random step with the square root of the diffusion coefficient, so that only for very low velocities ranges, the diffusive motion outbalances, the convection and the second moments are linear in time. By applying a simple Euler approximation to previous equation (8) the result will be in equation (8a).

$$\overrightarrow{x_L}(\overrightarrow{x_0},t+\Delta t) = \overrightarrow{x_L}(\overrightarrow{x_0},t) + \overrightarrow{u_L}(\overrightarrow{x_L}(\overrightarrow{x_0},t),t)dt + \sqrt{2D_m \Delta t}\vec{\xi}(t) \qquad (8a)$$

Where, (Δt) is the time (s) step which is calculated from the magnitude of the maximum flow velocity and the diffusion coefficient in such a way that a particle might not move over 10% of the distance of grid nodes used for both CFD and PTM simulation. Since the transformation of uniformly distributed random numbers to normal distributed ones (Box Muller transformation) usually is time-consuming, so the faster method of Maier et al., (2000) is used for the generation of $\vec{\xi}(t)$. [119]

An important aspect using the PTM is the implementation of a suitable boundary condition, because although the method causes precise solutions of the convection diffusion equation in the bulk phase, the quality of the wall boundary condition may considerably minimize the accuracy of the complete simulation [12]. Figure 2.10 illustrates the numerical algorithm by showing the procedure of the time loop.

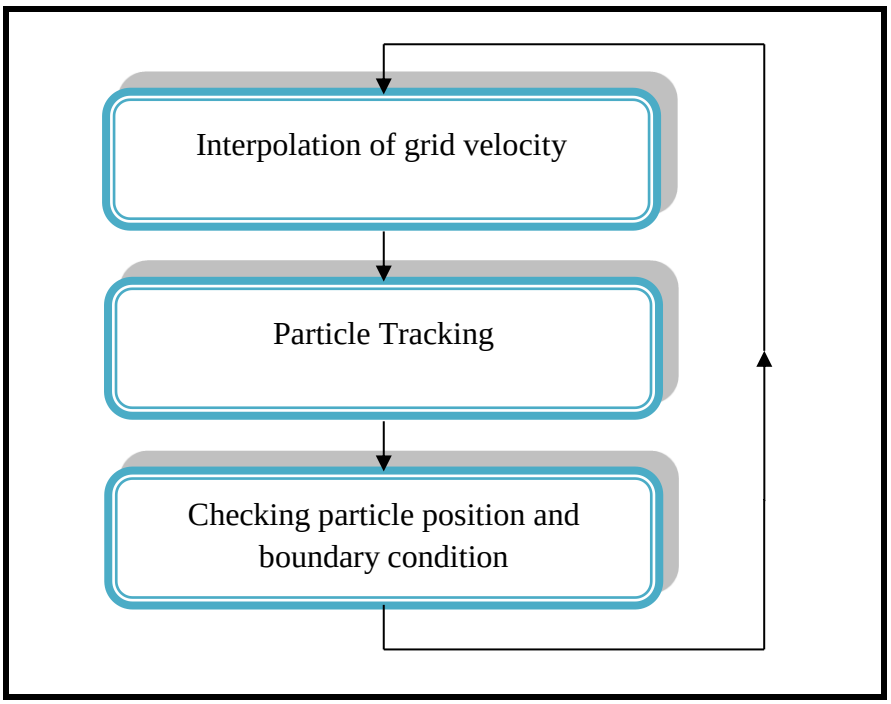

Figure 2.10. Time loop of the particle tracking [12]

Models of axial and radial dispersions in packed beds of low (AR) as a function of dimensionless Peclet number have been investigated by many authors. For instance, the two models as shown in equations (9) and (10) were developed by Freund et al., (2005). [12]

$$\frac{D_{ax/rad}}{D_m} = \frac{1}{\tau} + \frac{Pe^{\alpha_{ax/rad}}}{\beta_{ax/rad}} \qquad (9)$$

Where, α_{ax} =2; α_{rad} = 0.25; β_{ax} =29; β_{rad} =81; τ =1.39 , P_e: Peclet number

And,

$$\frac{D_{ax/rad}}{D_m} = \frac{1}{\tau} + a_1 Pe + a_2 Pe\ ln(Pe) \qquad (10)$$

Where, a_1= 0.005, a_2= 0.177 , τ =1.45

Chapter 3

3. Experimental and Numerical Methods

Majority of this work has done by modelling. A CFD study however needs experimental validation to assess the model. Pressure drop was selected as the validation parameter to be investigated experimentally at various scales of ARs.

3.1 Pressure drop tests

Since literature data of fluid flow for low ARs are limited, experimental tests of pressure drops for ARs ranging from 1.5 to 5 were carried out by using a range of ARs. Air was used as a flowing gas, and the flow rate was controlled by a mass flow controller (ROD-4A, Advanced Energy) which was connected to a cylinder of compressed air. The pressure drops over the bed were measured free of pressure loss with a U-tube manometer along with a differential pressure transducer (142PC02D, Sensortechnics GmbH), as shown in Figure 3.1 (a, b and c). [18 and 86]

(a)

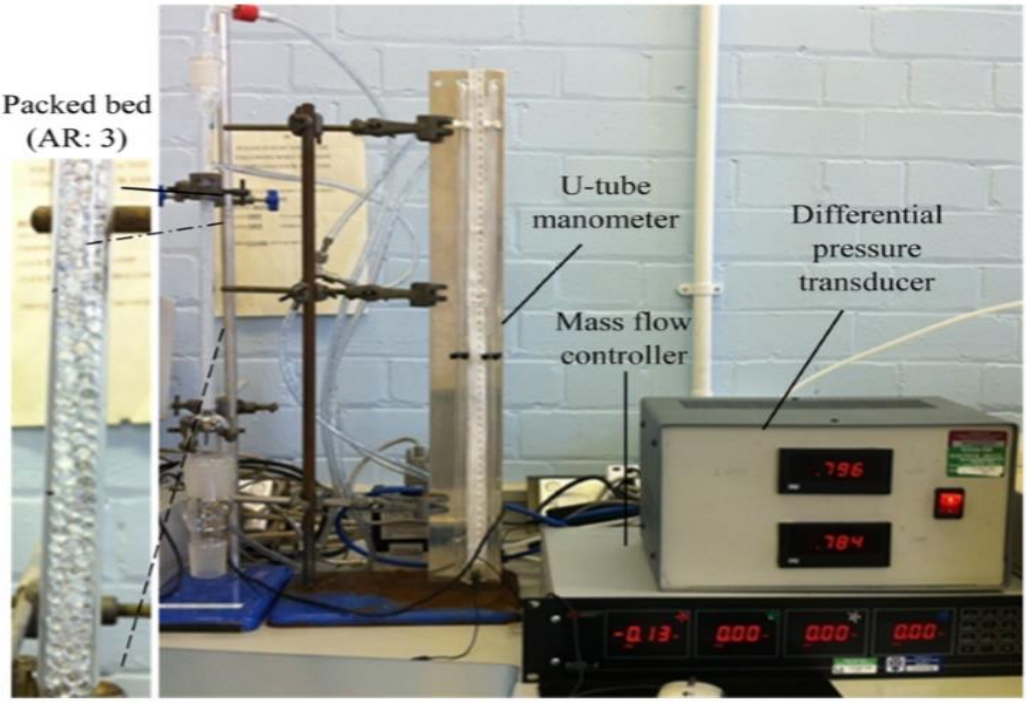

(b)

(c)

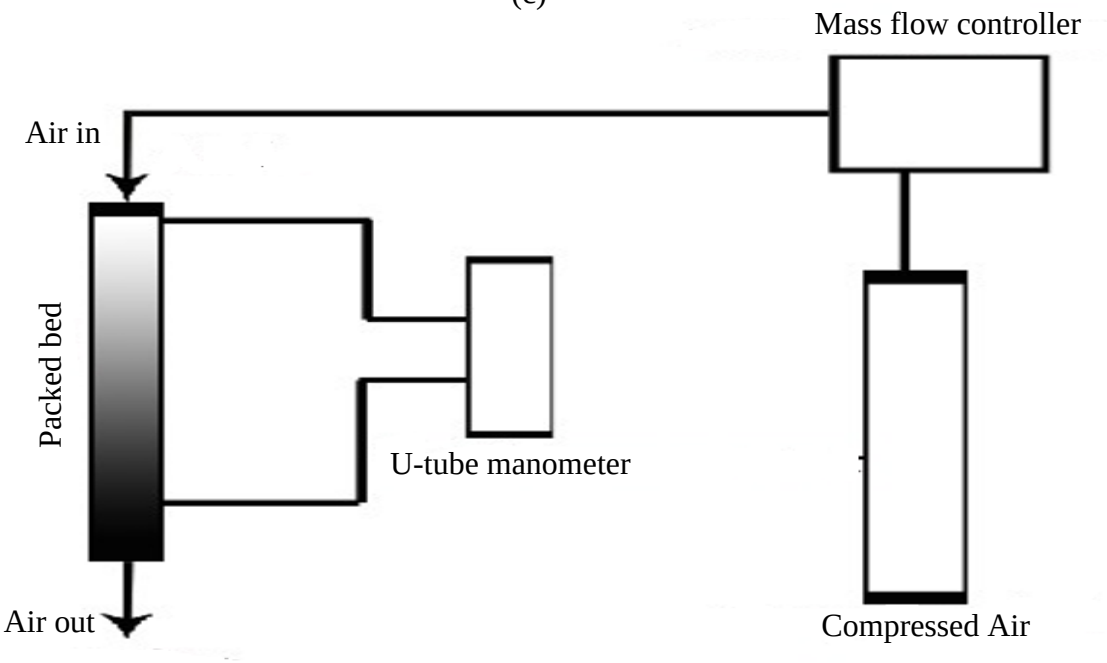

Figure 3.1. Experimental pressure drops setup [18, 86]

In order to get different aspect ratios, different particles sizes (d_p) were used (i.e., 6.66, 5, 4, 3.33, 2.85, 2.5, 2.22 and 2 mm). The packed bed was filled with one size of particles. Next, the mass flow controller was opened to the desired flow rate. Once stabilised, the monomeric reading was taken. To repeat the experiment, the mass flow controller was set to a zero value, and then, packing particles were removed to replace it by another size of particles and so on. Figure 3.2 shows some random arrangements of packing particles for different AR.

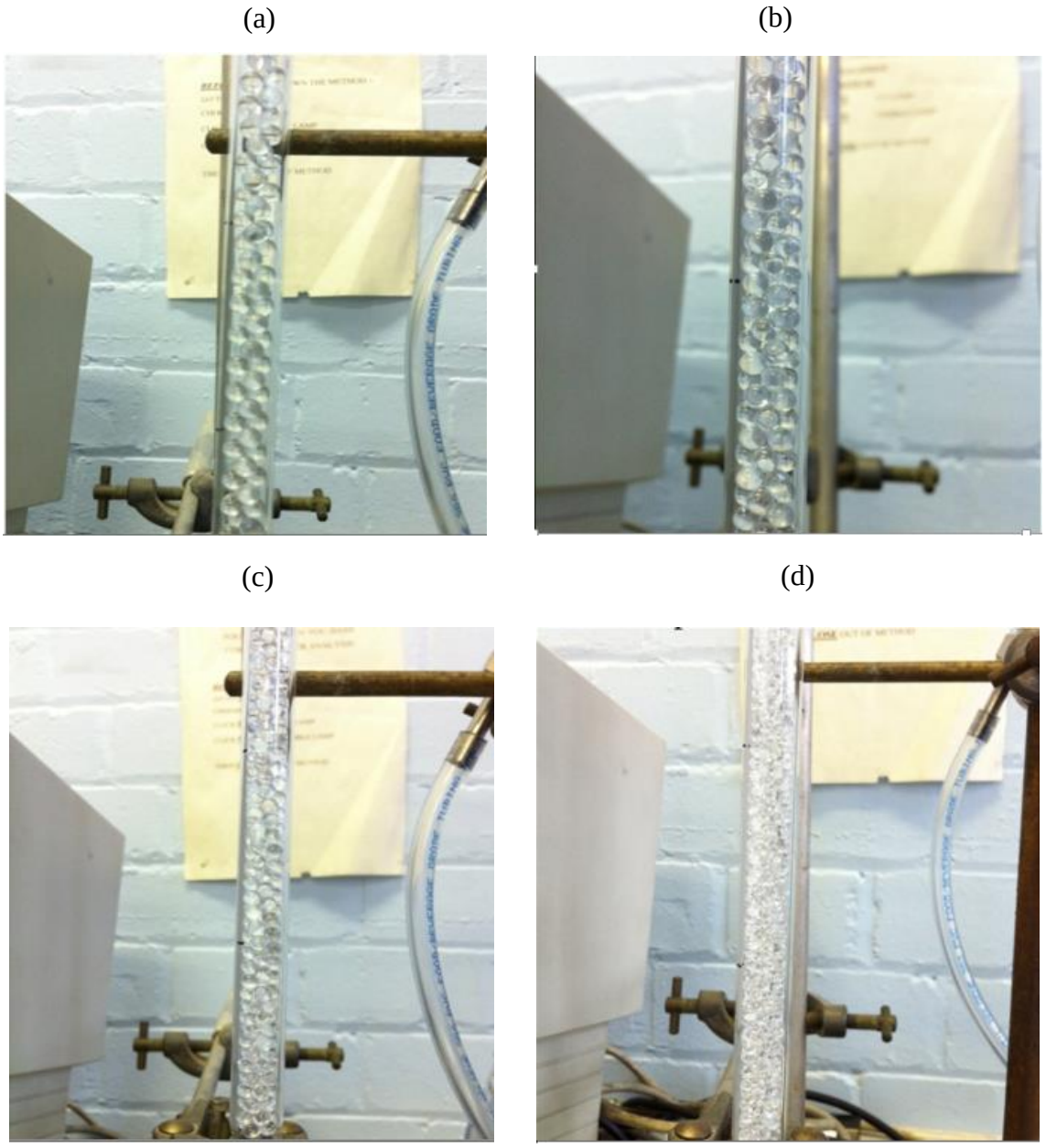

Figure 3.2. Random arrangements of various AR of the packed bed were built experimentally : (a) AR2 , (b) AR2.5 , (c) AR3.3 and (d) AR5 , for tube size =10 mm. [86]

3.2 CFD simulation part

3.2.1 Model development

CFD simulations of laminar flow, mass, heat transfer and reaction were carried out in a series of 3D tubes with ARs ranging from 1.5 to 5. A granular packing was built by DEM in order to construct a packing of densely spherical particles. The numerical sample is very similar to the experimental close-packed materials and its solid fraction can be adjusted by tuning friction or cohesion properties between particles. [120]

3.2.1.1 Packing generation by DEM

A granular packing of densely spherical particles was built by means of DEM in order to mimic experimental samples. The 3D DEM code was written in the built-in FISH programming language of particle flow code 3D (PFC^{3D}) and was used to generate realistic packing samples of random structures with ARs, as shown in Figure 3.3. The structure of the packing was function of properties of both the container and the particles, including the stiffness, the density and the friction coefficients between the particles or the particles and the confining wall. The compaction process was carried out until the maximum unbalanced contact force between particles reached a value of the order 10^{-7} N, resulting in a packing at static equilibrium. [18]

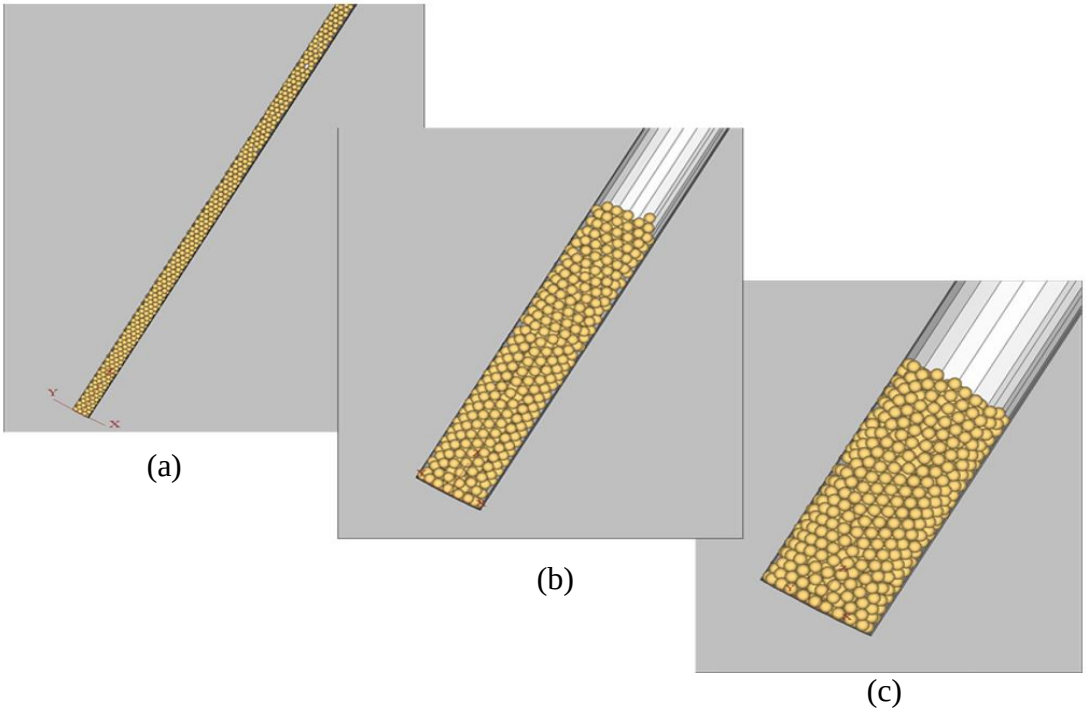

Figure 3.3. Three randomly generated packings by DEM (PFC^{3d}) for (a) AR: 3, (b) AR: 6 and (c) AR: 9

The stiffness coefficients of the wall and the particles were varied for maximum density of the packing. The overall setting parameters have been enlisted in Table 3.1 as below:

Table 3.1 Setting Parameters of DEM Based Modelling

	Wall parameters	Particle parameters
Normal stiffness coefficient	10^{13} N/m	2.5×10^{8} N/m
Tangential stiffness coefficient	10^{13} N/m	2.5×10^{8} N/m
Friction coefficient	0.2 (-)	0.2 (-)
Density	-	3900 kg/m^3

The packing geometry, which was defined by the 3D coordinates of particle centres, was then embedded into the commercial CFD package COMSOL Multiphysics 4.4 via 3D AutoCAD (Autodesk) processing. Then COMSOL Multiphysics 4.4 with interface function LiveLink™ for AutoCAD was able to import the packing and generate a 3D solid structure and of course is ready to use for simulation. In this case, allowing a dedicated meshing to take place by using a computer with 128 GB RAM.

Figure 3.4 summarizes all building steps of a random packed bed reactor for COMSOL modelling.

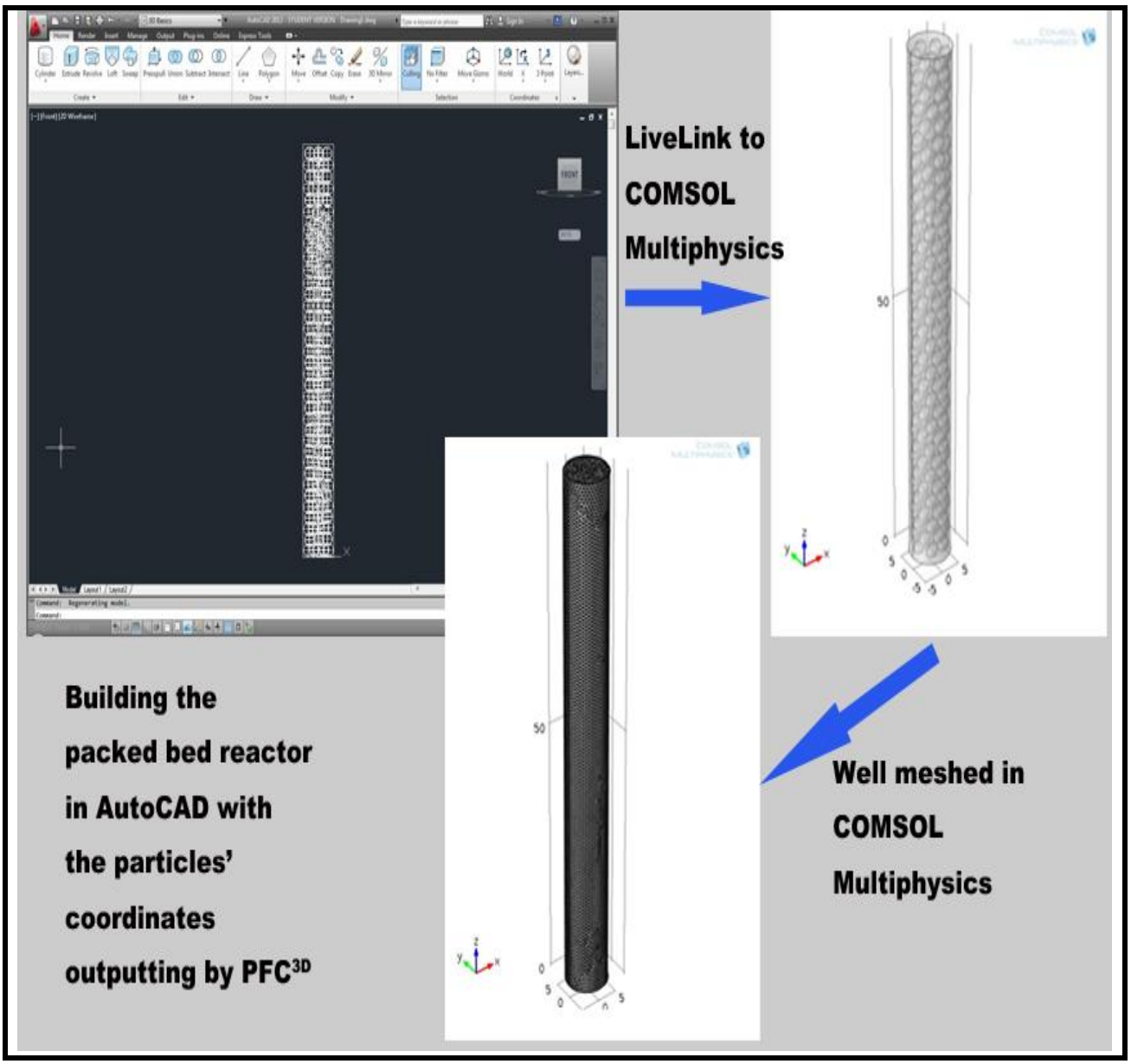

Figure 3.4. Building steps of a random packed bed reactor for COMSOL modelling (herein AR=3 as example)

The parameters of each generated packing are illustrated in Table 3.2 for various AR (all the models were built in unit of mm).

Table 3.2 Packing Parameter for different AR (mm)

Diameter of Tube D=10 mm			
Aspect Ratio (AR)	Diameter of particles d_p (mm)	Number of particles	Height of Packing (mm)
1.5	6.666	17	100
2	5.000	55	100
2.5	4.000	116	100
3	3.332	228	100
3.5	2.850	331	100
4	2.500	528	100
4.5	2.220	770	100
5	2.000	1075	100

3.2.1.2 Meshing modulation

One of the important steps during the modelling and simulation of phenomena using CFD codes after build the geometry is creation of mesh cells for the investigated zone. A well meshed model has a significant importance in CFD simulation. It is important to prepare a high-quality mesh for modelling. In fact, the mesh plays a very crucial role for the calculation of simulations and is therefore necessary to find an optimum balance between the number of cells and the hardware requirements for computing. [121] Also, the balance between accuracy, computation time and file size was considered in this work. This consideration will influence the user's choice of mesh which is specified in the geometry creation step.

The automatic meshing in COMSOL Multiphysics was the first choice, but sometimes and especially for large AR, some manually settings of meshes were required. Since the smaller the mesh is, the more accurate the data is. The ‘normal’ meshes were set at first for each simulation model, and then the mesh size was decreased while making sure that the output data keep the same quality until the meshes reach their lowest limits and this means (mesh-independent). In this step, any further refinement of the mesh quality will not yield any improved convergences in the model solution. However, although a more accurate result is obtained with a smaller mesh, this will require

increased computation times and much larger file size. Figure 3.5 shows images for two different sizes of meshes.

(a)

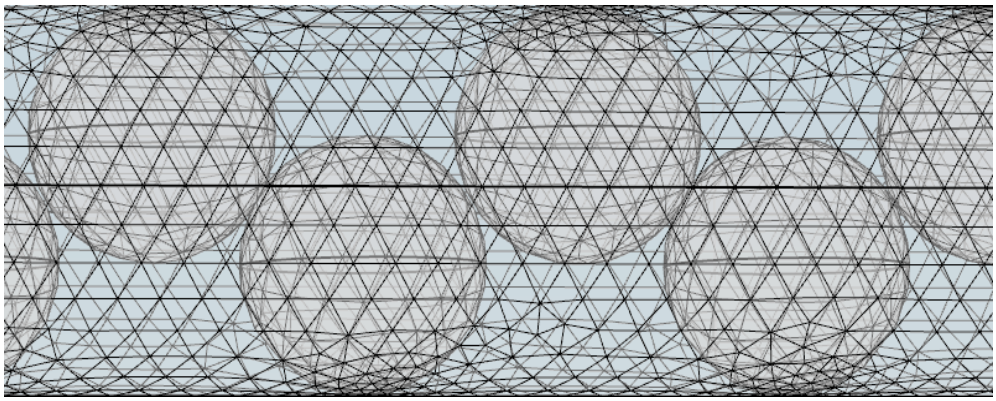

(b)

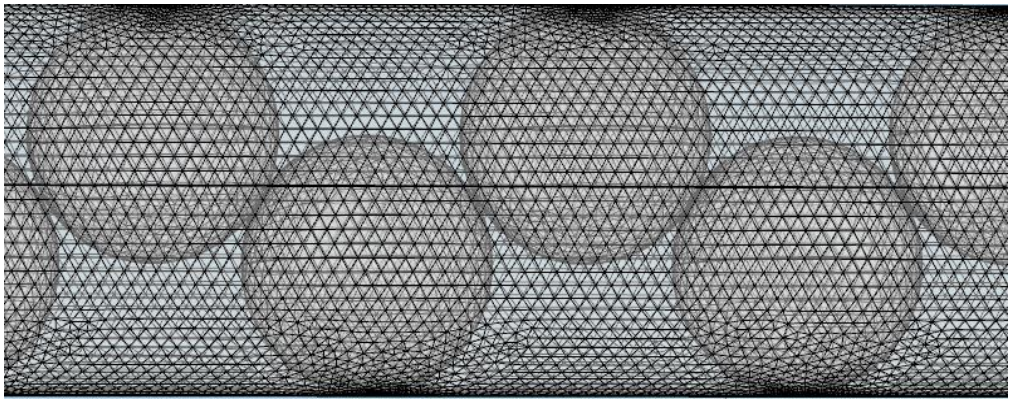

Figure 3.5. Different sizes of meshes applied for a random packed bed reactor by COMSOL,

(a) Large mesh and (b) small mesh for AR 1.5

Usually, CFD work in overall includes three steps which can be surmised as flow:

- **Pre-Processing:** Definition of the geometry of the region, flow parameters and the boundary conditions which need to be modelled.

- **Solver**: Once the problem is set-up and the boundary conditions defined, a solver software, for example, FLUENT, CFX, POLYFLOW or Comsol Multiphysics® will be using to solve the governing equations of the phenomena (flow, species transport, chemical reaction subject to the conditions provided) and suitable numerical methods will be used as a solver.

- **Post-processing:** it is the final step which is used to interpret, analysis the data and show the results in graphical and easy to read format by using various plots and tools. Figure 3.6 gives series of the steps that would be associated with analysis.

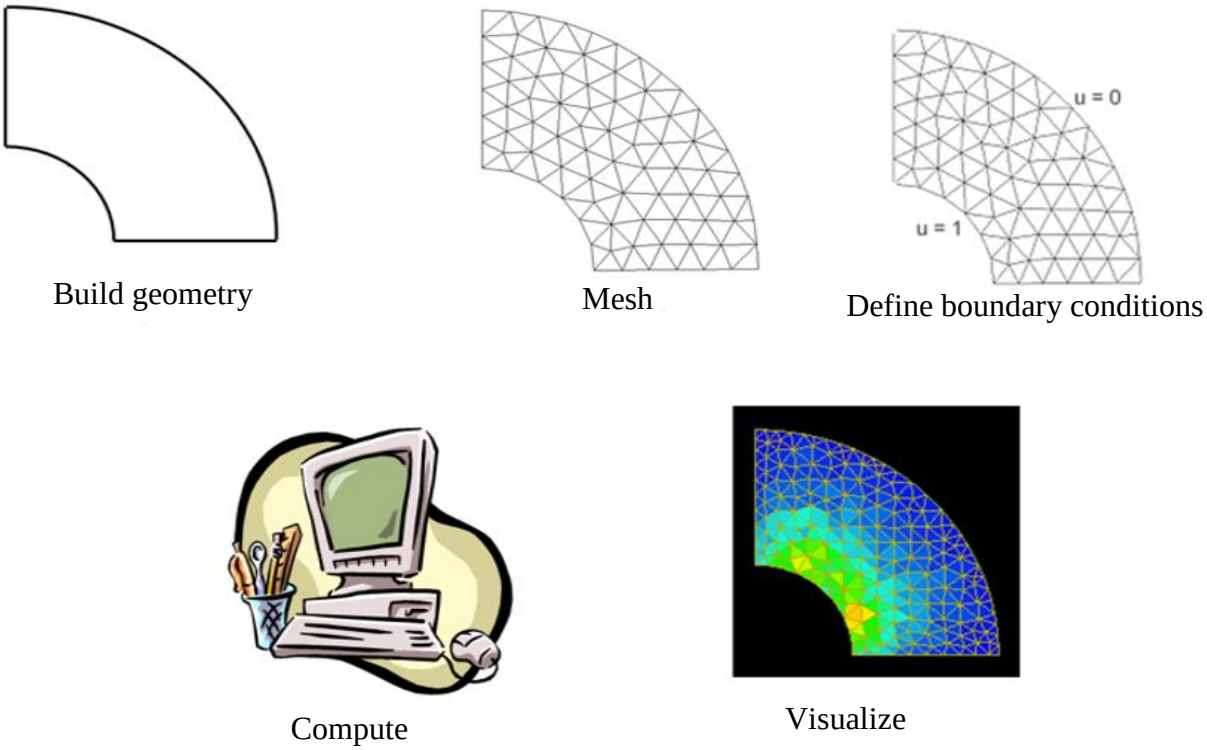

Figure 3.6. Calculation procedure of CFD modelling.

Chapter 4

4. Analysis of Fluid Flow

4.1 Introduction

Packed bed reactors (PBRs) as mentioned in literature survey (chapter 2) are used in many applications including, filtration, separation and purification units and etc. At low ARs, the behaviour of flow is complex because of strong interactions between fluid and packed particles, particles and column wall, and fluid and column wall. Especially for small AR where the in-homogeneities become dominant, resulting in significant wall impacts, local flows, axial and radial variations. This will influence on the results of different microscopic and macroscopic flow behaviours along the packed bed. In spite of interesting developments in applications of structured packings these years, the randomly one is still the state-of-the art reactor type in these fields. [3]

CFD simulations are proven to be useful for identification of the drawbacks of simplified semi-empirical modelling approaches and for their further improvement by developing better empirical correlations. The developed CFD based approach provided knowledge that often is difficult to obtain experimentally and could contribute to improving the design of low AR packed beds. In this chapter, DEM, which was coupled to CFD model of flow field in low AR packed bed is described. Realistic random packing was generated for a spherical particle by DEM as shown in chapter 3. Also, particle and mesh generations are reviewed (see chapter 3) and followed by porosity analysis of the generated packed beds and computation of the Navier–Stokes equations by collocated finite volumes.

Moreover, 3D modelling is used to visualize the fluid flow and spatial distributions of species in gas−solid packed beds of randomly distributed particles, subject to wall effects. The approach is extended to packed beds of ARs ranging from 1.5 to 5 and to flow regime ranging from laminar to transitional flow limits (Re ∼ 400). The results of experimental tests are used to validate 3D computer fluid dynamics (CFD) modelling. The work plan here includes the following steps: (1) generation by DEM of representative bed geometries and comparison of the bed structure properties such as average porosity and spatial distribution of porosity with literature models; (2) observation of pressure drops and local velocity distributions and comparison with 3D modelling as well as

relevant 2D literature models; and (3) observation of mass dispersion by CFD modelling and comparison with those obtained by 2D modelling and literature models.

4.2 DEM and CFD (Brief review)

As mentioned in previous section, DEM is an explicit numerical scheme which simulates the dynamic and static behaviour of assemblies of particles based on contact mechanics. A soft particle model was used to simulate the particle contact behaviour. The packing was generated by dropping spheres from a specified height into a tube. The launch position of the spheres at the specified height was randomly assigned in the tube to mimic the real filling procedure of the tube with particles. The commercial DEM software package PFC^{3D} by ITASCA was used. Once the packing structure of the packed bed was predicted with DEM, it was then exported to the CFD package. The structure of the packing in the tube changes locally based on geometry and the way the particles interact during the filling process. In addition to the geometric effects, the friction parameters also influence the packing. For the DEM simulation, the particle-particle friction as well as the particle-wall friction were considered. The visual observation of the DEM packing of AR of 3 (Figure 4.1, left) seems to show more void space at pore scale near the wall compared with the experimental packing (Figure 4.1, right) and this result was observed with all generated packing demonstrating a general loose structure of generated packings.

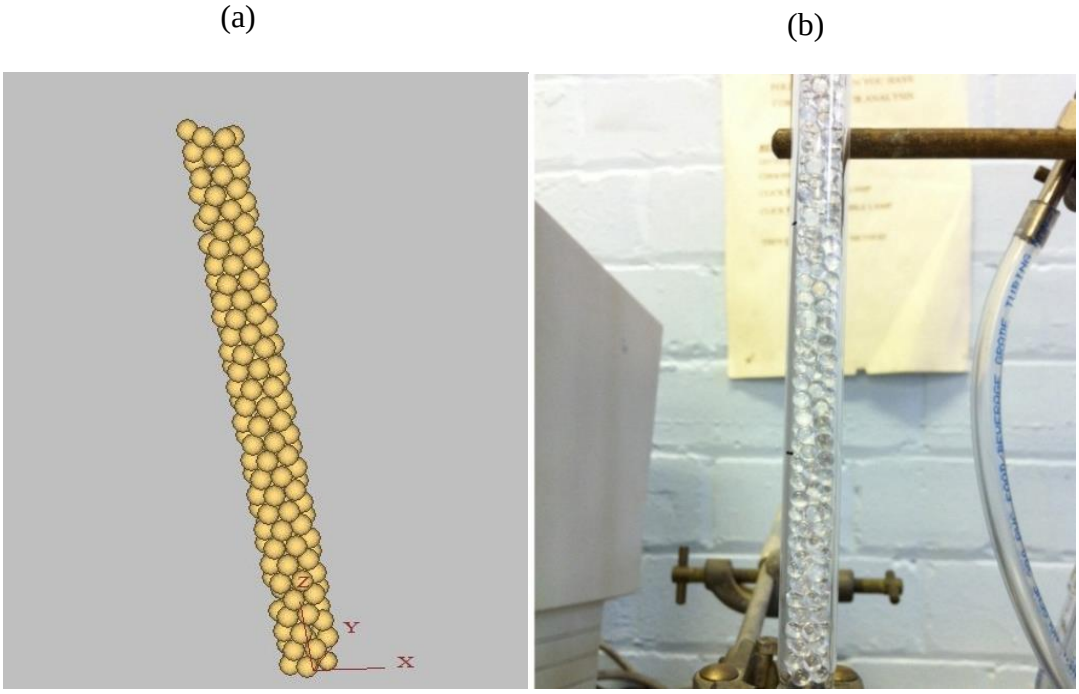

Figure 4.1. Comparison of the packing: (a) by DEM and (b) by experimental, for AR 3

4.3 Description of 3D Fluid flow model

The model of a laminar gas (air) flow in a 3D porous media is governed by both the mass conservation (equation 11) and the Navier−Stokes momentum (equation 12), where the inertial forces include both the pressure forces and viscous forces (the stress−strain tensor for a Newtonian fluid).

$$\rho \nabla . u = 0 \qquad (11)$$

$$\rho(u.\nabla u) = -\nabla p I + \nabla.\left[\mu(\nabla u) + (\nabla u)^T - \frac{2}{3}\mu(\nabla . u)I\right] \qquad (12)$$

In order to solve a system of differential equations, initial and boundary conditions must be given. The outlet boundary conditions are clearly harder to estimate. For instance, the velocity can be defined by an outlet pressure, because of the connection of velocity and pressure in the continuity and Navier-Stokes equation.

In our work, the inlet boundary was a fixed velocity inlet condition; this was spatially uniform over the inlet (equation 12a). At the outlet, a constant atmospheric pressure (p_0) boundary condition (equation 12b) was used. In addition, no slip conditions were assumed at wall−fluid and particle−fluid interphases.

$$u = -u_{in}\mathrm{n} = 0 \qquad (12a)$$

$$p = p_0, \qquad [\mu(\nabla u) + (\nabla u)^T - \frac{2}{3}\mu(\nabla . u)I]\mathrm{n} = 0 \qquad (12b)$$

In these equations, μ is the dynamic viscosity (kg $m^{-1}s^{-1}$), ρ is the fluid mass density (kg m^{-3}) , u is velocity (m s^{-1}), I denote the identity matrix, p is the pressure (Pa) and T is the absolute temperature (K).

The stationary solver of the Comsol package with default settings was used. The governing equations (11) and (12) were solved using the finite volume approach. The domain of interest between the solid particles was divided into numerous cells where the governing equations were integrated across the volume of each cell. The integrals converted the governing equations into a set of difference equations which were solved numerically using the generalized minimal residual method solver (GMRES) with the "Geometric Multigrid" pre-conditioner. The GMRES algorithm is an iterative method for the numerical solution of a non-symmetric system of linear equations. The method approximates the solution by the vector in a Krylov subspace with minimal residual. Trial studies with a variety of solvers (FGMRES, conjugate gradient, BiCgStab) indicated that, in these particular cases, the simulation result was fairly insensitive to the exact one. The convergence was evaluated based on relative tolerance, which was set to 0.0001.

The discretization was carried out by the built-in meshing module of Comsol using the Adaptative Mesh Refinement Method, which generated predominantly tetrahedral domain elements and triangular surfaces. The effects of the size of these elements on the viscous forces, particularly in areas where potential skewed meshes could be generated such as particle contact points, were investigated. This was ensured by a mesh convergence check for each packed bed by increasing the number of mesh elements and monitoring the pressure values at three arbitrary locations from the CFD simulation. It was observed that the packed beds of high AR required more refined meshing than the low AR to reach approximately stable values of pressure. This result was subsequently confirmed by using the Grid Convergence Index (GCI) to ensure if the results are independent of mesh size. This method was developed by Celik et al., (2008) as shown below. [122]

First the representative grid size h procedure is defined as:

$$h = \left(\frac{1}{N} \sum_{i=1}^{N} \Delta V_i \right)^{1/3} \qquad (13)$$

Where, ΔV is the cell volume and N is the number of cells. Three significantly different set refinement of grids were used, the grid refinement factor $r = h_{\text{coarse}} / h_{\text{fine}}$ is higher than 1.3. The apparent order m of the method is defined by equations 14 to 16:

$$m = \left| \ln\left|\Theta_{32}/\Theta_{21}\right| + q(m) \right| / \ln(r_{21}) \quad (14)$$

$$q(m) = \ln\left(\frac{r_{21}^{m} - s}{r_{32}^{m} - s} \right) \quad (15)$$

$$s = 1.\mathrm{sgn}\left(\Theta_{32}/\Theta_{21}\right) \quad (16)$$

Where, $h_1 < h_2 < h_3$, $r_{21} = h_2/h_1$, $r_{32} = h_3/h_2$, $\Theta_{32} = P_3 - P_2$, and $\Theta_{21} = P_2 - P_1$. P_k (k = 1, 2, 3) expresses the pressure values taken at three arbitrary grid locations in the packed bed, and also, sgn is the function signum. [122]

Equation (15) should be solved numerically for, m. This is then used to find the extrapolated value for the pressure (equation 17), the relative error (equation 18), and the fine grid convergence GCI (equation 19).

$$P_{ext}^{21} = \frac{r_{21}^{m} P_1 - P_2}{r_{21}^{m} - 1} \quad (17)$$

$$e_a^{21} = \frac{P_1 - P_2}{P_1} \quad (18)$$

$$GCI = \frac{1.25 e_a^{21}}{r_{21}^{m} - 1} \quad (19)$$

The GCI reached values below 2%, validating the reasons to trust the accuracy of the present numerical simulations and to ensure that the solution is independent of the mesh size. In addition, the quality of the mesh was analysed by the minimum element quality statistics method, which expresses the contribution of the skewed elements. The spherical particles in the packed bed were expected to release skewed elements, which were extensively reported in the literature.

These dealt with such elements by increase or decrease of particle sizes as well as using the range of features available in commercial CFD to smooth these skewed elements. Herein, the diameter size of particles was reduced by 1% in all our tests. Such shrinkage was found necessary to prevent highly skewed meshes at single-point contacts between particles while maintaining a reasonable computation time. [13 and 100−102] A shrinkage higher than this value would yield no advantage in producing more accurate results and would be computationally more expensive.

4.4 Fluid flow profiles by 3D modelling

4.4.1 Structural porosity profiles

It should be noted that the trends of packed bed porosity have been generally analysed by two methods. The first, which was followed by early studies, relied on experimental data of packing structures and where much attention was paid to the wall effects and periodic variation of porosity away from the containing wall. [123 and 124] The second used computer-generated packing through a variety of computational algorithms. [124 and 125] Both computer-generated or hand-built packing relied on models which use a two-point correlation function of sphere centres and the tessellation of the void space distribution of the interparticle interstices using a number of schemes such as tetrahedral , Dirichlet or Voronoi types. [60 and 126-131]

Although the tessellation permitted some statistical description of pores and interstices, it was unable to give a complete analysis which relies on the overall geometry of the individual pores. In contrast, direct analysis of the void space itself is possible via image analysis techniques, which take as input the 3D tomographic or 3D visualization data. [97] Compared with 2D images, the 3D visualization of the pore space allowed access to the 3D topology of the pore space (e.g., the connectivity of local elements) with similar resolution in each dimension.

These structural characteristics determined the velocity, pressure drop and mass transfer characteristics of the bed. Of course, the same information can be obtained by recording a succession of 2D slice sections for which the slice thickness is equal to or better than the in-slice resolution, and then reconstructing the 3D structure. It is the direct analysis via 3D visualization data that was followed in this work.

The procedure used available data in the 3D matrix that defines coordinates of particles inside the packed bed. For instance, Figure 4.1 illustrates generated packing arrangements for AR of 3 by DEM and experimental data. The porosity profiles of packed beds of different ARs were calculated by using the data of various spatial domains, which were denoted as “Domain Index (DI)” in COMSOL software. Domain index (DI) is a single integer number and was allocated to mesh boundaries of a single domain area (solid particle or between particles), allowing access to porosity distribution at any 3D coordinate with a spatial resolution at mesh size limits. Just like the distribution shown in Figure 4.2 (a), the cylinder container of the packed bed of 100 mm length was cut into 100 slices, allowing a spatial resolution along the axial direction.

A sample of DI data accessible for a single slice is shown in Figure 4.2 (b). It is interesting to see that the distribution of accessible DI data is not uniform, as it follows mesh distribution (i.e., dense data at particle contact points). The exported data files were then processed for the porosity distribution of the packed bed by developing a Matlab code for the procedure illustrated in Figure 4.2 (c).

(a) (b)

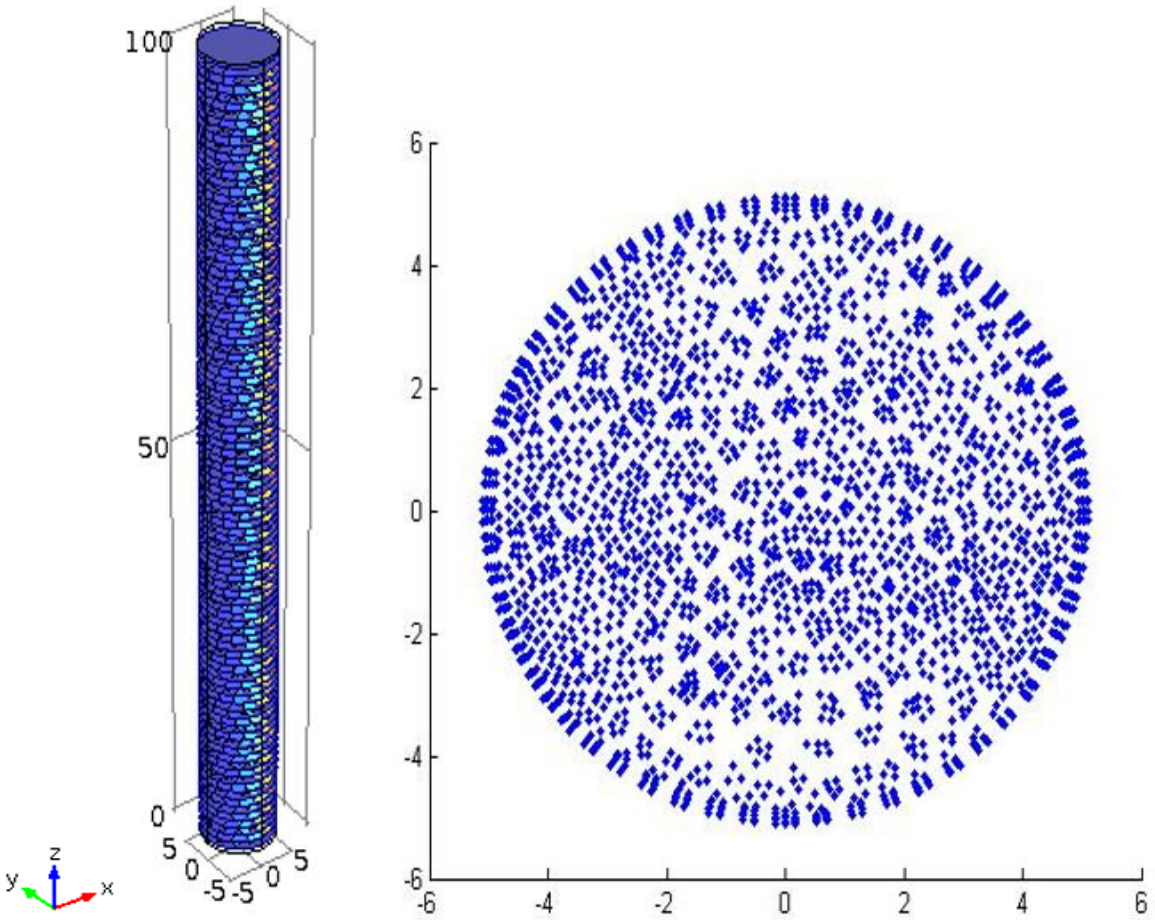

(c)

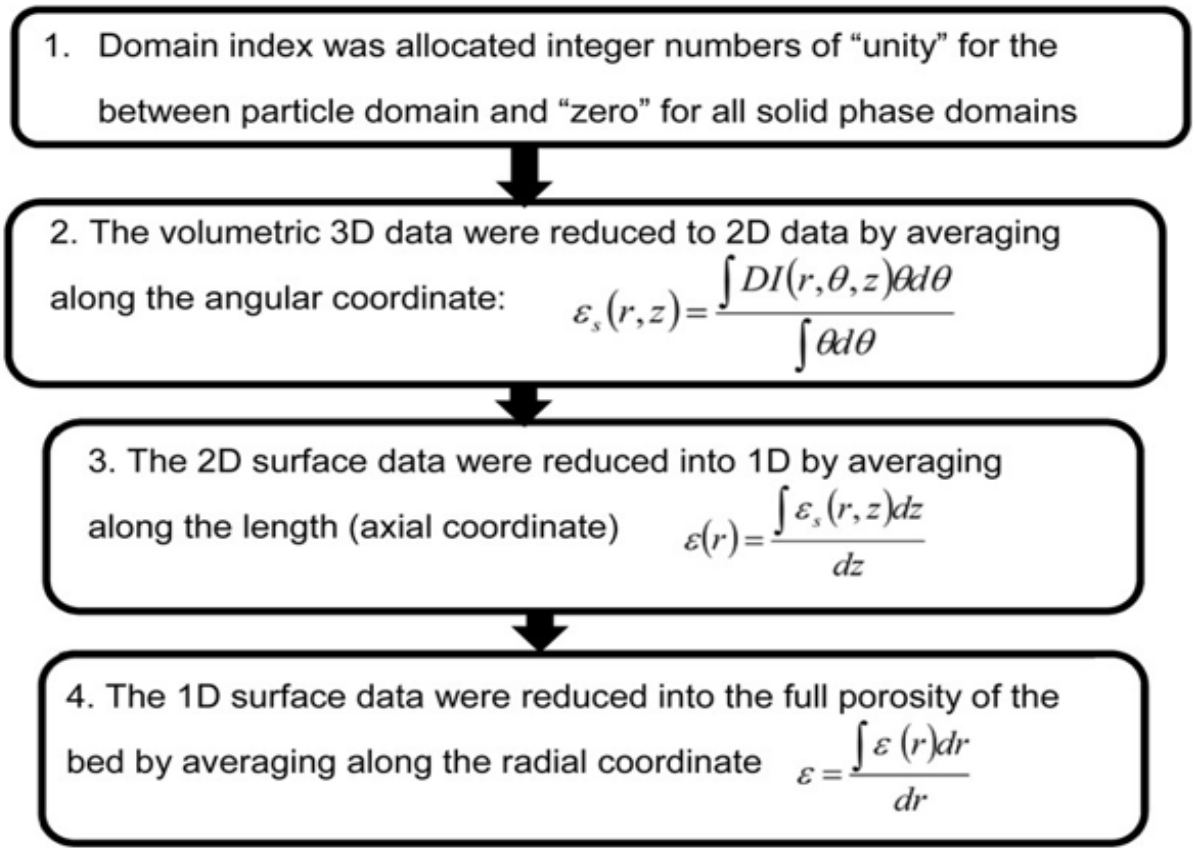

Figure 4.2. Reduction procedure of volumetric 3D domain index data. (a) Cross-sectional slicing of domain index, (b) irregular distribution of domain index data retrieved, and (c) averaging procedure from 3D domain index to 2D and to 1D data. [18]

First, the domain index of the area between the particles was considered fully porous with an integer number of unity, and the remaining domain indexes that belong to solid particles were considered nonporous with an integer number of zero (step 1 in Figure 4.2 (c)). The 3D DI data were angularly averaged into 2D data, where the angular weight of accessible DI data was taken into account (step 2 in Figure 4.2 (c)).

The released 2D data represent the surface fraction (ε_s) nonoccupied by the solid particles if the packed bed was represented by a 2D configuration. The surface fraction (ε_s) was subsequently

reduced into the “1D” axially averaged porosity (step 3 in Figure 4.2 (c)) and the global or averaged porosity of the full packed bed (step 4 in Figure 4.2 (c)).

Table 4.1 illustrates the averaged porosity data obtained in the present simulation for various aspect ratios (ARs). A comparison with a model from Zou et al., (1995) shows a good agreement, particularly for low AR. [97] With the exception of AR of 2, the loose structure of generated packing by shrinking the particles by 1% was well observed and it increased to a large AR. More insights into the loose structure have been shown in the 2D maps of the circumferentially averaged DI data in Figure 4.3.

Table 4.1 Porosity trends for ARs from 1.5 to 5

Aspect Ratio D/d_p	Porosity (ε)	Porosity (ε) by Zou et al [97]	Deviation (%)
1.5	0.688	0.658	4.360465
2	0.575	0.578	0.521739
2.5	0.530	0.522	1.509434
3	0.528	0.517	2.083333
3.5	0.572	0.539	5.769231
4	0.547	0.532	2.74223
4.5	0.525	0.496	5.52381
5	0.498	0.473	5.02008

The loose structure along the axial coordinate is confirmed along the axial coordinate of the packed bed for various ARs. The surface fraction of empty space ε_s of a selected location of the packed bed could be larger or smaller than the entire corresponding bed, depending on where the location was selected and how many particles were included in the selected location.

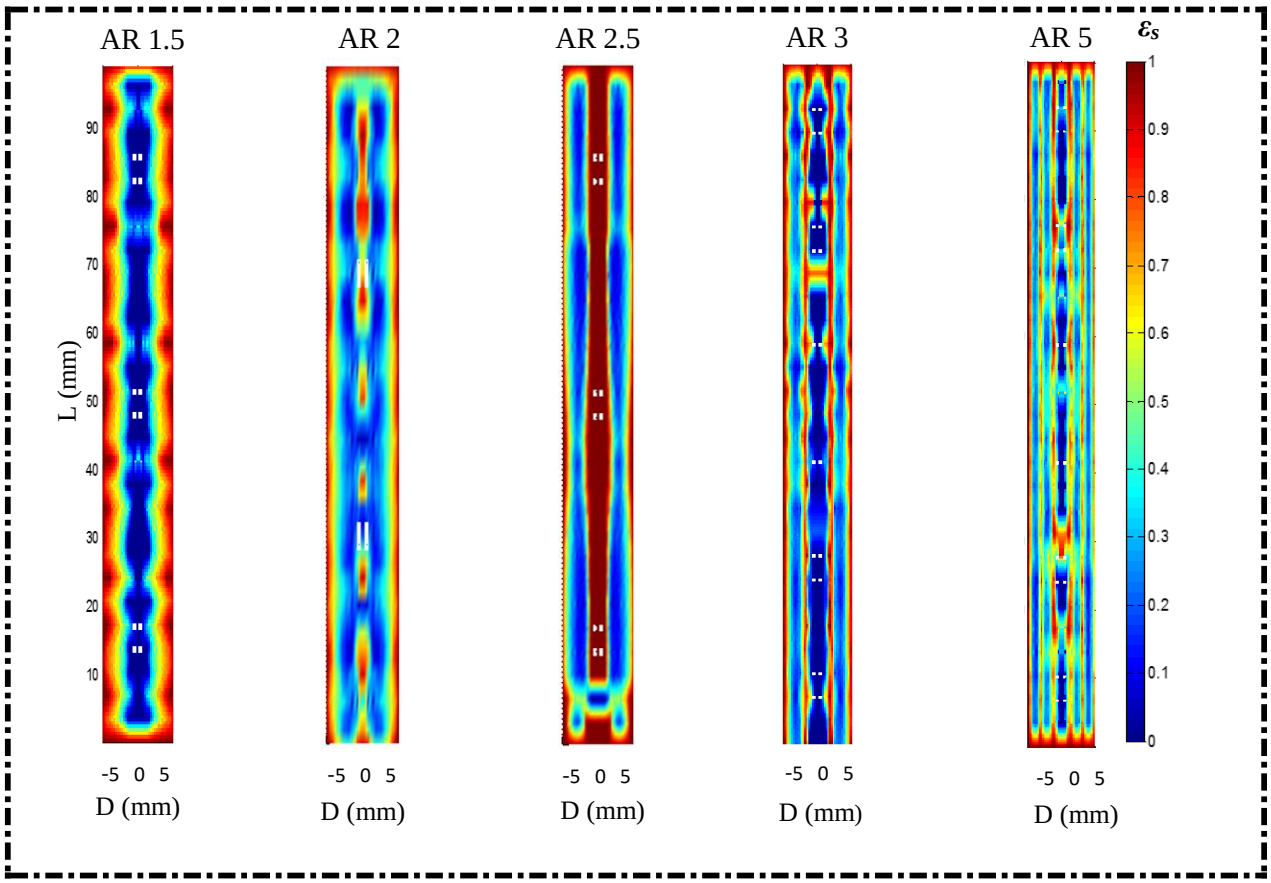

Figure 4.3. Spatial distribution of surface fraction ε_s of the solid particles for packed beds of ARs from 1.5 to 5. [18]

Moreover, Figure 4.3 shows ε_s of the selected locations and how it deviated from the entire packed bed porosity in Table 4.1 when the numbers of particles in the segments varied. It is interesting to see the periodic variations of ε_s for all AR arrangements, corresponding to the layer changes in the packing.

The deviations suffered from a jump every time additional particles constituted a new layer of packing and then decreased as more particles were added to the same layer. For high AR, the particle number further increased. The local porosity could be either larger or smaller than the entire bed, but the deviation was relatively small. The larger the AR was, the more particles were needed to reach this low-level deviation of packing porosity. This is because sufficient layers were required to represent the entire packed bed, and a packing with a larger AR contains more particles per layer. Such cyclic changes of the porosity of the height of the bed could be reflected by cyclic variations of interstitial flow velocity and mass dispersions.

Taking the axially averaged porosity for these figures, which represents the distribution of porosity along the radial coordinate within the packing system, was the next step to compare simulation results with the semi-analytical model of the radial porosity distribution by Mueller et al., (2010) as shown in Figure 4.4. [104] Similar oscillation trends with damping profiles toward the centre of the packed beds were observed. The discrepancies in regions toward the centre confirm the loose structure of the generated packing. On the other hand, the radial distribution of porosity obtained was in a good agreement with the model of Mueller, especially close to the wall, while the porosity increased at low AR due to high porosity near the wall in packed beds. Such property distribution of porosity impacts the flow dynamics and mass transfer, as described in the following sections.

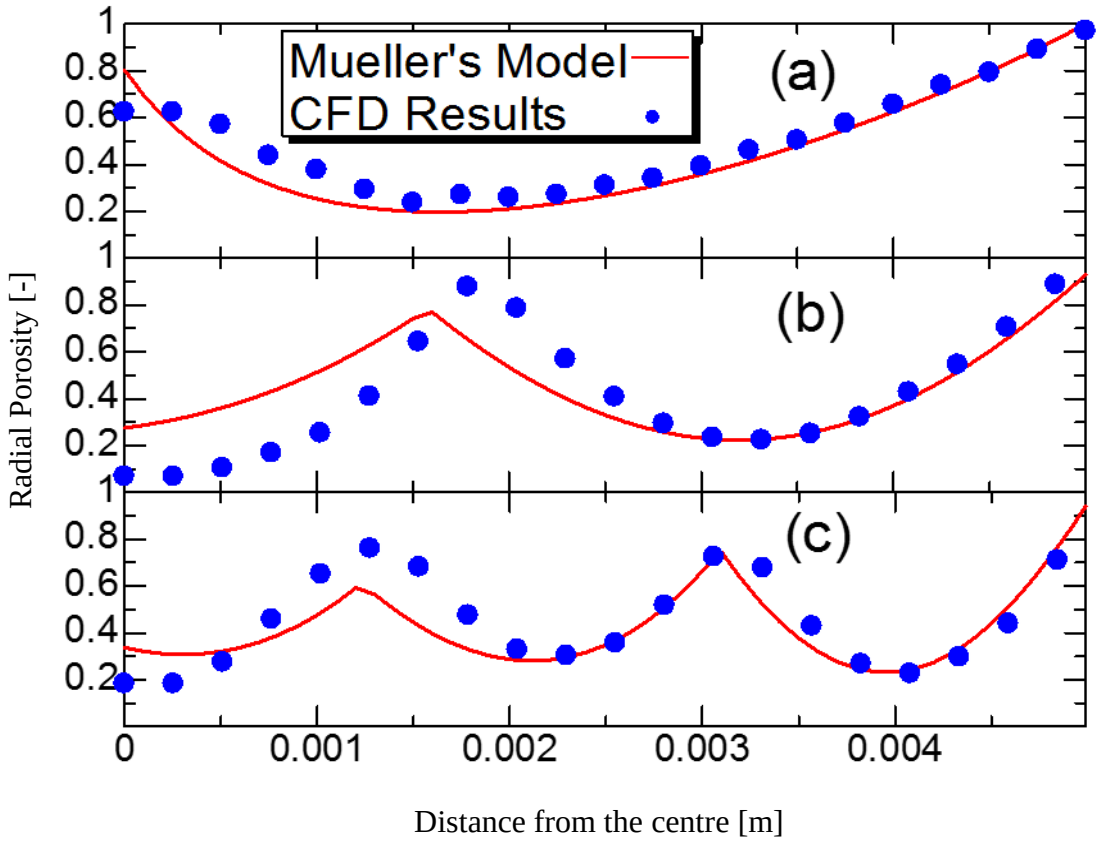

Figure 4.4. Averaged porosity variation along the radial coordinates at (a) AR: 2, (b) AR: 3, and (c) AR: 5. (Dots: simulation data; lines: Mueller's model. [104])

4.4.2 Pressure drop profiles

Among well-established models, Carman (1997), Ergun (1953), Zhavoronkov et al., (1949) and Reichelt (1972) are often cited in the literature to estimate pressure drops in low AR packed beds. [106, 96,132 and 133] Ergun proposed a semi-empirical correlation (equation 20) by linking the Kozeny–Carman equation for the creeping flow regime and the Burke–Plummer equation for the turbulent regime.

- Ergun's correlation accounts for viscous and inertial energy losses and relates them to the dynamic variable, the velocity of the fluid, as well as the structure of the bed, as characterized by the bed average porosity, ε. The dimensionless pressure drop, ψ is expressed by equation (20).

$$\psi = \frac{150(1-\varepsilon)^2}{Re_{dp}\varepsilon^3} + 1.75\frac{1-\varepsilon}{\varepsilon^3} \qquad (20)$$

Where,

$$\psi = \frac{\Delta p}{L}\frac{dp}{\rho u} \qquad (20\ a)$$

The above equation holds for the case of large AR (AR > 15), where the condition of near uniformity prevails in the porosity throughout the bed.

- The Carman model, as shown by equation (21), predicts well pressure drop at large AR and therefore can be used as reference model to estimate pressure drop deviations at low AR.

$$\psi = \frac{6^{3-n}k}{Re_{dp}^{2-n}}\frac{(1-\varepsilon)^{3-n}}{\varepsilon^3} \quad (21)$$

Where, n=1 and k=5

- The Zhavoronkov equations is illustrated by equation (22):

$$\psi = \frac{165.35A_w}{Re_{dp}}\frac{(1-\varepsilon)^2}{\varepsilon^3} + 1.2B_w\frac{1-\varepsilon}{\varepsilon^3} \qquad (22)$$

Where,

$$A_w = B_w = 1 + \frac{1}{2\left(\frac{D}{dp}\right)(1-\varepsilon)} \qquad (22a)$$

- The Reichelt model is illustrated by equation (23):

$$\psi = \frac{154A_w^2}{Re_{d_p}}\frac{(1-\varepsilon)^2}{\varepsilon^3} + \frac{A_w}{B_w}\frac{1-\varepsilon}{\varepsilon^3} \qquad (23)$$

With the wall correction terms,

$$A_w = 1 + \frac{2}{3\left(\frac{D}{d_p}\right)(1-\varepsilon)} \qquad (23a)$$

$$B_w = \left[1.15\left(\frac{d_p}{D}\right)^2 + 0.87\right]^2 \qquad (23b)$$

Where, A_w and B_w are model constants, d_p is particle size (m) and D is the tube diameter (m).

The last two models of Zhavoronkov and Reichelt are based on extensive experimental data where Ergun's constants are corrected by considering wall effects.

Also, the Particle Reynolds number (Re) can be calculated as below:

$$Re = \frac{\rho u d_p}{\mu} \qquad (24)$$

Where, ρ = fluid density (kg m^{-3})

u = velocity in flow field (m s^{-1})

d_p = particle's diameter (m)

μ = fluid dynamic viscosity (kg $m^{-1}s^{-1}$)

The pressure drops, in terms of dimensionless pressure drop ψ , in packed beds of ARs of 1.5 and 5 at different values of Re were compared with established models of Carman, Ergun, Zhavoronkov, and Reichelt as shown in Figure 4.5. The results of pressure drops by CFD simulation fit the models predicted by Zhavoronkov, Reichelt, and Ergun well at high Reynolds numbers, but showed disagreements with the Carman model, which is suitable for packed beds of large AR.

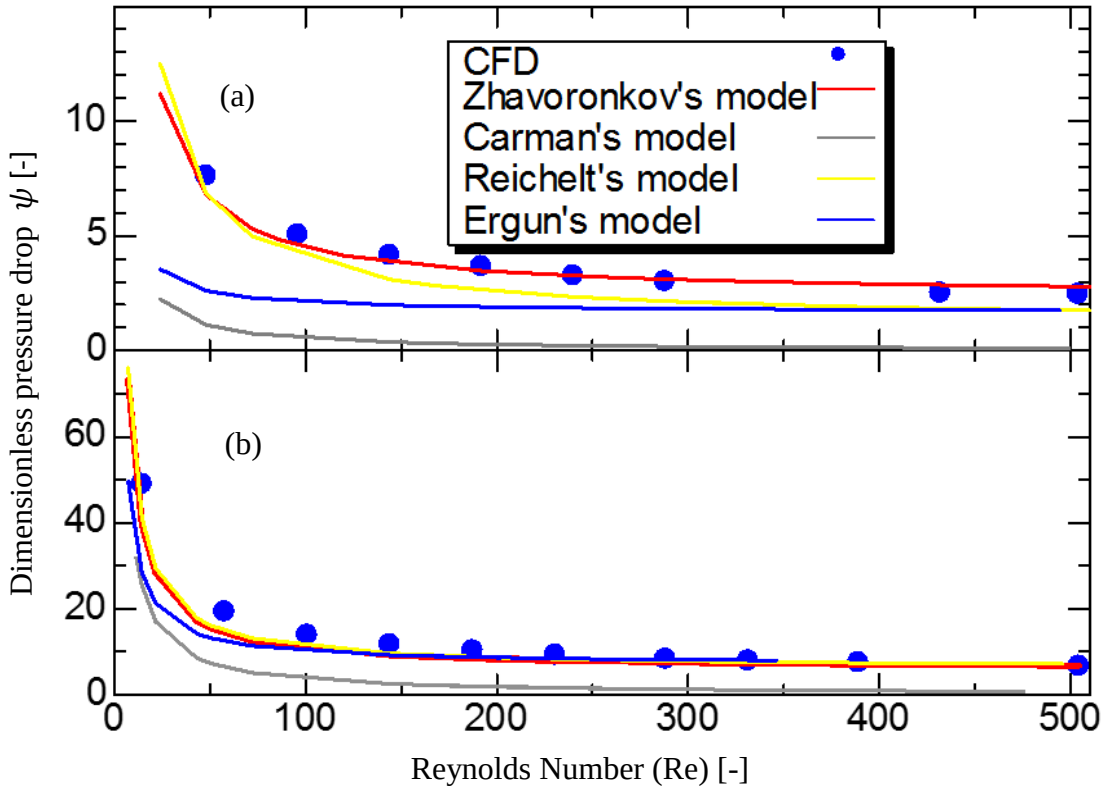

Figure 4.5. Pressure drop profiles for (a) AR: 1.5 and (b) AR: 5; dot: CFD simulation. [18]

The pressure drops are as well represented in terms of pressure drops ratios, ψ / ψ_{inf}, in order to account for the effect of the wall for low AR values. ψ_{inf} is the dimensionless pressure drop for an infinite AR. The simulation results, as the effect of AR of packed beds on pressure drops at laminar and transitional flows, are shown in Figure 4.6 (a) and were validated using experimental data and literature models, as shown in Figures 4.6 (b1−b4), respectively.

An increase of pressure drop ratios at low AR packed beds was observed at AR less than 3, while those obtained by the Carman and Ergun models were not sensitive to AR values. The simulation results fit the Reichelt model better, and the decrease in the pressure drops at AR lower than 3 was

interpreted by Eisfeld and Schnitzlein (2001) by two counteracting effects of the wall: one to offer additional resistance due to wall friction (this effect will be less at Re > 200) and the other positive effect, which represents reducing the pressure drop with Reynolds number due to increased porosity in the vicinity of the wall. [110]

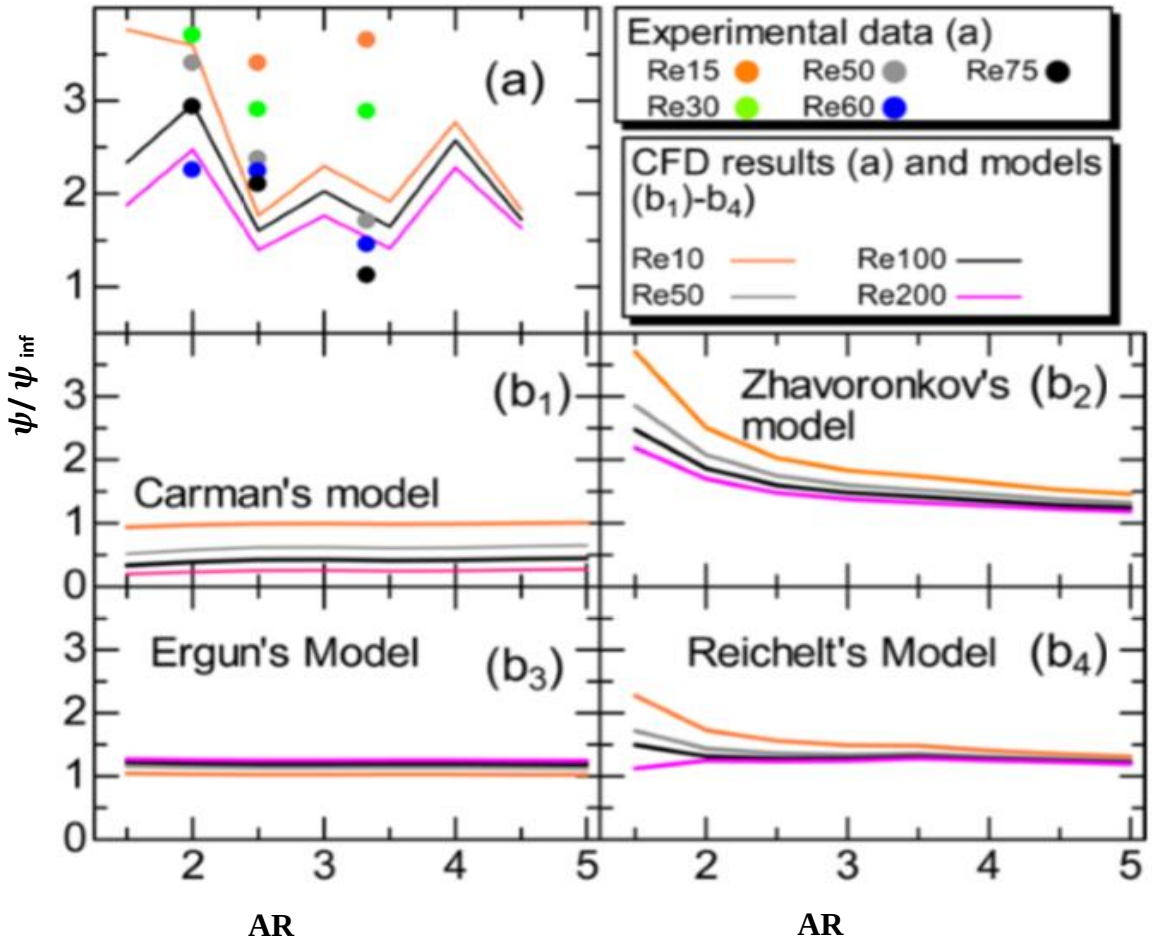

Figure 4.6. Ratio of pressure drop to pressure drop of infinite packing profiles, (a) simulation, and experimental data, and (b1−b4) Carman, Zhavoronkov, Ergun, and Reichelt models. [18]

In order to ascertain this important finding of the decrease of the wall effect at AR lower than 3, the fluid flow in a 2D porous medium of packed map of circumferentially averaged porosity in Figure 4.3 was carried out. The fluid flow model was computed from a 2D Brinkman− Forchheimer model that accounts for porosity changes along the radial coordinate of the packing. [134 and135]

$$\nabla u = 0 \qquad (25)$$

$$\nabla \varepsilon \rho u u = -\varepsilon \nabla P + \varepsilon \mu \nabla^2 u + \varepsilon F \qquad (26)$$

The drag force per unit of volume F is expressed using Ergun's relation as:

$$F = -\frac{\mu u}{K} - \beta \rho u^2 \qquad (26\ a)$$

The permeability of the porous media K and the non-Darcy term β are calculated from Zhavoronkov's model.

$$K = \frac{\varepsilon^3 dp^2}{A(1-\varepsilon)^2},\ \beta = \frac{B(1-\varepsilon)}{\varepsilon^2 dp} \qquad (26\ b)$$

The porosity distribution map for the 2D model was obtained by interpolation with a spline function, allowing access to data which were not visualized by the 3D non-transparent arrangement. As expected, in Figure 4.3, the results clearly showed more porosity distribution in the centre of the packed bed for even numbers of AR values such as (AR 2) and less porosity distribution for uneven numbers of AR (i.e., 3 and 5).

Between consecutive even and odd numbers of AR, the trends were found, however, nonlinear for AR less than 3, shown by AR of 2.5. For this value of AR, the porosity distribution shifted toward the AR value of 2, allowing more flow in the centre of the packed bed than AR values of 2, 3, or 5.

The wall effect and subsequent porosity distribution along the radial direction thus took place progressively as the porosity increased in the vicinity of the wall toward AR of 3, offering more

selective channelling and, by inference, velocity in these regions. The wall effect decreased again for AR higher than 4, owing to more mixing in the centre of the packing. Thus, there is a nonlinear wall effect, which is exclusively function of fluid flow rate as shown in Figure 4.6.

4.4.3 Velocity field profiles

Since no symmetry exists in the unstructured (randomly) packing, the flow structure is expected to be highly dependent on the topology of the intergranular space at pore scale. Figure 4.7 shows the projections of local velocity on cross-sectional and vertical planes along the bed length at ARs of 1.5 and 3. It is clear that interpreting a suitable visual output of velocity is a challenging task without a direct line of sight through the full packed bed. The disorder of the flow structure by 3D view, however, can reveal the presence of vortices and eddies in the pores, particularly at high velocity fields.

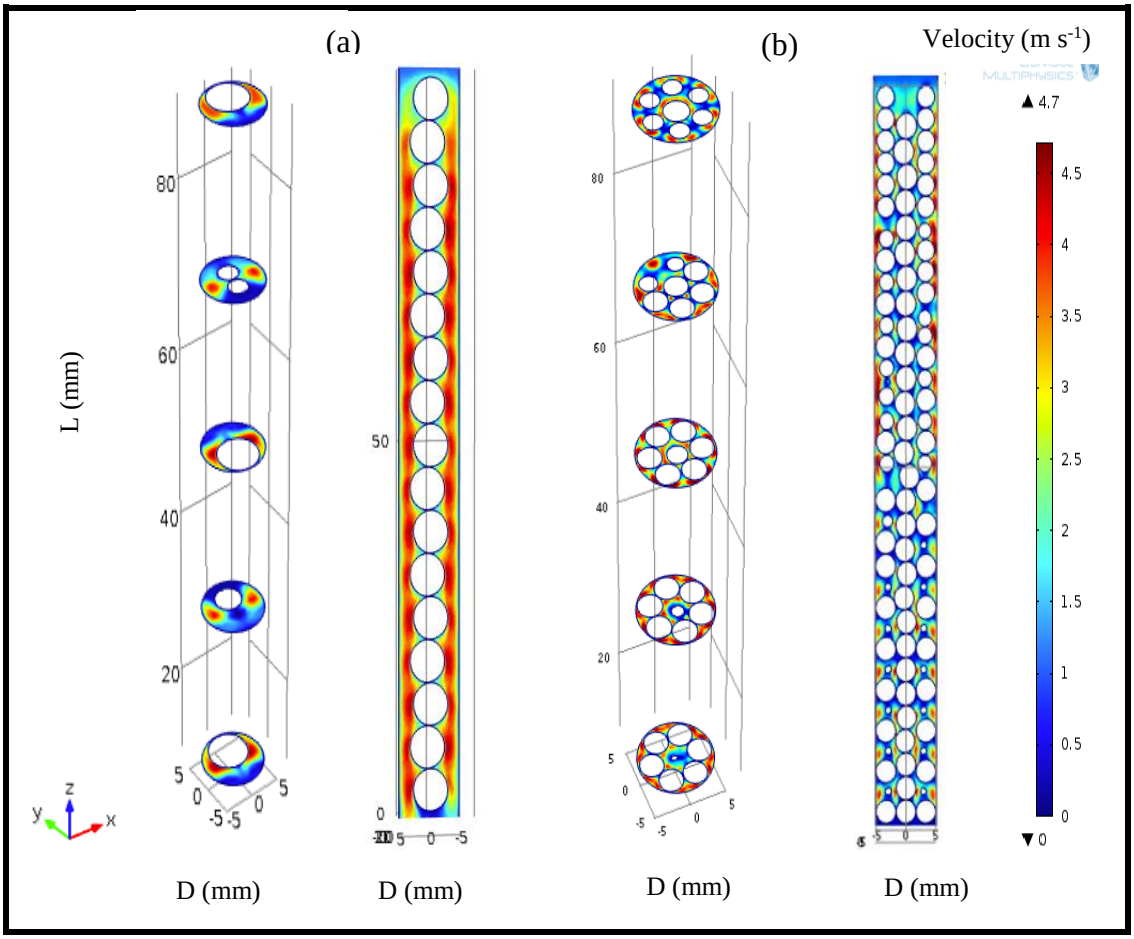

Figure 4.7. Cross-sectional and vertical cuts of the velocity (m s^{-1}) inside a packed bed reactor: (a) AR 1.5, Re = 375 and (b) AR3, Re = 187. [18]

An alternative viewing option of the complex 3D domain is by a 2D angularly averaged domain, as it offers a more realistic full picture of flow behaviour, as shown in Figure 4.8 for ARs of 1.5, 2, 2.5, 3 and 5. Such detailed analysis of flow structure would be relevant provided that the 2D porous structures in Figure 4.3 are as close as possible to the real 3D structures.

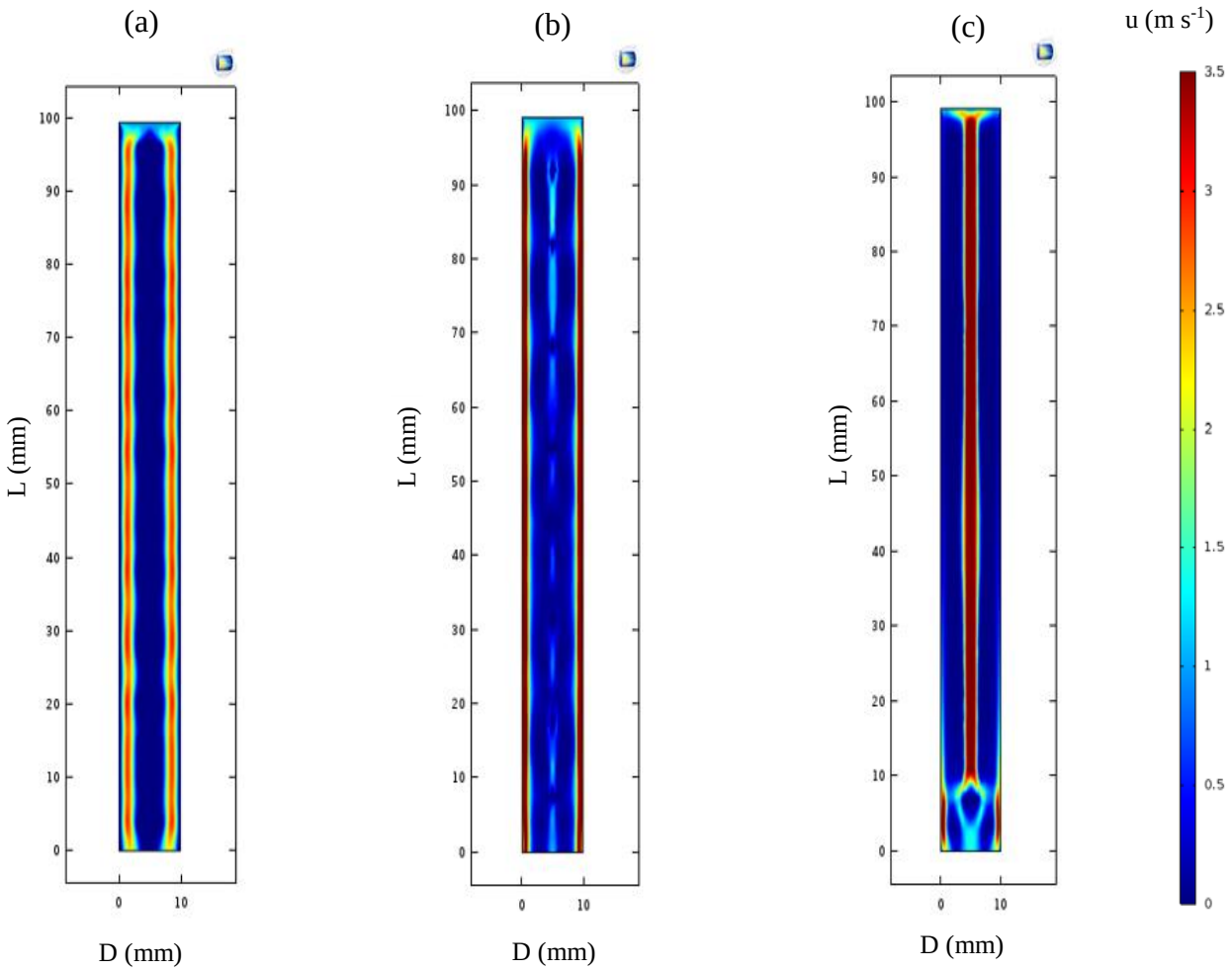

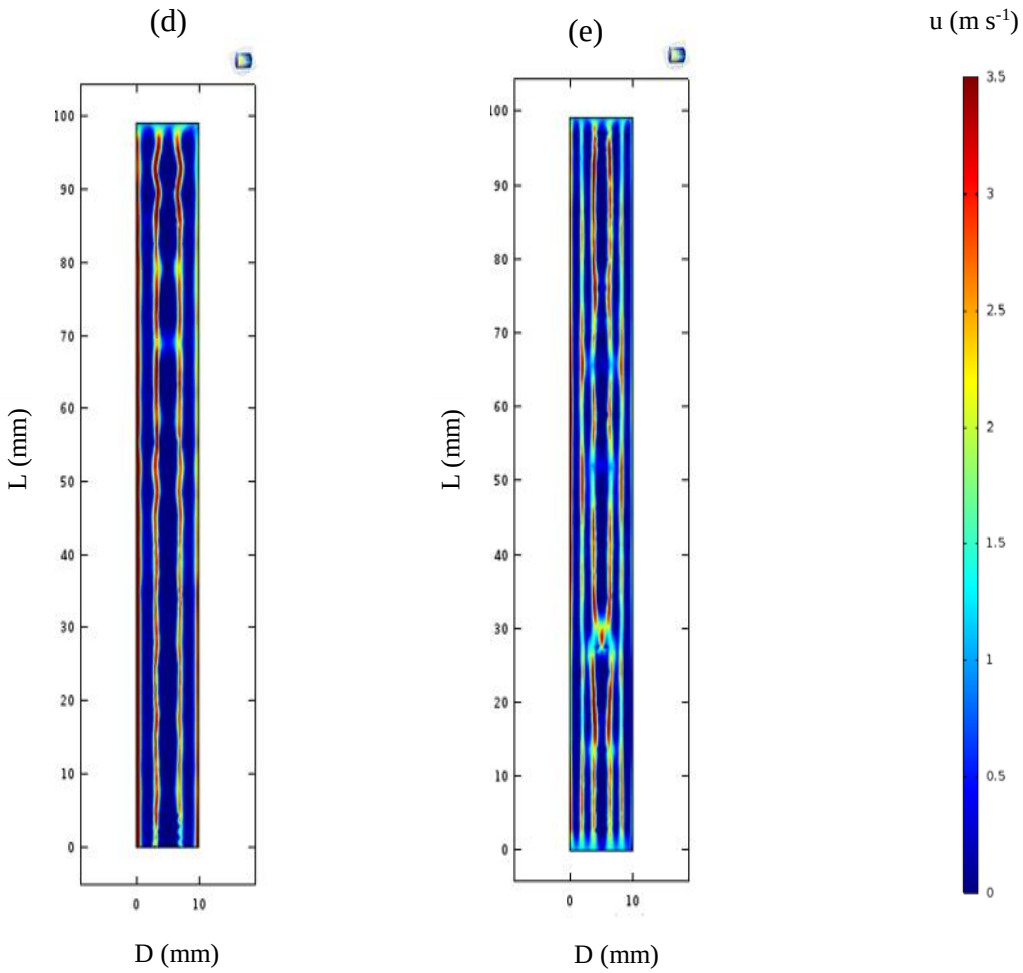

Figure 4.8. Velocity distribution in 2D profile in a packed bed reactor: (a) AR1.5, (b) AR2, (c) AR 2.5, (d) AR3, and (e) AR5. [18]

Figure 4.8 (a) shows the velocity distribution for AR of 1.5 mainly in the near-wall regions, demonstrating the effect of the wall. This effect slightly decreases for AR value of 2, as shown in Figure 4.8 (b), where some spots of velocity are displayed along with the continuous distributions near the wall regions. Increasing the value of AR to 2.5 promoted the spots of values into continuous values, which correspond to a more homogeneous velocity than those observed at an AR of 2, which in turn displays less homogeneous velocity than that at 3. This later packing, however, shows less homogeneous velocity distributions than at AR of 5, yielding to expected trends of the effect of the confining wall on fluid flows at low AR.

Contrary to the magnitude of velocity inside the packed bed of AR of 2, the magnitudes of the spots along the tube wall for ARs of 3 and 5 are not sufficiently high, confirming the looseness of the packing in these regions. These results are in agreement with experimental data reported by Aiouache et al., (2011) where preferential channelling near the wall has been experimentally demonstrated. [69]

The fluid velocity was the greatest in the narrow spaces at ARs of 3 and 5 because it occurred in between particle-to-particle contacts and particle-to-wall contacts, where the flow was forced to accelerate through a relatively smaller space. Similar to porosity trends, cyclic variations of velocity along the bed height are again observed, confirming local variations of fluid flow in low AR, particularly those of less than 3. This caused several areas of local maximum velocity where the fluid sometimes found its way into the channels. The 2D modelling approach was ascertained by comparing the results of pressure drops with those obtained by 3D modelling, as shown in Figure 4.9. A deviation of 0.5% is observed for Re of 284, confirming the benefit of using the porosity distribution from 3D maps to access insights into industrial packed beds of large computation time and hardware power.

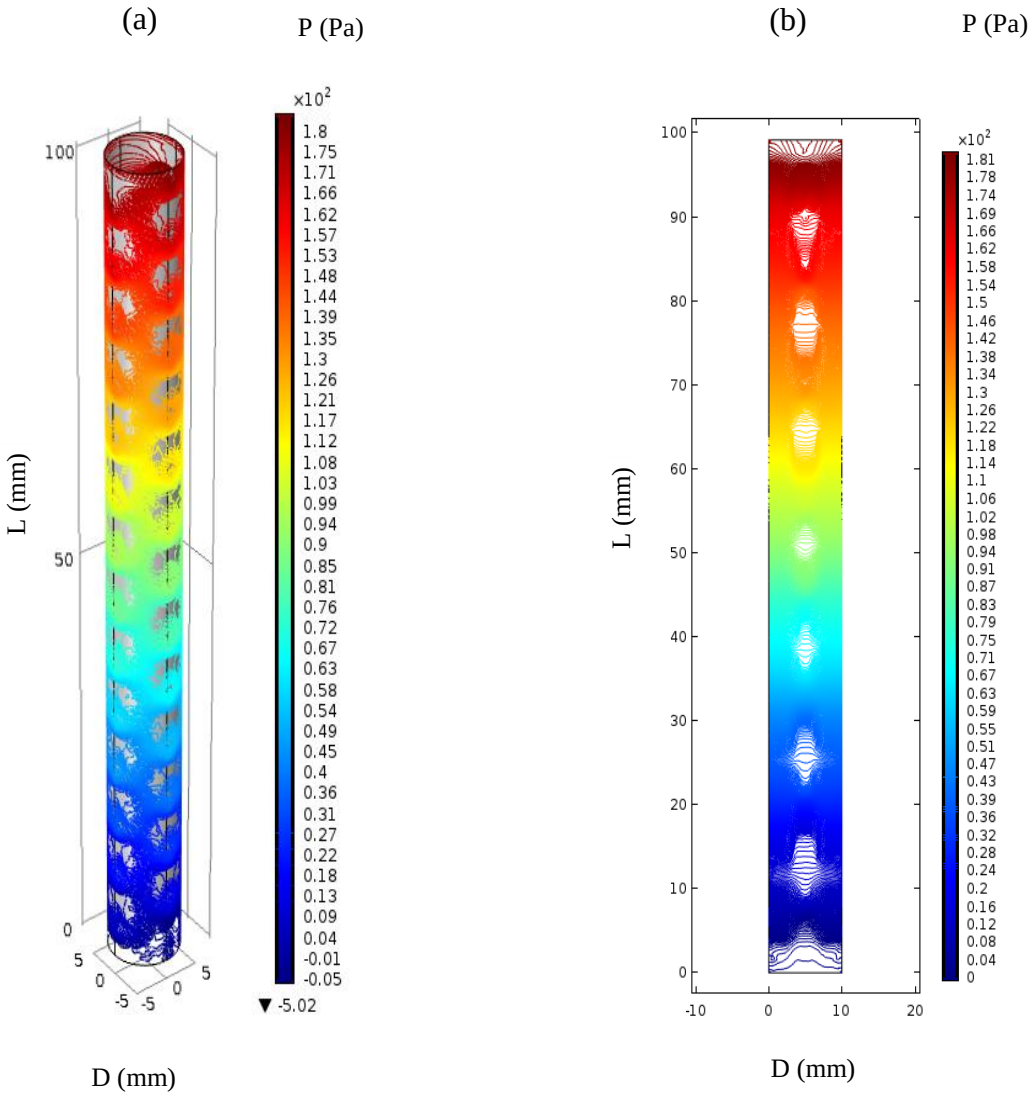

Figure 4.9. Pressure drop contours for AR = 2: (a) 3D modelling and (b) 2D modelling (Re = 284). [18]

4.5 Mass dispersion model

Dispersion of species in porous media is generally characterized by five regimes: pure molecular diffusion regime ($Pe < 0.3$), superposition regime ($0.3 < Pe < 5$), where the effects of molecular diffusion and dispersion are comparable; predominant mechanical dispersion regime ($5 < Pe < 300$); pure mechanical dispersion regime ($300 < Pe < 100000$), where the effect of molecular diffusion is negligible; and dispersion out of the Darcy domain regime ($Pe > 100000$), where the effects of inertia and turbulence cannot be neglected. [136]The dispersion in a packed bed is well described

by the two-dimensional diffusive and convective model equation, assuming constant velocity *u* and constant dispersion coefficients.

$$\frac{\partial C}{\partial t} = D_{ax}\frac{\partial^2 C}{\partial z^2} + \frac{1}{r}\frac{\partial}{\partial r}\left(D_{rad} r \frac{\partial C}{\partial r}\right) - u\frac{\partial C}{\partial z} \qquad (27)$$

The analytical solutions, by assuming a maximum concentration at the centre of the packed bed, as expressed by equations 28 and 29, require continuous species tracing under steady-state transversal and dynamic axial mass dispersion experiments.

$$\frac{C}{C_o} = \frac{1}{2} erfc\left(\frac{r}{2\sqrt{(zD_{rad}/u)}}\right) \qquad (28)$$

$$\frac{C}{C_o} = \frac{1}{2} erfc\left(\frac{z-ut}{2\sqrt{D_{ax}t}}\right) + \frac{1}{2}\exp\left(\frac{uz}{D_{ax}}\right) erfc\left(\frac{z+ut}{2\sqrt{D_{ax}t}}\right) \qquad (29)$$

Where C_0 is the inlet concentration (mol m^{-3}). An alternative discontinuous approach relies on the Lagrangian method by following distinct particles along a trajectory in a steady-state velocity field. The method of moments, as shown in equation 30, is used to calculate axial and radial dispersion coefficients. [12]

$$D_{ax/rad} = \frac{1}{2}\frac{d\sigma^2_{ax/rad}}{dt} \qquad (30)$$

Here, $D_{ax/rad}$ is axial or radial dispersions coefficients (m^2 s^{-1}) and $\sigma_{ax/rad}$ is the second moment or mean square deviation, as defined by equations 31 and 32:

$$\sigma_{ax}^2(t) = \frac{1}{NP}\sum_{n=1}^{NP}(x_n(t) - \bar{x}(t))^2 \quad (31)$$

$$\sigma_{rad}^2(t) = \frac{1}{NP}\sum_{n=1}^{NP}(r_n(t) - \bar{r}(t))^2 \quad (32)$$

Here, n is the particle index, NP is the total number of tracked particles, t is the time and (x, r) are displacements of particles along the axial and radial coordinates (m), respectively. $\bar{x}$ and $\bar{r}$ are the averaged displacements of all particles along the axial and radial coordinates (m), respectively.

4.5.1 Mass dispersion profiles by CFD

The Lagrangian method of particle tracking was used to describe their trajectories: thus the macroscopic mixing of tracer particles along the axial and the radial directions of the packed beds. Herein, the particle tracking module of Comsol was coupled with the 3D fluid flow model equations (11) and (12) to give trajectories to individual particles of similar trends to those developed by the carrying fluid. The particles were assumed to be negligible mass and subject to bounce conditions at the fluid−solid interphase. The design of the packed bed required addition of an inlet for particle flow by using a small cylinder of 1 mm I.D. and 2 mm height at the top centre of the packed bed. The size of the small cylinder was effective in terms of meshing requirements. About 500,000 particles were released for each test, and the displacement of these particles was followed with time.

Interaction of AR and mass transport was investigated by using two values of AR (i.e., 2 and 4) and two values of *Pe* (0.01 and 100). Although the particles were released at the centre of the packed bed, their propagation at *Pe* of 100 along the axial direction was significant for both AR 2 and AR 4

and was dominant in comparison with the diffusive propagation along the radial direction, as shown in Figure 4.10. Significant holdups should be associated with zones where the fluid entered stagnant regions of reduced convective flow, leading to significant transport by diffusion. At *Pe* of 0.01, the particles, however, happened to collide at the solid/fluid interface, causing a significant diffusion along the radial direction.

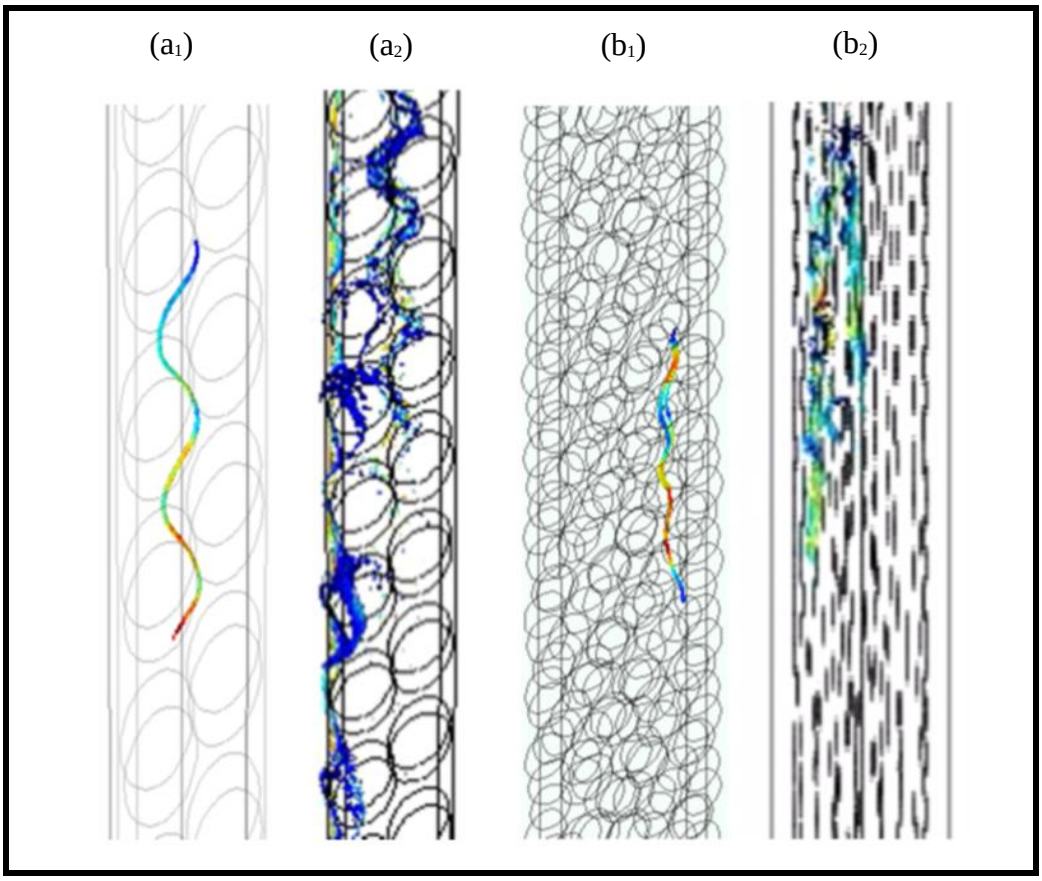

Figure 4.10. 2D vertical slices of particle tracers. AR 2 (a_1: Pe = 0.01 and a_2: Pe = 100) and AR 4 (b_1: Pe = 0.01 and b_2: Pe = 100). [18]

Compared with those observed in the vicinity of the wall at AR of 4, the particles were seen to circulate mainly along the centre of the packing at AR of 2, which agrees with the results of porosity and fluid flow. Beyond this value of AR, particles again circulated more in the central region of the packed bed. It should be noted that no particle was seen as trapped in stagnation zones, except at the interface fluid/solid. This means that if there were vortices inside which the current

lines loop on themselves, they would be too small in number to be observed. Owing to the no-slip assumption, particles that reached the wall were eliminated for the computation of mass transfer dispersions.

Quantitative values of dispersion coefficients were then computed by accessing first the trends of individual particle positions with time. These positions were used to compute trends of the second moment or mean square deviation of positions of these particles along axial and radial directions according to equations (31) and (32), respectively. These values served to calculate the asymptotic values of dispersion coefficients according to equation (30). The profiles of axial and radial dispersion coefficients normalized to molecular diffusion were added to Figure 4.11, along with those computed by the semi-analytical models of Freund and Delgado. [12, 137]

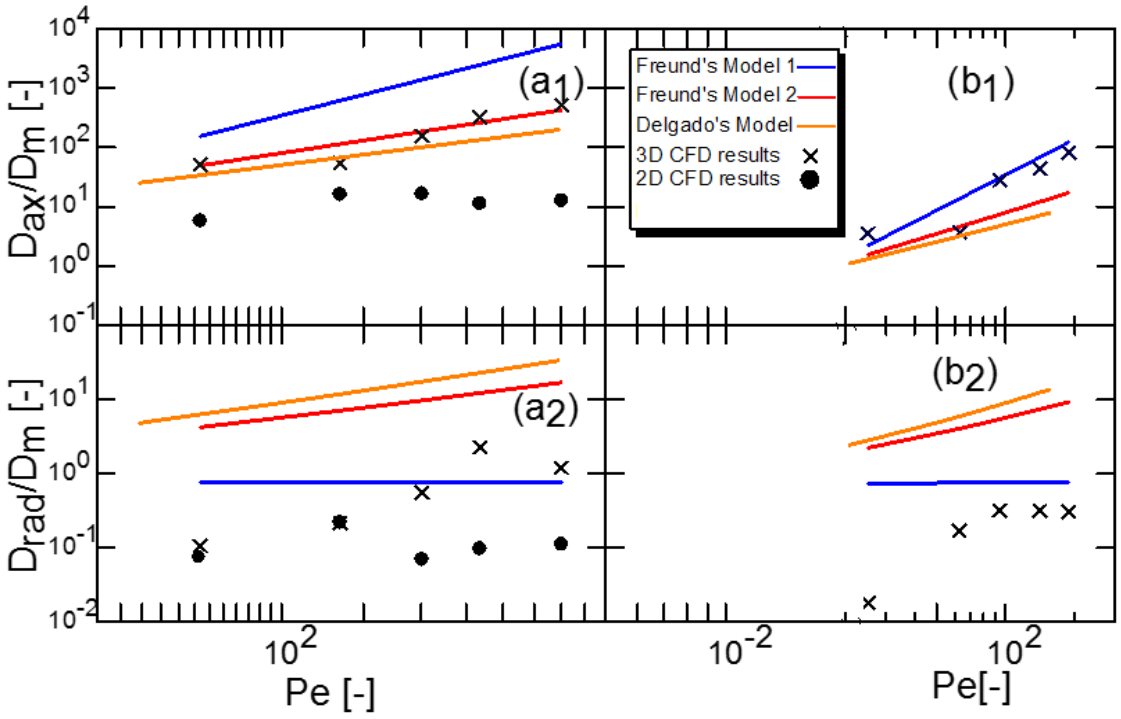

Figure 4.11. Axial and radial dispersion coefficients along with flow dynamics, respectively: (a_1, a_2) for AR of 2 and (b_1, b_2) for AR of 4. [18]

The prediction of axial dispersion is in a good agreement with those obtained by literature models. The radial dispersion by CFD showed some discrepancies with literature models, although for an AR value of 2, there is some reasonable agreement with Freund's model. Similar trends were reported by Augier et al., (2010) and the explanation could be given by the size of the packed bed,

which was not large enough to allow asymptotic profiles of velocity to be reached by the particles. [138] Axial dispersion values for a larger aspect ratio of packed bed (AR of 4) were between the models of Freund and Delgado.

Unlike the radial dispersion, the axial dispersion was more promoted by the wall, confirming the impact of the wall on global mixing within low-AR packed beds, and suggesting that the CFD approach is a helpful tool to characterize such a phenomenon. Finally, the validated results from the 3D CFD were compared with those obtained from the 2D CFD, which used 2D angularly averaged porosity, as shown in Figures 4.11 (a1) and (a2). Radial and axial dispersions by 2D modelling are in a reasonable agreement with those obtained from 3D modelling, and thus again validates the benefit of using 2D averaged maps of porosity for large-scale packed beds for mass dispersion studies.

4.6 Summary of the chapter

In this chapter, gas/solid behaviour in narrow packed beds was investigated by 3D modelling. Bed configurations of low ARs were generated by DEM and the structural porosity trends (3D, 2D, and 1D) of randomly distributed particles subject to wall effects were compared with semi-analytical models. The results contributed to more understanding of fluid flow and mass transport in these low AR packed beds where knowledge is still scarce. The porosity profiles were in a good agreement with the semi-analytical models such as Mueller's expression, especially in the zone near the wall. Similar oscillation trends with damping profiles toward the centre of the packed beds were observed.

The discrepancies in regions toward the centre may have originated from the loose structure of the generated packing. In addition, the averaged porosity obtained by the CFD simulation was in a reasonable agreement with Zou's model, where the porosity increased at low AR. The simulation results were validated by a pressure drop, and the results fitted well with Reichelt, Zhavoronkov, and Ergun's models at high Reynolds numbers. Distribution of velocity was investigated, and the results of high velocities were mainly observed in the regions near the confining wall owing to high local porosities in these zones.

The results of 2D model were in a good agreement compared to 3D modelling, confirming the benefit of using the porosity distribution from 3D maps to access insights into industrial packed beds of large computation time and hardware power.

Flow heterogeneity was also characterized by mass dispersion using a Lagrangian approach. Particles were released at the centre of the packed bed and their propagation along the radial and axial directions was examined. The results have shown changes in axial and radial dispersions and confirmed the impact of the wall on global hydrodynamics inside low AR packed beds. Some discrepancies for radial dispersion coefficients were observed due to the very short domain length, particularly for small values of AR. Unlike radial dispersion, axial dispersion showed agreements with CFD results and literature models.

Chapter 5

5. Analysis of Mass and Heat transfer in PBRs

5.1 Introduction

Inside the packing, fluid elements randomly move between the particles and lead to additional heat and mass transport towards the radial and axial directions. Mixing of the fluid elements takes place because turbulence, molecular diffusion and conduction. Mass and heat transfer problem in a packed-bed reactor is a major concern in the design of chemical reactors. Mass transfer from the bulk of the fluid to the particle interface in gas – solid systems has been a main objective for different investigations during the last few years. For low ARs of packed bed reactors, the wall effect dominates the packing structure by building inhomogeneous patterns of particle locations, especially those in the vicinity of the wall. [139] As consequences, fluid flow, fluid/solid mass and heat transfers are found to be influenced, as demonstrated by various applications, including gas/solid contactors, reactors and adsorbers. [140]

The design of packed bed reactor requires a detailed knowledge of local transport phenomena inside the bed. For example, within a packed bed including heat exchanges, the evaluation of temperature profile and the heat transfer rates is a characteristic to assess performance of catalytic reactors. [8] At particle scale level, the design of these is governed by different competing considerations; smaller particles have less internal resistance to diffusion but the larger ones result lower pressure drop of the fluid. [9] Access to temperature trends in these reactors is not simple, particularly in the catalytic phase, these are estimated through heat transfer characteristics between the catalytic phase and the gaseous phase as well as with the containing wall. [8] This is even more challenging with low aspect ratios (AR) of tube to particles diameter which exhibit uneven distribution of flow, heat and mass transfers. [19-22]

In addition, heat transfer may play a critical role in determining the optimal performance of chemical reactors. The analysis of non-isothermal influences on the overall reaction rate through packed beds is important since majority industrial packed beds are operated at considerable temperature gradients and therefore, temperature control is considered as one the challenges during design these reactors. [11] In fact, majority of previous studies, which have primarily concentrated on heat transfer in packed beds, only measured radial temperature distribution at the outlet of the bed. The detailed temperature distribution inside the bed and the temperature difference between packed particles and flowing gas are mostly unknown. [141]

Several studies have examined fluid –packed particle heat transfer, transient response of packed beds, and effective variables under steady state which involve radial and axial thermal conductivities, effect of wall to fluid heat transfer coefficient and the overall heat transfer coefficients. [141] Packed bed reactors with low AR are used in highly exothermic or endothermic systems e.g., partial oxidations and steam reforming of methane where the heat is expected to be sharply transferred into or out of a narrow reactor tube, validating the role of the confining wall on heat transfer and flow around the catalyst particles. These in turn affect some properties during catalytic reactions process such as catalyst activity, selectivity and deactivation possessing. [23]

Also, exothermic reactions lead to significant temperature variations in a catalyst particle which when coupled with external mass and heat transfer limitations and intra-particle concentration gradients cause hotspots formation and as result of this, reaction rate will be strongly influenced. [11] There were several works that investigated heat transfer through the packed beds. For instance Dongsheng and Yulong (2006) have studied distribution of temperature experimentally, retrieved relevant data at different axial positions of the bed for different Reynolds numbers (Re) and found that there is a proportional relationship between the axial distance and temperature rise. [141] Despite the fact that the use of CFD to simulate geometrically complex flows through randomly packed tubes is expensive and unpractical currently for routine design and control of packed bed reactors, its contribution to this area is observed through recent achievements on understanding interactions of transport and reaction phenomena events taking place inside the packed reactor. In this chapter, CFD by 3D modelling is used to obtain local distribution of mass and heat fields inside the reactor and achieve comprehensive information on global behaviour of flow, temperature and species inside the packed beds.

5.2 Carbon monoxide (CO) oxidation

5.2.1 Theoretical background

The oxidation of carbon monoxide on noble metals is selected for this work because it has been extensively studied for packed bed instabilities. A large amount of information is available for its role in the catalytic control of automotive emissions at a wide range of conditions. Special attention was paid to ignition (or light-off) taking place with increasing inlet temperature. Physically, the ignition is related to instability and self-acceleration of exothermic reactions because of the heat release. Before ignition, the system is in a low-reactive state and also the mass-transfer limitations are negligible. However, after ignition, the system will be in a high-reactive state and the reaction rate is controlled by mass (external) transport. [12 and 66] Decreasing inlet temperature below the light-off temperature leads to reaction extinction due to transition from a high reactive state to a low-reactive state. This bi-instability and its impact on catalyst deactivation have been studied experimentally and by pseudo-homogeneous modelling. [12, 50, 56, 60, 63, 66, 80 and 142]

In fact, through the low-reactive regime, which is observed at relatively high CO pressure, the surface of catalyst is primarily covered by CO and the reaction rate is controlled by O_2 dissociation. In contrast, the high-reactive regime takes place at relatively low CO pressure, the surface is mainly covered by oxygen and the reaction rate is proportional to CO pressure. The stepwise changes inside the reaction rate observed with an increase or decrease reactant pressure was found of first-order kinetic phase transitions. [143] Recent publications have been focusing on catalyst formulation, characterization and performance such as activity, conversion of CO and stability of catalyst. In the CO selective oxidation reaction system, the following two oxidation reactions take place. [144]

$$CO + \frac{1}{2}O_2 \rightarrow CO_2 \qquad \Delta H = -283 \text{ kJ mol}^{-1}, \quad \text{(desired reaction)} \qquad (33)$$

$$H_2 + \frac{1}{2}O_2 \rightarrow H_2O \qquad \Delta H = -242 \text{ kJ mol}^{-1}, \quad \text{(undesired reaction)} \qquad (34)$$

The relevant model of CO oxidation mechanism would occur through the following detailed kinetics stages:

$$CO + Pt \rightarrow Pt.CO \qquad (35)$$

$$O_2 + 2Pt \rightarrow 2\ Pt.O \qquad (36)$$

$$Pt.O + Pt.CO \rightarrow 2\ Pt.CO_2 \qquad (37)$$

The first step of the mechanism is CO adsorption due to the low initial sticking coefficient of oxygen on platinum as compared to CO. The second step is the dissociative adsorption of oxygen. [145 and 146] Majority of researchers believe that the last step is driven by interaction between the adsorbed CO and the adsorbed atomic oxygen by a Langmuir–Hinshelwood (L-H) mechanism. The final stage is the desorption of CO_2 from platinum catalyst that is believed to take place instantaneously. [147] Reactions in equations 33 and 34 are extremely exothermic and for these kind of reactions it is then important to remove the heat from the reactor. Temperature control can also be crucial to catalyst selectivity. Based on the relative heats of adsorption of CO and H_2 on platinum. It is very likely that the selectivity of the catalyst at higher temperatures would lead preferentially to CO oxidation before H_2. [144, 148 and 149] An approximate first order rate expression was found appropriate then for the reaction mechanism. For precious metal catalysts, many different kinetic rate expressions have been reported. Power law models are easy to implement in CFD simulations as they reduce non-linearity issues when combined models of mass and heat balances. Herein, we cite some power laws expressions relevant to CO oxidation on Pt/Al_2O_3 catalyst. Amphlett et al., (1996) developed a simple first-order rate expression as illustrated in equations (38 and 39): [144]

$$r_{CO} = k_{co} C_{co}\ , \qquad (\text{mol s}^{-1}\ \text{kg}^{-1}) \qquad (38)$$

$$\text{Where}\ ,\ k_{co} = A \exp\left(-\frac{E}{RT}\right)\ , \quad (\text{m}^3\ \text{s}^{-1}\ \text{kg}^{-1}) \qquad (39)$$

Where, C_{co} (mol m^{-3}) represents concentration, k is the reaction rate constant, r_{CO} is reaction rate, T is temperature in (K) , E is the activation energy (J mol^{-1}), A is the Arrhenius constant (s^{-1}), ΔH is heat of reaction (kJ mol^{-1}) and R is the gas constant (J mol^{-1} K^{-1}) . Moreover, a different kinetic expression was derived by Kahlich et al., (1997) by introducing a process parameter λ which is defined as the concentration ratio of O_2 to CO:

$$r_{CO} = kP_{CO}^{0.42}\lambda^{0.82} \quad (40)$$

$$\text{Where,} \quad \lambda = \frac{2c_{O_2}}{c_{CO}} = \frac{2P_{O_2}}{P_{CO}} \quad (40\ a)$$

According to this kinetic expression, the reaction rate of CO can be determined with activation energy about 71 kJ mol^{-1}. [150] Another similar expression was used by Kim and Lim (2002) as illustrated in equation 41. [151]

$$r_{CO} = 1.4 \times 10^8 \exp\left(\frac{-78}{RT}\right) P_{CO}^{-0.51} P_{O_2}^{0.76} \quad (41)$$

In this work, CO oxidation over alumina (Al_2O_3) catalyst support was used and relevant kinetic model that was developed by Amphlett et al.,(1996) as written in equations (38) and (39), was considered. [144] The kinetic model along with 3D CFD modelling of flow, heat and mass was investigated and the results were validated by published works.

5.3 3D Modelling description

5.3.1 Model equations

Realistic random packing was generated for spherical particles by DEM as discussed in chapter 3. Phenomena of hydrodynamics, mass and heat in the granular media, containing several thousands of spheres, were described for selected ARs (i.e., 1.5, 2.5, 3, 4 and 5). The solid particles do not move and the void between them remains constant. The Transport of diluted species, heat transfer

module with chemical reaction was applied, which included diffusion and convection to model the component concentrations trends in the fluid. The fluid was assumed laminar and the simulation was carried out by including the governing equations which couple balances of momentum, mass and heat transfers in 3D random packed bed reactor as follows:

Governing Equations:

$$\rho(u.\nabla)u = \nabla.\left[-pI + \mu(\nabla u + (\nabla u)^T) - \frac{2}{3}\mu(\nabla.u)I\right] \quad (42)$$

Continuity equations:

$$\nabla.(\rho u) = 0 \quad (43)$$

In these equations, p is the applied pressure (Pa), μ is the fluid dynamic viscosity (kg $m^{-1}s^{-1}$), ρ is the fluid mass density (kg m^{-3}), u is velocity vector (m s^{-1}), I denote the identity matrix, T is the absolute temperature (K). Atmospheric pressure at the exit of the packed bed was considered. The inlet boundary was a fixed velocity inlet condition; this was spatially uniform over the inlet. At the outlet, a constant pressure boundary condition was used. The transport of diluted species user interface assumes chemical species transport through diffusion and convection and implements the mass balance equation. The interface assumes that all species present are dilute, and that their concentration is small compared to a solvent fluid.

Mass balance:

The diffusion of reaction species (CO and O_2) was considered as molecular (Fickian) due to low values of velocity and concentration used (turbulent diffusion and concentration based diffusion coefficients were neglected). Mass transfer in the catalytic phase was assumed to be driven by diffusion and free of convection (negligible velocity) and the chemical reaction occurs in the catalytic phase only (Al_2O_3). The mass transfer in gaseous phase domain is given in the equations (44):

$$\frac{\partial c_{i,g}}{\partial t} + \nabla.\left(-D_{i,g}\nabla c_{i,g}\right) + \mathcal{U}.\nabla c_{i,g} = 0 \quad (44)$$

$$N_{i,g} = -D_{i,g}\nabla c_{i,g} + Uc_{i,g} \quad (45)$$

In the reactive packing phase, the equation will be:

$$\frac{\partial c_{i,s}}{\partial t} + \nabla.\left(-D_{i,s}\nabla c_{i,s}\right) = R_i \quad (46)$$

Where,

$$R_i = \ A\ e(-\frac{E}{RT})\ C_{CO} \quad (46\ a)$$

And, $$D_{i,s} = \frac{\varepsilon_c D_{i,g}}{\tau_c} \quad (46\ b)$$

$$N_{i,s} = -D_{i,s}\nabla c_{i,s} \quad (47)$$

Where, $D_{i,g}$ and $D_{i,s}$ denote the diffusion coefficients ($m^2\ s^{-1}$) in the gaseous and solid phases, respectively, c_i is the species concentration (mol m^{-3}), $\mathcal{U}$ is the velocity vector (m s^{-1}), R_i is the reaction rate expression for the species (mol $s^{-1}\ kg^{-1}$) and N_i is the molar flux (mol $m^{-2}\ s^{-1}$), porosity ε_c , tortuosity τ_c , E is activation energy and A is the pre-exponential Arrhenius factor. The first term on the left-hand side of Equation (44) represents the accumulation or consumption of the species. The second term on the left-hand side of this equation accounts for the diffusion transport (interaction between the dilute species and diluting gas). The third term ($u.\nabla c$) accounts for the convective transport due to the velocity field u. This field could be achieved from coupling the transport of diluted species user interface to one that describes fluid flow (CFD or momentum balance). Lastly, the R_i term represents a source or sinks term, owing to presence of the chemical reaction.

Heat balance:

The energy equation for gaseous phase was used as below:

$$\rho_g Cp_g \frac{\partial T}{\partial t} + \rho_g \, Cp_g u.\nabla T = \nabla.(k\nabla T) + Q \qquad (48)$$

Where, k is the thermal conductivity (W $m^{-1}K^{-1}$), Cp_g is heat capacity of gas (J kg^{-1} K^{-1}), ρ_g the density of gas (kg m^{-3}) and Q is the generated heat was zero.

For the conjugate heat transfer in the solid particles the equation became as:

$$\rho_s Cp_s \frac{\partial T}{\partial t} = \nabla.(k_s \nabla T) + Q \qquad (49)$$

$$Q = \Delta H_R R \quad (49\ a)$$

Where, k is the thermal conductivity of catalyst particles (W m^{-1} K^{-1}), and Q is the generated heat from the exothermic process of CO oxidation of enthalpy ΔH_R.

5.3.2 Boundary conditions and solver details

These equations are subject to the following boundary conditions. At the inlet of the reactor, velocity and temperature were set at various values. At the outlet of the reactor, the pressure boundary condition was set to zero gauge pressure. Stationary solids (both walls and catalyst particles) with no slip boundary condition were assumed. The governing equations were discretised by the Finite volume Method (FVM). Momentum equations were combined with the transport of diluted species model and heat transfer model and then were solved in 3D transient formulations. Table 5.1 shows a summary of properties for different ARs which were used in this chapter.

Table 5.1 Properties of particles used.

(AR)	Diameter of particles d_p (mm)	Number of particles	Height of Packing (mm)
1.5	6.666	17	100
2.5	4.000	116	100
3	3.332	228	100
4	2.500	528	100
5	2.000	1075	100

Again, the contact points between the spheres were avoided by shrinking the diameter of solid particles by 1% .The actual porosity after shrinkage was used for all ARs during our simulations. The mesh was examined by Grid Convergence Index (GCI) which was discussed in chapter 4 to ensure the results are independent of mesh size and to check the accuracy of CFD model.

COMSOL Multiphysics 4.4 was used for detailed simulations of flow, mass and heat transfer inside a randomly packed bed of spherical particles of various ARs. The conjugate heat transfer problem used “Heat Transfer Module” where the “Heat Transfer in Fluids” model was set up first, then the “Heat Transfer in Solids” model was added to it, which ensured that the two models would couple temperature and flux correctly across the fluid-solid interface. Also, the dispersion of mass was dealt by using “Transport of Dilute species” model in both gaseous and solid phases, ensuring that the two models would couple concentration of species (CO) and mass flux correctly across the fluid-solid interface. The simulation was run first by studying the fluid flow alone and the results were then set as initial values for the subsequent study of simultaneous flow, heat and mass transfers.

5.4 Results and Discussions

5.4.1 Validation of CFD model for CO oxidation

The validation of the results was achieved by comparing the CFD results with the experimental and numerical data obtained from different authors. In this chapter the deactivation phenomena of this reaction will not be considered as it will be discussed in details in chapter 6.

- **Mass transfer**

5.4.1.1 Effect of inlet temperature on total conversion rate of CO oxidation

The validation of CFD model was carried out by observing the conversion rate trends of CO with temperature at steady-state operations, for AR 3, d_p = 3.33 mm , temperature range 433-553 K, feed composition: CO = 1.3 mole % and O_2 = 1.68 mole %. The degree of conversion is expressed by equation (50):

$$CO\ conversion(\%) = \frac{CO_i - CO_t}{CO_i} * 100 \qquad (50)$$

Where, $CO_i$is the initial CO concentration (mol m^{-3}) and CO_t is the outlet concentration (mol m^{-3}) at time, t (s), during the dynamic operations.

The general trend shows an increase in conversion with increasing reaction temperature as shown in Figure 5.1. These results were validated by comparison with experimental data and model results from literature. The conversion increased smoothly from 433-475 K with conversion about 42%, became more noticeable above T = 475 K, and reached 100 % conversion at T = 553 K. The light-off impact or "T_{50}", which is defined as the temperature value at 50 % conversion of CO. In this work, T_{50} was around 480 K and relevant CFD results were in good agreements with literature data, particularly with those obtained by Dong (2002) and Yongtaek (2004) for whole temperature range. [151 and 152] Unlike Sarp's results (2009), those obtained by Akkarat (2008) were in agreement with the CFD ones at early temperatures from 433-475 K. It should be noted that the maximum conversion in our simulation was obtained at 553 K. [153 and 154]

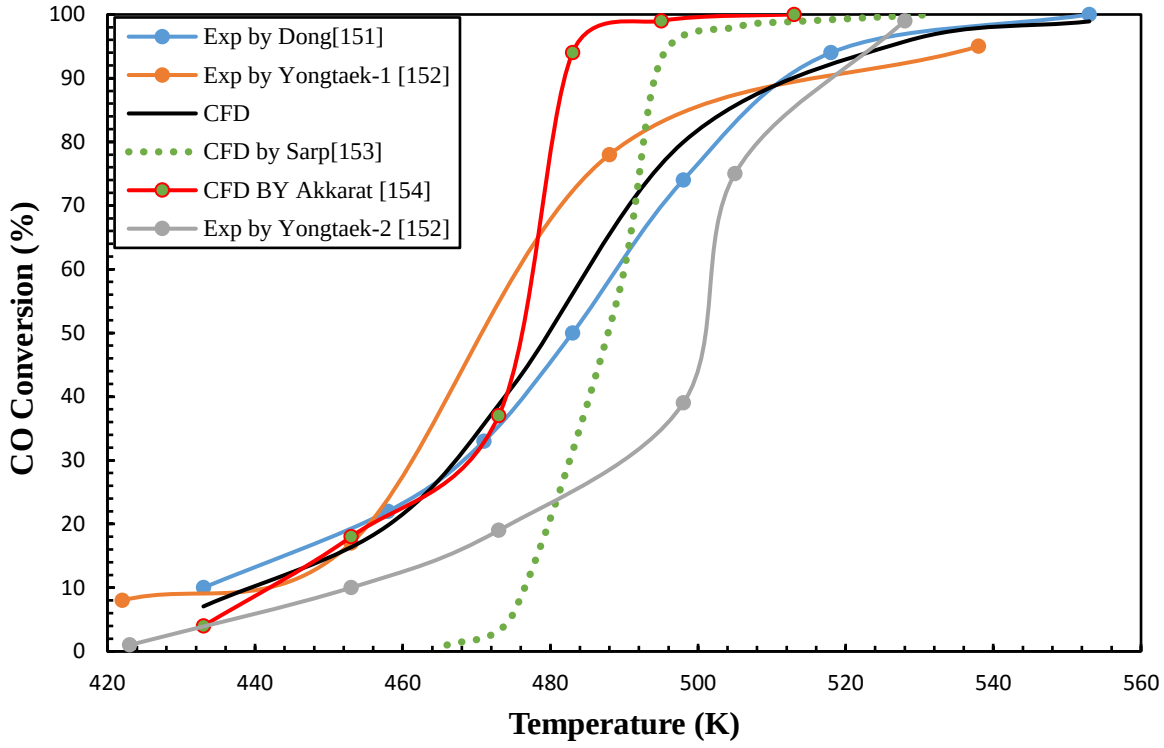

Figure 5.1. Conversion extent of CO versus temperature for (AR3)

The following figures 5.2 (a_1, a_2) give another insight into the distribution of conversion inside the column at inlet temperature, T_0 = 553 K. These figures show that the conversion of CO throughout the packed bed and the depth of local conversion inside the catalytic beads. In general, at the narrow zone (channels), where the temperature and rate of reaction are the highest, the reaction reached a complete conversion toward the end of the reactor. Also, when the temperature and/or concentration at the surface of the particle vary from its value in the fluid phase, the mass and/or heat exchange between the fluid and the particles take place as well.

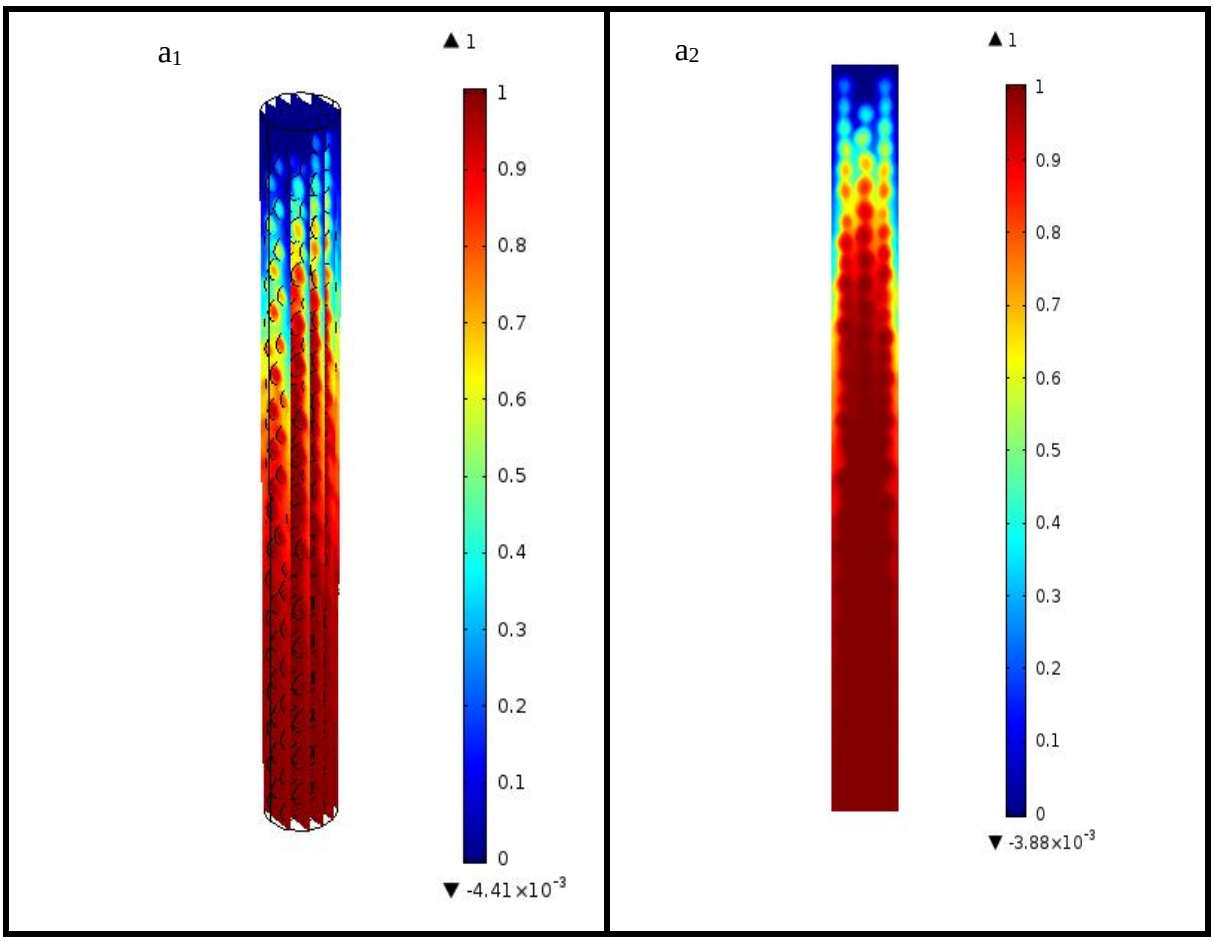

Figure 5.2. Conversion distribution of CO obtained by CFD for AR 3: (a_1) 3D view on slices and (a_2) 2D contour plot.

In figures 5.3 (b_1, b_2), propagation of temperature and profiles of temperature, respectively, from the inlet towards the outlet of the reactor are presented. The temperature of packed bed had a tougher distribution especially through the axial direction due to the particle heat transfer by conduction and the velocity distribution between particles. When the feed temperature decreased, the position of the reaction front moved downstream as more catalyst was needed to compensate starting lower temperature and reaction rate.

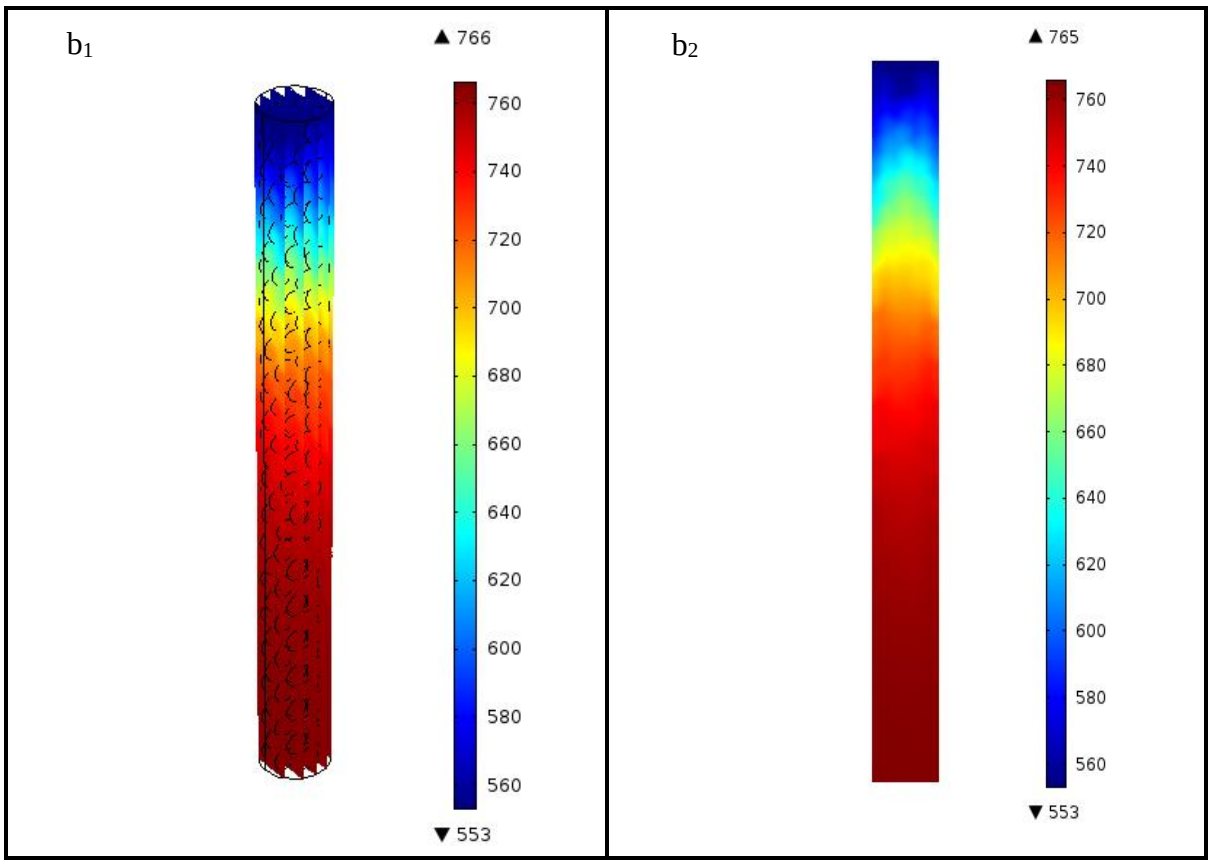

Figure 5.3. Temperature profiles of CO obtained by CFD for AR 3: (b_1) 3D view on slices and (b_2) 2D contour plot.

5.4.1.2 Effect of flow on conversion of CO oxidation

The conversion of CO into CO_2 was investigated as a function of the Re number in the range 300 - 900 as shown in Figure 5.4. CFD results were validated by comparison with experimental data and simulation results of Anna et al., (1998). [155] It can be seen that with increasing flow rates, the total conversions decreased owing to less contact (residence) time in the reactor. It is interesting to see that at low Re numbers (300-400), deviations between the CFD results and experimental data of Anna et al., (1998) were in agreement, unlike those obtained at high Re values. However, these results were close to CFD results obtained in the same work, demonstrating underestimation of reaction activity at high flow rates and this could originates from the simplified assumption of laminar flow regime, including the model by Anna et al., (1998), while transitional flow toward turbulent should have been considered for Re values higher than 400.

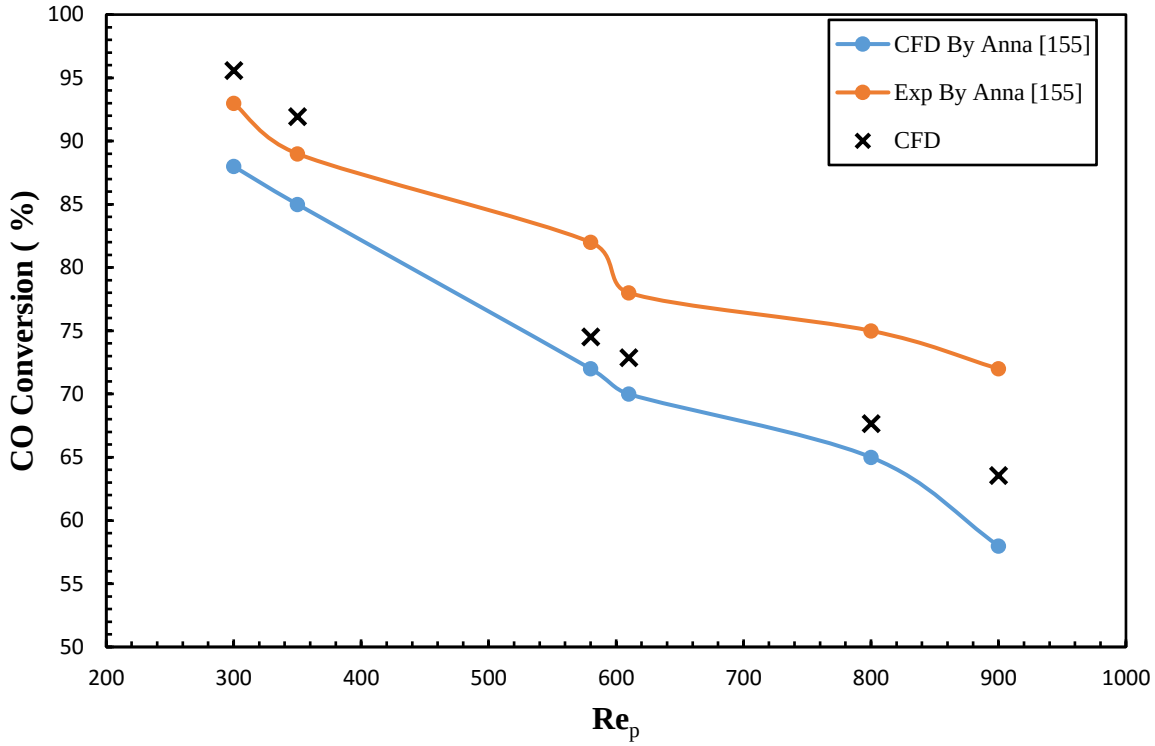

Figure 5.4. The simulated and measured conversions as function of Re. AR3

5.4.1.3 Effect the size of ARs on the CO oxidation

The effect size of catalyst particles on conversion of CO for different ARs (1.5, 3 and 5) was assessed as shown in Figure 5.5. It shows the influence of particle size on the value of CO conversion rate. The trends of conversion curves are similar at the early stages of the reaction and until around 20% conversion rate and then the packing of smallest particle size shows the highest conversion rates. Higher values of CO conversion obtained at 528 and 553 K for AR5 (d_p = 2 mm), however the maximum conversion was achieved at final stage of the CO oxidation for AR 3 (d_p = 3.33 mm). On the other hand, the conversion range for AR 1.5 (d_p = 6.66 mm) was the lowest. Similar trends were reported by Abdel Halim et al., (2007) for CO oxidation with different catalyst sizes of Fe_2O_3. [156]

The complete oxidation of CO to CO_2 was observed with (AR5) d_p =2mm at *T* 553 K. This result validates those obtained by Abdel Halim et al., (2007) and demonstrates that conversion of CO is sensitive to particle size as it is driven by mass transfer limitations, particularly at temperature above the light-off temperature.[156] These results reveal that with increasing the diameter of catalyst particles, the reaction rate per unit volume of catalyst decreases because of decrease of the reactant concentrations towards the centre of particles leading to decrease in CO conversion. At large ARs (i.e., AR5), the number of particles used was higher than the other ones (see table 5.1), causing more surface area, more reaction and contact between CO gas and solid catalysts (Al_2O_3) and leading to high conversion of CO.

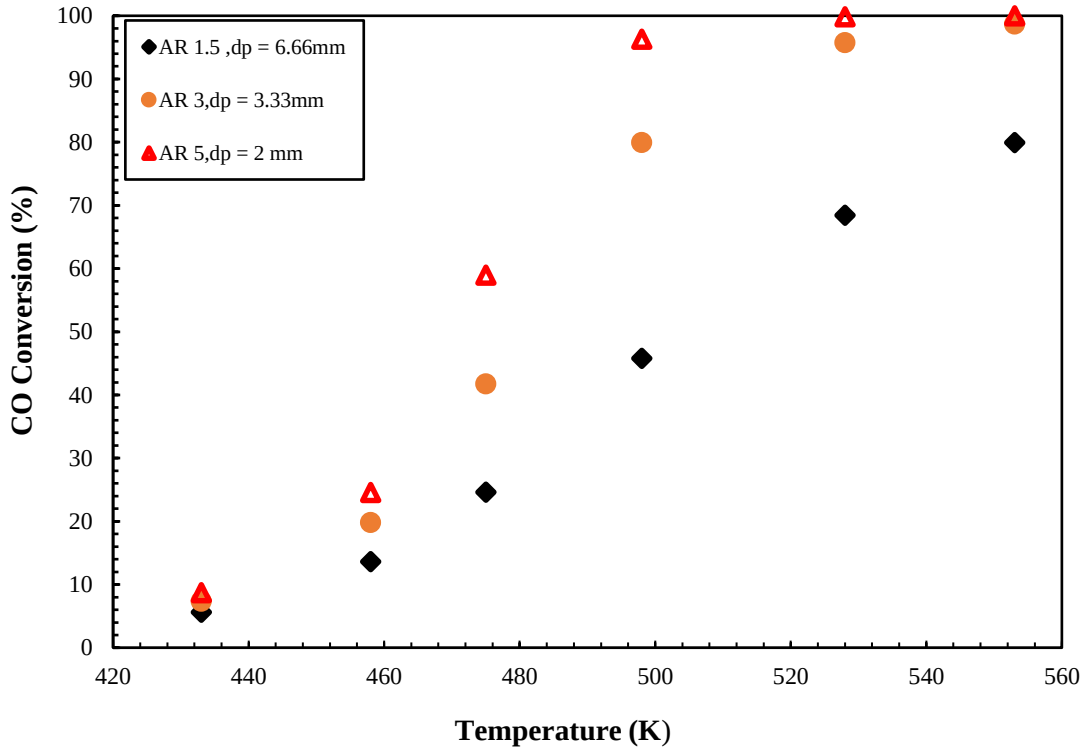

Figure 5.5. Effect of size of aspect ratio AR on steady-state conversion for carbon oxidation of CO, inlet velocity u_0 3.11 (m s^{-1})

- **Heat transfer**

Simulation works were also extended to heat transfer profiles within the gas phase and the solid phase, where both conduction and convection types of heat transfer are expected to take place. In this section, the fluid was assumed as (air) and the solid phase was assumed as alumina particles (Al_2O_3), and the study was done without consideration of the chemical reaction.

5.4.2 Temperature profiles inside the packed bed reactor

Previous studies have primarily concentrated their objectives on the heat transfer phenomena in 3D designed packed beds by measuring radial temperature distribution at the outlet of the bed. The detailed temperature distribution in the interior of the bed and the temperature difference between packed particles and flowing gas are still challenging experimentally as well as by modelling when a limited number of heat transfer correlations are used. In this section, we aim to obtain a comprehensive information, by CFD modelling of fluid flow and heat transfer on trends of temperature field inside the bed, including radial and axial temperature distributions. The fluid inlet temperature was set to T_0= 458 K.

Figures 5.6 (a, b and c) show that temperature at the centre of the packed bed as a function of axial distance of the packed bed for Re values ranging from 187 to 556 and AR values of (2.5, 3 and 5). It can be seen that at a given Re value, temperature increases slowly along the first 20 mm length and then increases significantly until the end of bed and the distribution is S-shaped for all Re values. At high values of Re (i.e., 494 and 556), the increase in temperature is not sufficiently noticeable, however at end of packed bed (z=100 mm), there is a slight decrease in temperature and which could be attributed to non-uniform temperature distribution of the flow inside the bed. An increase in Re values has given then a limited contact or residence time of the flowing gas throughout the column with the heating wall, reducing thus temperature gradient between the walls and flowing fluid and validating the resistance to heat transfer on the fluid side in packed beds with a constant wall surface temperature. These results are consistent with those obtained experimentally for Re values of 187 to 556 by Dongsheng and Yulong (2006). [141]

(a)

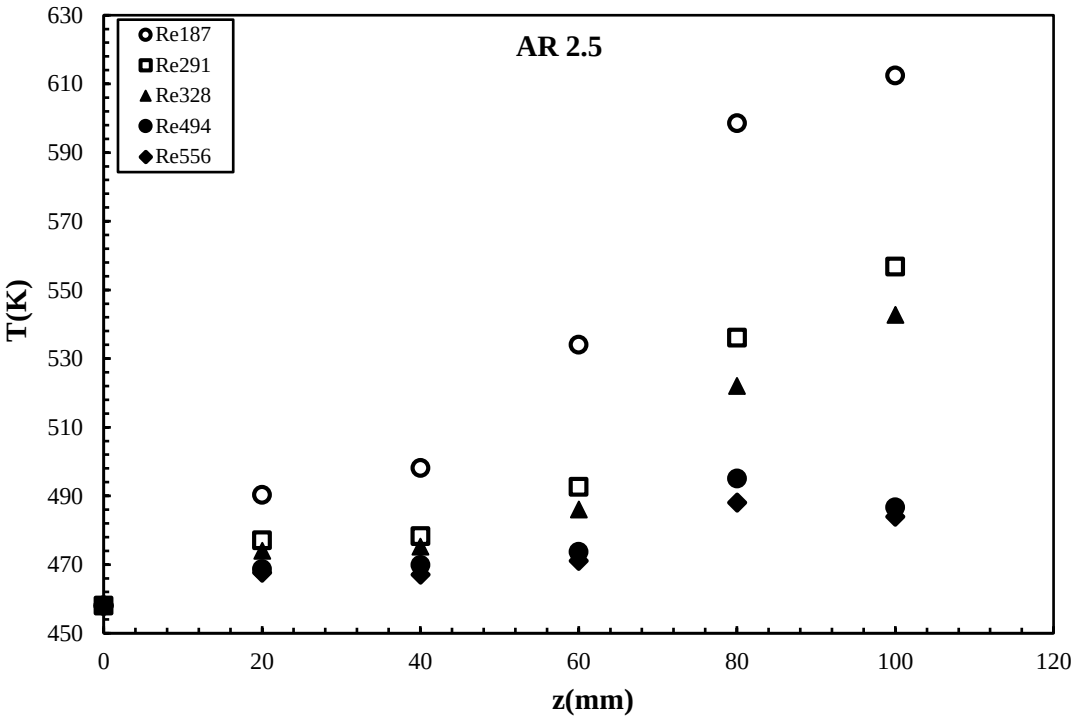
AR 2.5
Re187
Re291
Re328
Re494
Re556
T(K)
z(mm)
630
610
590
570
550
530
510
490
470
450
0
20
40
60
80
100
120

(b)

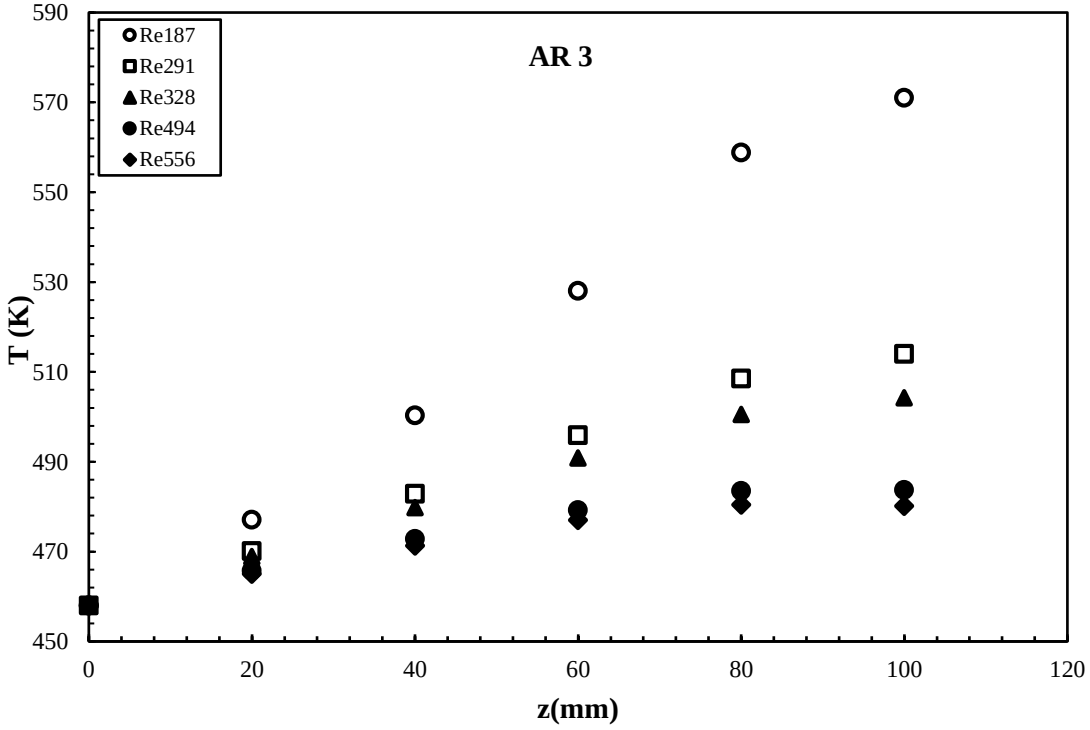
AR 3
Re187
Re291
Re328
Re494
Re556
T (K)
z(mm)
590
570
550
530
510
490
470
450
0
20
40
60
80
100
120

(c)

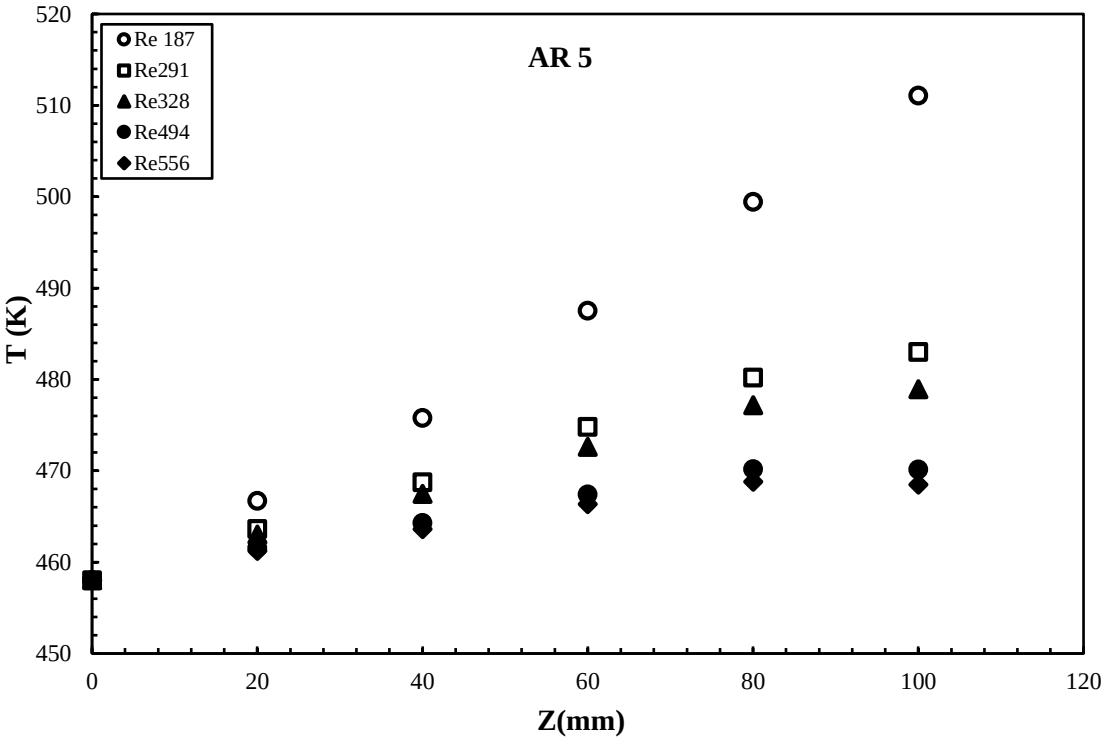

Figure 5.6. Axial temperature distributions at different values of Re for AR: (a) AR 2.5, (b) AR 3 and (C) AR5, inlet temperature T_0 458 K.

The maximum values of temperature obtained were 610, 570 and 510 K for AR values of 2.5, 3 and 5, respectively, at Re value of 187 and thus the highest temperature obtained was at the lowest values of AR. Owing to relevant high porosity, low AR were demonstrated to exhibit high axial, but more importantly radial flow which is responsible of the convective heat transfer from the wall to core the packed bed. This packing feature extended contact time with the heating wall at low Re and promoted temperature gradients or heat transfer rates, particularly by convection, between the heating wall and core of the packing. This is well observed at high values of Re (494 and 556), where insignificant difference in trends of temperatures are exhibited at any value of AR.

A typical temperature profile from the CFD results shows a higher density of data and better continuity than a temperature profile acquired experimentally. Simulations were next extended to the heat transfer distribution inside the packed bed for AR4 (both gaseous phase and solid particles): inlet temperature of fluid, T_0 =298 K, wall temperature T_w= 368 K and Re value of 240

(i.e., laminar regime) as shown in Figure 5.7 (a). The penetration of the heat from the heating wall and toward the radial direction of the bed progressed within the limits of length of the bed. The spatial distribution of temperature reveals that the distribution was not developed smoothly from the inlet to the outlet of the bed, but unevenly propagated towards the centre of the bed. These results by CFD were validated by a good fit with those obtained by Behnam et al., (2013) with a relative deviation about 1.35 %. [23]

The uneven distribution of temperature is well visible in the cross-sectional map of temperature as shown in Figure 5.7 (b). For instance, extends of both the cold region in the centre which forms funnel-like shape and the surrounding warmer region close to wall, depend on the random arrangement of the solid particles, and thus AR values.

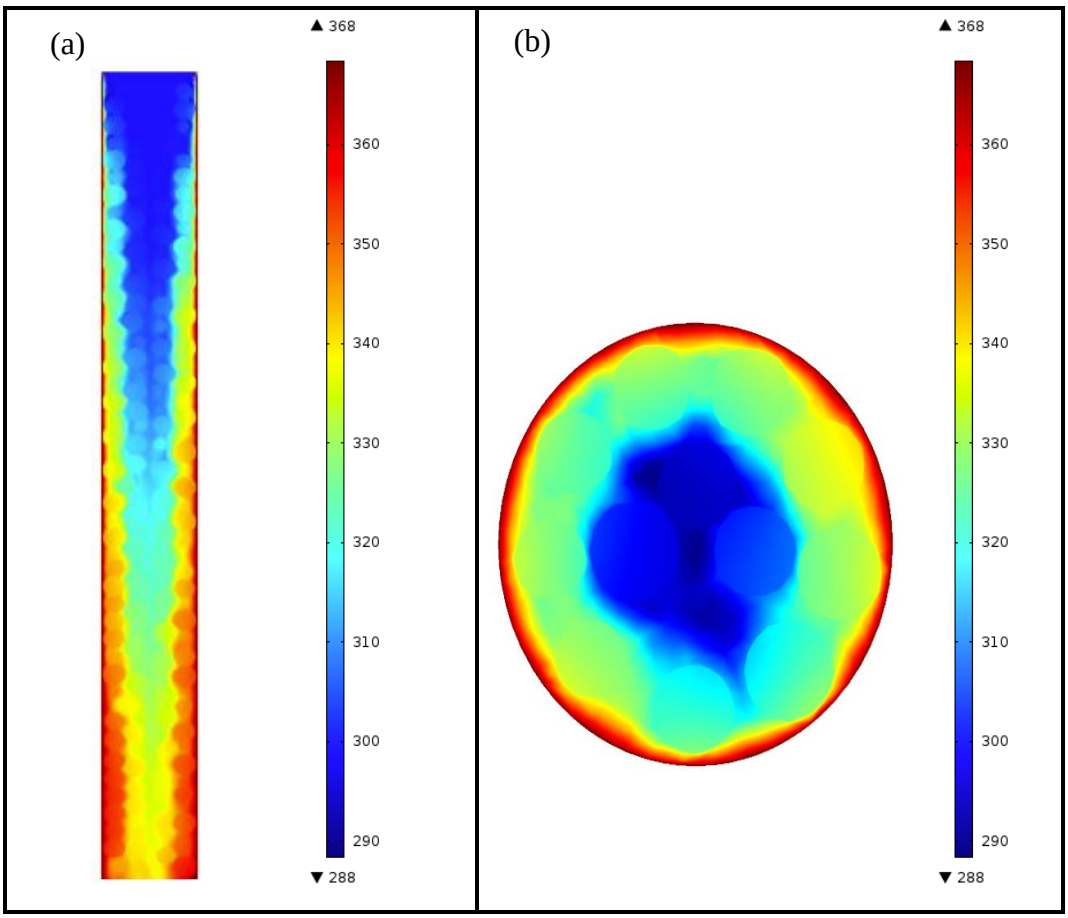

Figure 5.7. (a) 2D contour plot of temperature on the mid-plane. (b) 2D contour plot of temperature on cross section, Re 240. (AR 4)

This figure demonstrates that non-uniformity of the radial temperature distribution decreases with increasing axial distance as shown by the large temperature drop in the vicinity of the wall, particularly at positions in the entrance zone. The large temperature drop is mainly because of the contact resistance at the wall as the wall itself has a low heat transfer resistance. For models for heat transfer in packed bed reactors often lump the contact resistance into the effective wall–fluid heat transfer coefficient, the above results suggest that the heat transfer coefficient is a function of the axial position.

Majority of previous investigations on heat transfer in packed beds only measure the radial temperature distribution at one axial position, mostly at the bed outlet. Figure 5.8 illustrates a comparison of the predicted radial temperature distributions by CFD with those obtained by Behnam et al., (2013) at two different bed depths inside the bed (z/L= 2/3, z/L=1) for same conditions ; T_0 = 298 K , T_w = 368 K and Re value of 240. [23] From the main trend, it is observed that the temperature profile increases when the axial coordinate increases. A deeper coordinate denotes a position further downstream in the bed; since the residence time is larger, therefore the overall temperature is higher.

When the fluid enters through the heated zone, it will experience a large difference in temperature between the centre of the column and the wall. CFD results were in a reasonable agreement with those obtained by Behnam et al., (2013) along the bed. [23] Another aspect that becomes clearer from comparing temperature profiles at different bed depths is the fact that the CFD results were found to be of higher values than the literature ones and this deviation might be attributed to difference in diameter of tube used in this work, which was very small (i.e. 0.01 m) compared with the literature one (i.e. 0.1009 m).

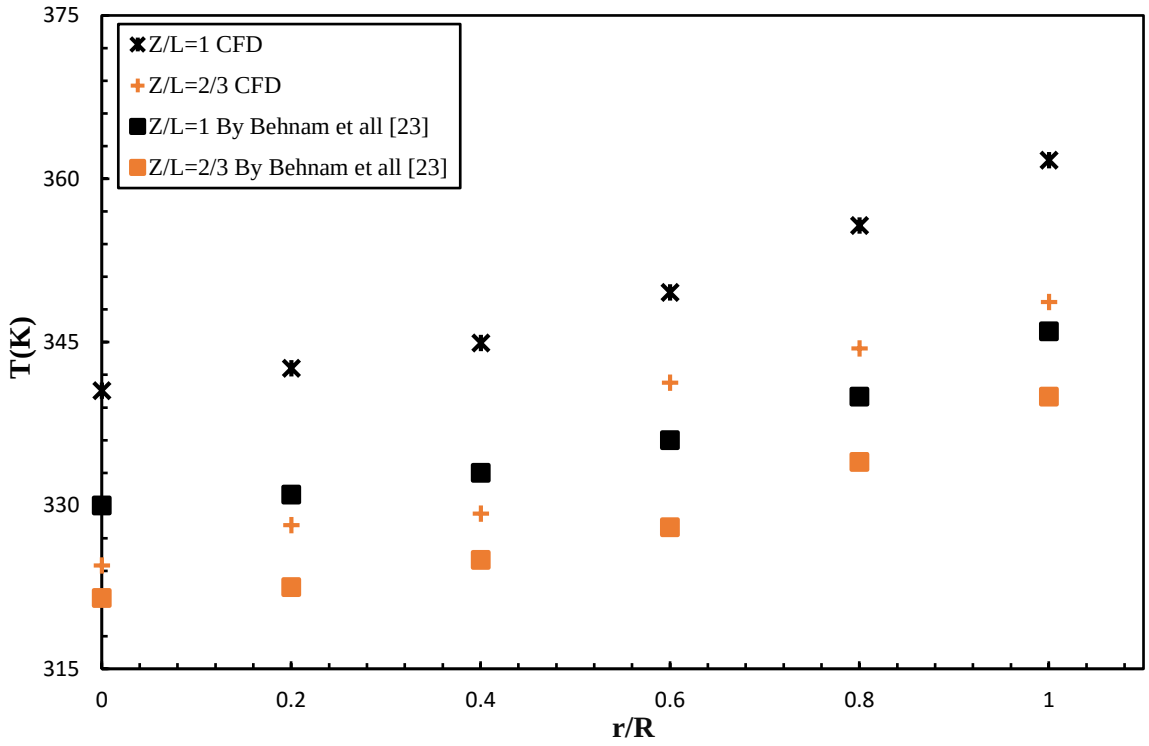

Figure 5.8. Temperature distributions at different bed depths for AR4. (Cross sign: simulation data; square shape: literature data by Behnam et al. [23])

The capability of the CFD tests were validated as well by comparing the heat transfer coefficient from the particle-to-fluid with literature models. The temperature distribution data was therefore investigated by another path which was based on some specific parameters such as the heat flux q (W m^{-2}) and heat transfer coefficient h (W m^{-2}K^{-1}) which was determined by equation (51):

$$q = h.(T_s - T_b) \qquad (51)$$

Where, T_b and T_s are temperature at bulk fluid and solid particles (K), respectively. The non-dimensional heat transfer coefficient, expressed by the Nusselt number(Nu) was generated using equation (52):

$$Nu = (h.dp)/k \qquad (52)$$

Where dp is particle diameter (m) and k is the thermal conductivity (W m^{-1}K^{-1}).

Figure 5.9 shows the relation between Nusselt and Reynolds numbers for the model developed in the present study along with correlations and experimental data reported in the literature. [19,141 and 157] It can be seen that there is a good qualitative agreement among the published correlation, experimental data and the CFD results. Some discrepancies with those obtained by Dixon (1985) are noticed though. [157] These deviations between the CFD results and the literature can be attributed to the use of materials with a wide range of physical and transport properties during the experimental and simulation work. In fact, the heat transfer coefficient depends on both the thermal properties of the bed and the flux rate. The CFD simulation reveals that when the Re values increase, the value of Nu increases as well. In addition, the discrepancies in Nu values were promoted by the differences in experimental conditions (i.e., particles characteristics, height and diameter of the packed bed and assumptions of boundary conditions).

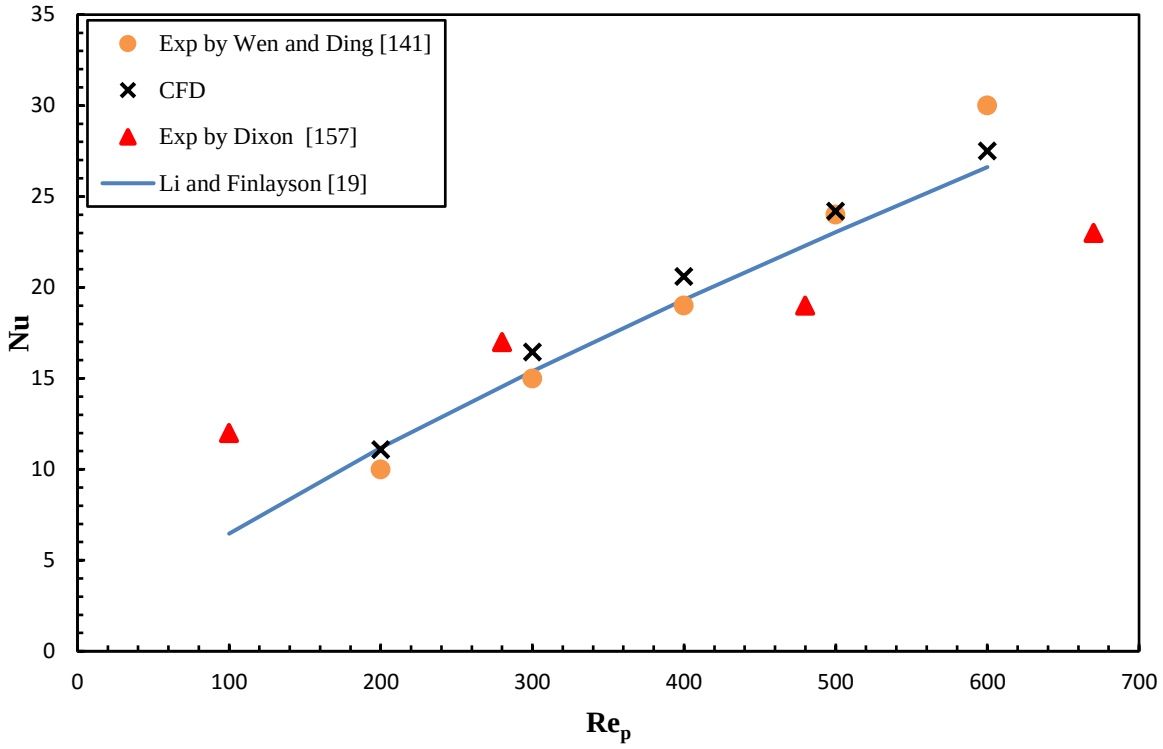

Figure 5.9. Compression of the simulated Nusselt number, Nu with published correlations, for AR 4

Moreover, the effect of inlet feed temperature along the packed bed was studied and validated by comparison with Jaree et al., (2003) as shown in Figure 5.10. It can be seen that there is a reasonable agreement in temperature trends between CFD results and literature ones. [64] It should be noticed that at each steady operating condition, temperature profile reached maximum values and then slowly dropped toward the end of the packed bed. A maximum value of CFD was found at 455 K while it was reported about 440 K by Jaree et al., (2003) both operated at inlet feed temperature T_0 of 406 K. [64] In fact, perturbations of feed temperature, flow or cooling rate took place on a shorter time scale, short enough that the reactor could not remain in a steady state. The resulting of this situation is non-steady state or dynamical response. The deviation between CFD results and literature ones and again is attributed to the different scales used such as particles characteristics, height and diameter of the packed bed.

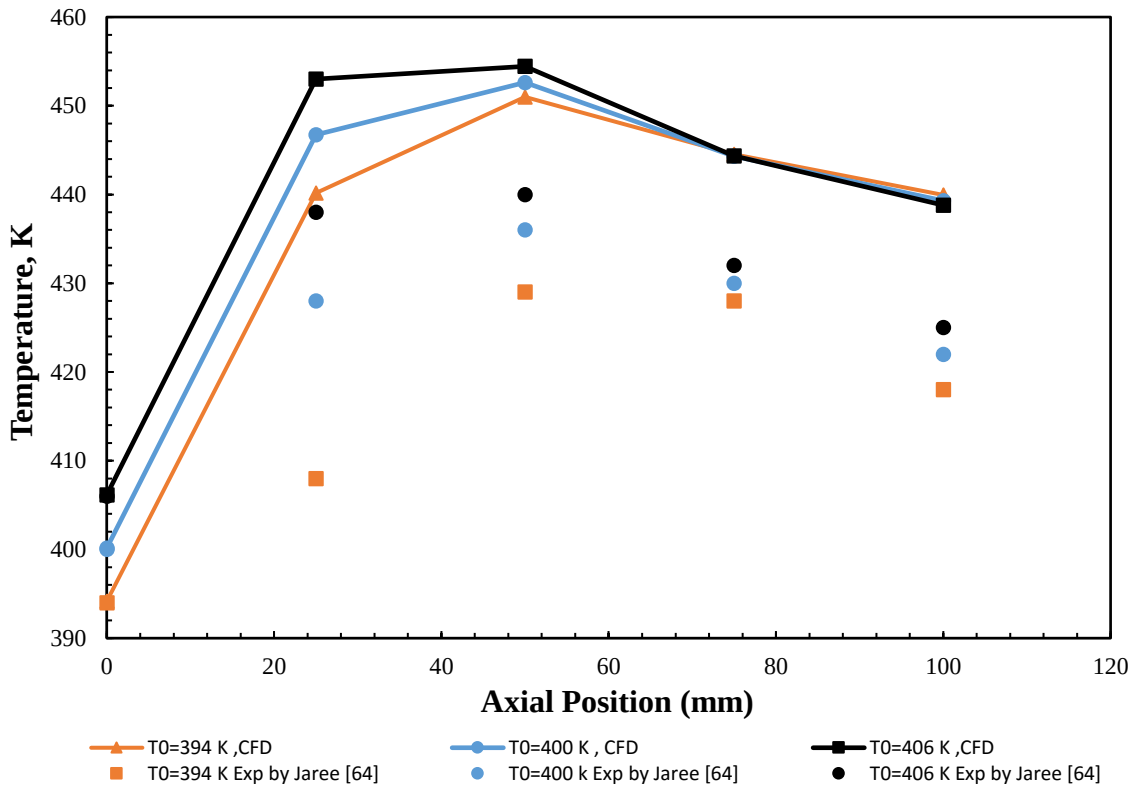

Figure 5.10. Temperature profiles for different inlet feed temperature, T_0; (lines: simulation data; Dots: Experimental data by Jaree et al. [64]

The contribution of heat conduction in the solid was significant depending on its thermal conductivity and the fluid velocity. When the fluid temperature changes around the solid particles, temperature gradients over these particles develop as well. The distribution profiles of temperature along the packed bed with time progressing for ARs 2.5 and 5 under inlet feed temperature T_0 458 K and Re 187 were examined as shown in Figure 5.11(a, b). It shows that the type of behaviour of temperature obtained from the model depends on the random arrangement of particles inside the bed. It is interesting to observe that the strong effect of positions of particles on the temperature profiles, particularly for small AR i.e. 2.5, as demonstrated in Figure 5.11 (a). It can be seen that the maximum value of the temperature is located in the region close to the end of the bed for both ARs 2.5 and 5. Also, there is a rapid variation in value of temperature at t=0.83 min with less uniformity of distribution of the heat for both AR 2.5 and 5.

It should be noticed that by increasing the time, low temperature values (cold zones) are found for AR 2.5 at the centre of the bed which is attributed to the high porosity in this region (as discussed that in chapter 4), while large values of temperature are observed on the solid particles and the wall. On the other hand, the variation of temperature for AR 5 after t = 0.83 min was slower along the packed bed and the propagation of heat transfer was more uniform as shown in Figure 5.11 (b), which is attributed to presence of more solid particles in this packing. At t=16.6 min, both ARs 2.5 and 5 reached steady state conditions as shown in Figure 5.11(a, b). The influence of heat transfer was more visible for AR 2.5 than the large one AR5. Moreover, this figure reveals that the maximum value of temperature was 618 K for AR 2.5 and 521 K for AR5.

(a)

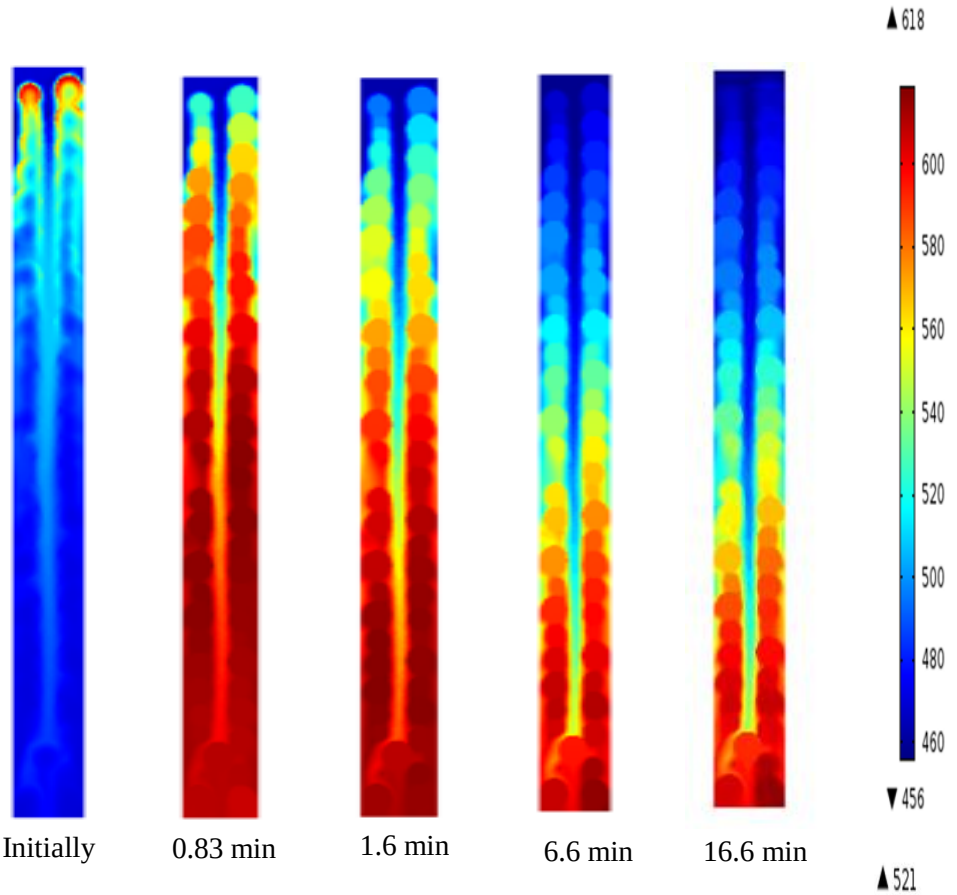
618
T, (K)
600
580
560
540
520
500
480
460
456
Initially
0.83 min
1.6 min
6.6 min
16.6 min

(b)

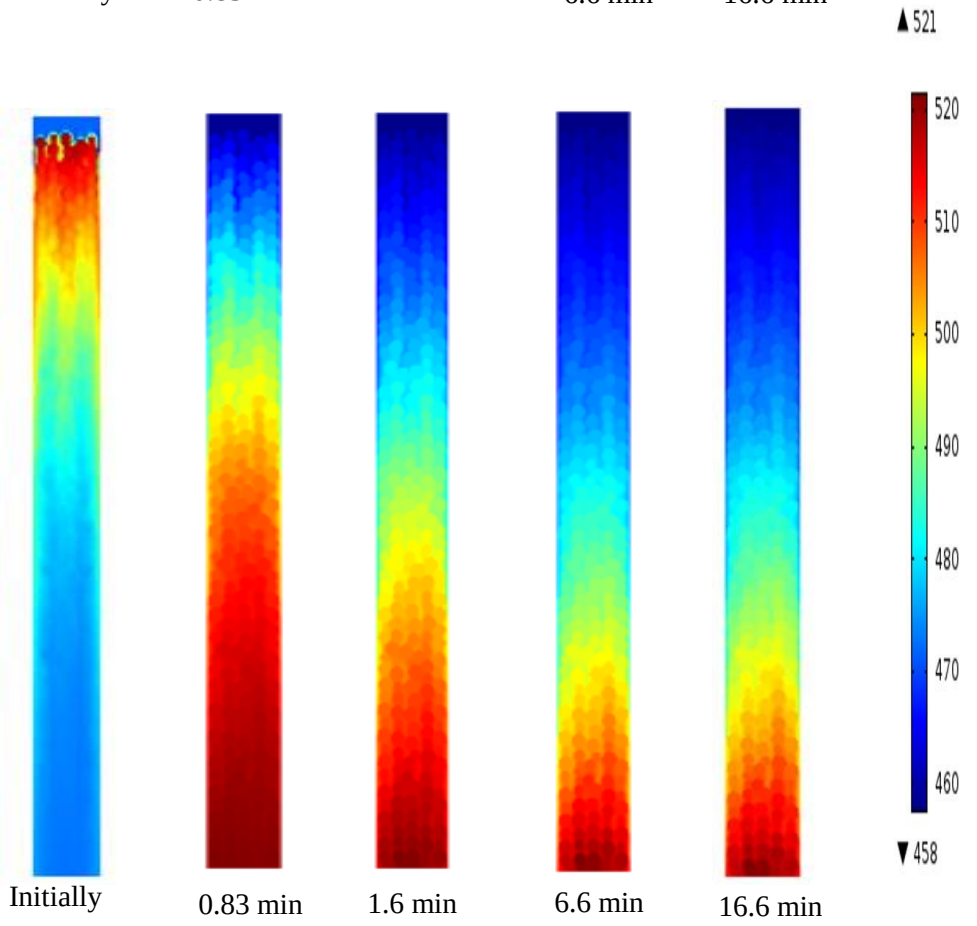
521
T, (K)
520
510
500
490
480
470
460
458
Initially
0.83 min
1.6 min
6.6 min
16.6 min

Figure 5.11. 2D map of temperature distribution obtained by CFD with time at; T_0 458 K and Re 187: (a) AR 2.5 and (b) AR 5.

5.4.3 Summary of the chapter

Heat and mass transfer were simulated by 3D CFD modelling in a cylindrical packed bed of spherical catalyst particles of gas/solid reactive system for different ARs (1.5, 2.5,3,4 and 5). Since exothermic reactions such as the catalytic CO oxidation are carried out in a heated narrow reactor tube, the results of this chapter validated temperature gradient, uneven flow and heat and mass inside the packed bed. The kinetics of the CO oxidation on alumina catalysts was well described by 3D simulation. The conversion of CO oxidation was significantly function of reaction temperature and feed compositions. Flow rates and size of particles played a significant role in the catalytic oxidation reaction. The conversion profiles from CFD simulation were in a reasonable agreement with those obtained from the different published works.

The 3D CFD modelling, as a tool for predicting temperature trends of exothermic reaction, could offer a clear vision on behaviour of the flow and the heat inside the reactor. This behaviour is sometimes not possible to capture experimentally. The 3D CFD modelling provided a detailed vision of temperature distribution in the interior of the bed and discriminated between temperature of the solid and gaseous phases. It allowed analyse of heat transfer phenomena and achieved results that are qualitatively and quantitatively comparable with those published. Radial temperature distributions and heat transfer coefficients were in good agreements with existing empirical models. Contour maps of temperature also showed that temperatures propagation with time evolution throughout the bed were function of operating conditions and the scale of the packed bed.

Chapter 6

6. Analysis of Catalyst Deactivation in Packed Bed Reactors

6.1 introduction

The deactivation of catalysts is an important issue in any catalytic process, e.g. steam reforming, dehydrogenation of alkanes, cracking and so on. In case of local carbon laydown, this may lead to heterogeneous mechanical or chemical breakdown of catalyst particles and decrease reaction rates in unpredictable way, and thus associated heat sink and hot spots would not be avoided. This is particularly a problem for reactors with at low AR (i.e., $3 \leq AR \leq 10$). [24] The catalyst deactivation affects the lifetime, the activity and the possibly selectivity of catalyst. As a result, catalyst deactivation decreases the rate, the conversion and the productivity of the process. In addition, catalyst deactivation causes an interruption of process operation for either replacement or regeneration of catalyst. The detailed deactivation information inside a reactor plays then an important role in industry. However, in almost all industrial reactors there is no mean available to directly measure the local catalyst activity.

As reported in the literature section (chapter 2), extensive works have been carried out on modelling catalyst deactivation in packed bed reactors using 1D approach .[56, 66 and 151] However, only two investigations to our knowledge have been carried out by using a 3D modelling which were published by Dixon's group (2010) and Wehinger et al., (2015) .[24 and 158] Works based on 1D modelling allowed understanding the physical phenomena inside packed bed reactors but were not be able to reflect local information in terms of velocity, mass and heat transfers and catalyst deactivation. As to the work on 3D modelling and deactivation, it was limited by operations under stead-state operations. Herein, both 2D and 3D models were investigated in order to get a comprehensive understanding of detailed catalyst deactivation in packed bed reactors which is difficult to achieve experimentally.

In this chapter, the catalyst activity is studied by simulation using (COMSOL Multiphysics version 4.4) which allows get access into the inner tube. This investigation operates carbon monoxide oxidation which was discussed in previous chapter, as first-order exothermic reaction model of a

gas/solid system in a packed bed reactor. Some important properties such as the effect of (1) deactivation rate expressed in terms of dimensionless activation energy of deactivation γ_D and the Damköhler number of the deactivation Da_D (ratio of residence time and reaction time; (2) Peclet number in terms of mass and heat dispersions Pe_1,Pe_2, respectively; (3) wrong-way behaviour of the temperature; (4) internal mass transfer coefficient; and (5) thermal inertia in terms of heat capacity of the solid packed bed, on the deactivation profiles are investigated by 2D and 3D CFD modelling.

6.2 Model development of deactivation

A combination of heat, mass and momentum balances along with the kinetic model of reaction and catalyst deactivation are used for screening local catalyst activity inside the porous media. The catalyst activity is studied by simulation using (COMSOL Multiphysics version 4.4), which allows to obtain access to the internal packing inside the tube. This investigation was carried out on carbon monoxide oxidation in a gas/solid system for ARs 3 and 4 under dynamic (transient) operations. The PBR was built by DEM as shown in chapter 3. The CFD code numerically solved the Navier-Stokes equations and associated with differential equations for energy and mass balances as well as deactivation model.

6.2.1 Model description by 2D modelling

In this study, a 2D pseudo-homogeneous model through porous media was first used to simulate an adiabatic packed-bed reactor operating a first-order exothermic reaction. The 1D pseudo-homogeneous mass and energy balances developed by Jensen and Ray (1982) and Jaree et al., (2008) were extended in this work to 2D modelling which includes a momentum balance. [159 and 59] A first-order deactivation model was applied in order to study the effect of catalyst deactivation on the thermal behaviour at various ARs of the packed bed. The 2D modelling was carried out for two reasons: (1) to justify our CFD modelling by comparing the results with the 1D modelling of Jensen and Ray (1982) and Jaree et al., (2008), and (2) to consider the results of 2D modelling, which do not require large memory and computation time and these results will be compared with 3D modelling later. [159 and 59]

- Momentum balance :

$$\nabla \varepsilon \rho u u = -\varepsilon \nabla P + \varepsilon \mu \nabla^2 u + \varepsilon F \qquad (53)$$

$$\nabla u = 0 \qquad (53\ a)$$

The drag force per unit of volume F is expressed using Ergun's relation as:

$$F = -\frac{\mu u}{K} - \beta \rho u^2 \qquad (53\ b)$$

The permeability of the porous media K and the non-Darcy term β are calculated from Zhavoronkov's model.

$$K = \frac{\varepsilon^3 dp^2}{A(1-\varepsilon)^2},\ \beta = \frac{B(1-\varepsilon)}{\varepsilon^2 dp} \qquad (53\ c)$$

$$u\big|_{\tau=0} = u_0, \nabla u\big|_{\tau=1} = 0, \qquad (53\ d)$$

- Mass balance for both (gas and solid phases)

$$\frac{\partial C_i}{\partial t} + \nabla \cdot (-D_i \nabla_{Ci}) + u \cdot \nabla C_i = R_i \qquad (54)$$

- Heat balance for (both gas and solid phases)

$$(\rho_g Cp_g + \rho_s Cp_s)\frac{\partial T}{\partial t} + \rho_g Cp_g u \cdot \nabla T = \nabla \cdot (k \nabla T) + Q \qquad (55)$$

$$Q = \Delta H_R R \qquad (55\ a)$$

Where μ is the viscosity (kg m^{-1} s^{-1}), C_p is the heat capacity (J kg^{-1} K^{-1}), k is the thermal conductivity(W m^{-1} K^{-1}), D_i is the diffusion coefficient (m^2 s^{-1}), R_i is the stoichiometric chemical reaction rate (mol s^{-1} kg^{-1}), Q is the heat generated by the chemical reaction, and subscripts *s* and *g* refer to the solid (catalytic) and gas phases, respectively. A linear first-order kinetic model was assumed as it eliminates effects of reactant or product activation or inhibition of surface kinetics (model of Eley, Langmuir-Hinshelwood, etc.) and facilitates model convergence. The model was applied to the reaction rate model of CO oxidation by Amphlett et al., (1996) as reported in previous chapter and it can be written as shown in equation (56): [144]

$$Rco = a\, Ae^{-\frac{E}{RT}} c_{co} \qquad (56)$$

Where, A is the pre-exponential Arrhenius factor, (A = 0.026 s^{-1}) and a, is the catalytic activity, E is activation energy J $mol^{-1,}$ R is the universal gas constant (R=8.314 J mol^{-1} K^{-1}) and $C_{co,}$ is concentration of CO (mol m^{-3}). [144]

- Deactivation rate

A simplified power law deactivation rate model was assumed. This model applies to a single mechanism of activity deactivation (parallel deactivation) which was discussed in details in chapter (2).

$$\frac{d_a}{d_t} = -k_d C_{co} \qquad (57)$$

Where k_d is the deactivation rate constant ($k_d = A_D e^{-\frac{E_D}{RT}}$), E_D is the activation energy of deactivation and A_D is the pre-exponential Arrhenius factor of deactivation.

Initially, the reactor was set at steady-state and then the deactivation process was switched on causing transient profiles of temperature, concentrations and catalyst activity. The operating conditions were selected based on conditions of 1D model of Jaree et al.,(2008) and expressed as follows: velocity u=0.5 m s^{-1}, inlet concentration C_0 = 0.533 mol m^{-3}, inlet temperature T_0 = 413 K, ρ_s= 1230 kg m^{-3}, ρ_g = 1 kg m^{-3}, Cp_g = 1045 J kg^{-1} K^{-1} and Cp_s = 900 J kg^{-1} K^{-1}. [59]

6.2.2 Model description by 3D modelling

The simulation by 3D modelling was carried out under similar operating conditions used in the 2D modelling. The effect of deactivation rates, mass and heat transfer on local deactivation under steady-state and transient operations was investigated. Governing equations which couples balances of momentum, heat and mass transfers in 3D random packed bed reactor of various ARs.

- Momentum balance:

Navier–Stokes and continuity equations for momentum and mass conservations, respectively, were used. A uniform velocity profile was assumed at the inlet whereas the pressure at the exit was assumed to be fixed to the local atmospheric pressure. In addition, no-slip boundary condition at the entire solid (packing or wall)-fluid interface was considered.

$$\rho(u.\nabla u) = -\nabla pI + \nabla.\left[\mu(\nabla u) + (\nabla u)^T - \frac{2}{3}\mu(\nabla.u)I\right] \qquad (58)$$

$$\rho\nabla.u = 0 \qquad (58\ a)$$

$$u\big|_{\tau=0} = u_0, P\big|_{\tau=1} = P_0 \qquad (58\ b)$$

- Mass balance in the gas phase :

$$\frac{\partial Ci}{\partial t} + \nabla\cdot(-D_i\nabla_{Ci}) + u\cdot\nabla C_i = 0 \qquad (59)$$

- Mass balance in the catalytic phase:

Mass transfer in the catalytic phase was assumed to be driven by diffusion and free of convection (negligible velocity) and the chemical reaction occurs in the catalytic phase only.

$$\frac{\partial Ci}{\partial t} + \nabla \cdot (-D_{ie} \nabla_{Ci}) = R_i \qquad (60)$$

Where D_{ie} is the effective diffusion coefficient which was approximated based on the bulk diffusion coefficient , D_i and the catalyst particle properties (porosity ε_c and tortuosity τ_c):

$$D_{ie} = \frac{\varepsilon_c D_i}{\tau_c} \qquad (60\ a)$$

The diffusion coefficients were assumed to be unaffected by catalyst deactivation. The reaction rate was written as follows:

$$R_i = a\ A\ e(-\frac{E}{RT})\ C_{CO} \qquad (60\ b)$$

- Heat balance in the gas phase:

$$\rho_g Cp_g \frac{\partial T}{\partial t} + \rho_g Cp_g u \cdot \nabla T = \nabla \cdot (k \nabla T) \qquad (61)$$

- Heat balance in the catalytic phase:

$$\rho_s Cp_s \frac{\partial T}{\partial t} = \nabla \cdot (k_s \nabla T) + Q \qquad (62)$$

$$Q = R \Delta H_R \qquad (62\ a)$$

- Deactivation rate

Finally, the deactivation rate was written as follows:

$$\frac{\partial a}{\partial t} = A_D \; e \; (-\frac{E_D}{RT}) C_{CO} \qquad (63)$$

The first step in 3D modelling was to use same operating conditions illustrated in the 2D modelling. The only change here was then the use a 3D geometry and 3D flow dynamics model inside a generated PBR by DEM, instead of the simplified 2D geometry. The effect of deactivation rate in terms of dimensionless activation energy of deactivation Υ_D, Damköhler number of the deactivation Da_D, wrong-way behaviour of the temperature, internal mass transfer coefficient, mass and heat dispersions and thermal inertia of the solid catalytic phase were investigated at various ARs (i.e., 3 and 4) of the packed bed. The results obtained by 3D modelling were compared with those achieved by the 2D modelling.

6.3 Results and Discussions

6.3.1By 2D Model

6.3.1.1Effect of dimensionless activation energy of deactivation (Υ_D)

The dimensionless activation energy of deactivation can be defined as shown in equation (64):

$$(\Upsilon_D = E_D/RT_0) \qquad (64)$$

An increase in the activation energy of deactivation, Υ_D is expected to promote the deactivation. Figures 6.1 (a, c) show the main trend of the catalyst activity coefficient along dimensionless axial position ($\zeta = z/L$) of the packed reactor by 2D model as a function of dimensionless activation energy of deactivation, Υ_D ranging from 0 to 17. Deactivation constant profiles from Jaree et al., (2008) are also listed in same Figure at (b) and (d). [59] Because of the deactivation, the catalyst activity is not uniform through the reactor while it exhibits monotonic increase in temperature towards the end of the bed as shown in Figure 6.1 (e).

The front section of the bed has a small degree of deactivation because the thermal impact of the Arrhenius term in the rate of catalyst deactivation. The temperature increases throughout the reactor coordinate until it reaches the adiabatic temperature rise. This causes a rapid drop in catalytic activity in the reaction zone. After most of the reactant molecules are consumed, the deactivation rate decreases quickly as indicated by the jump in catalyst activity near the exit-end of the reactor bed. Increasing Υ_D speeded up the reaction rate of CO oxidation, releasing thermal energy, which in turn accelerates the deactivation rate. Decreasing Υ_D causes however the zone of catalyst deactivation to shift forward to the front section of the reactor while the reaction zone was still further down in the catalyst bed as shown in Figure 6.1(a). The case of zero deactivation energy Υ_D, the rate of catalyst deactivation will depend only on the reactant concentration.

(a)

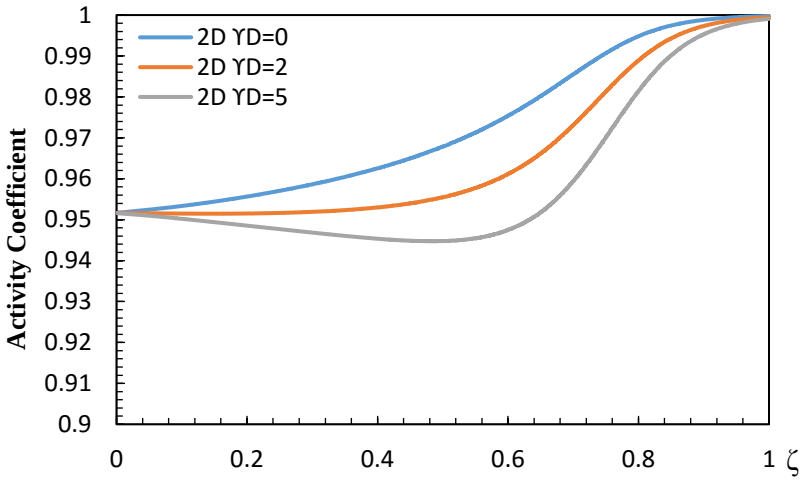

(b)

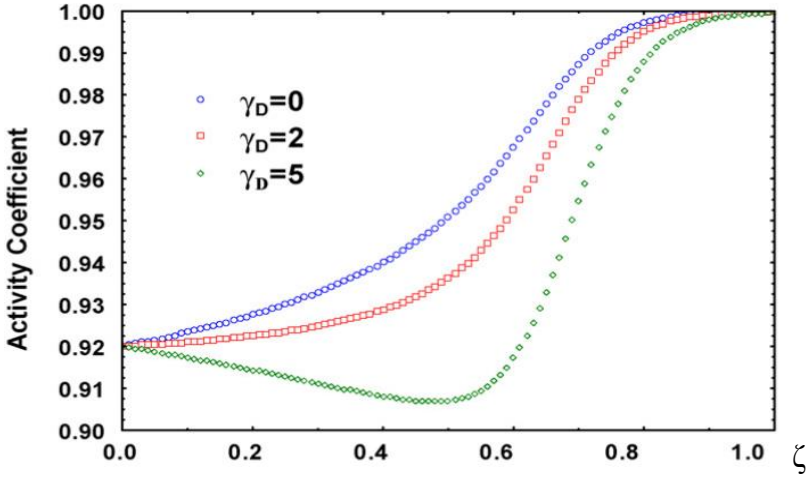

(c)

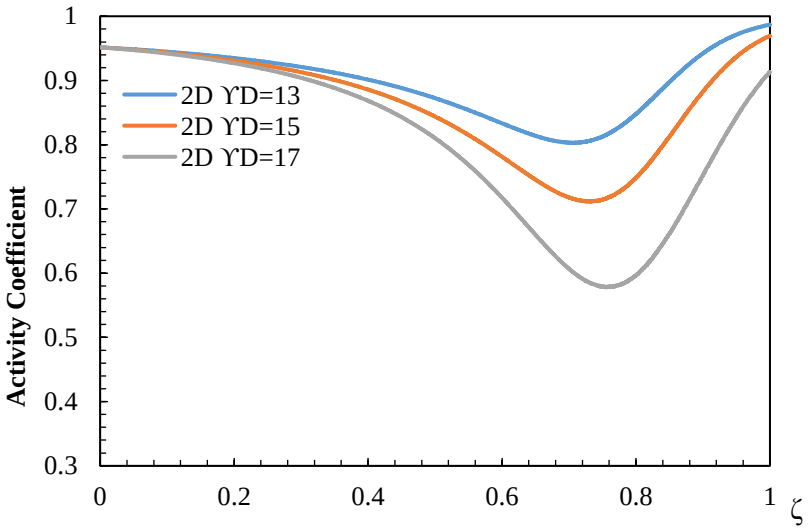
Activity Coefficient
1
0.9
0.8
0.7
0.6
0.5
0.4
0.3
0
0.2
0.4
0.6
0.8
1
ζ
2D ϒD=13
2D ϒD=15
2D ϒD=17

(d)

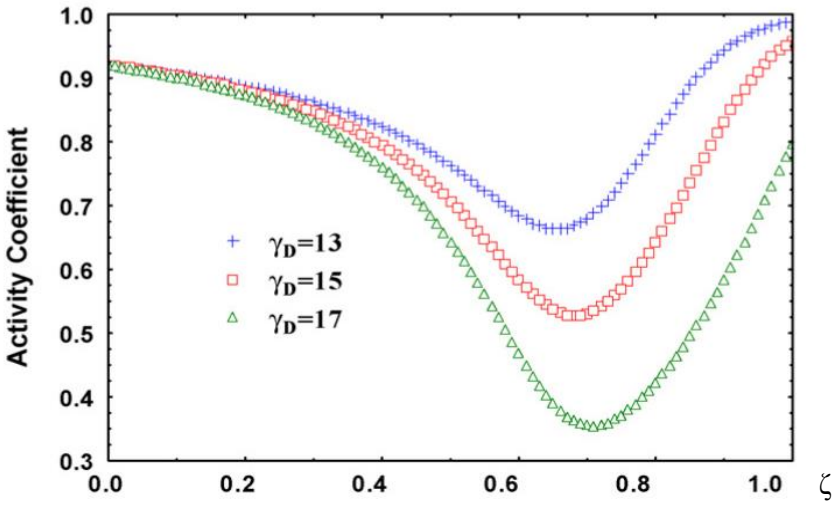
Activity Coefficient
1.0
0.9
0.8
0.7
0.6
0.5
0.4
0.3
0.0
0.2
0.4
0.6
0.8
1.0
ζ
γD=13
γD=15
γD=17

(e)

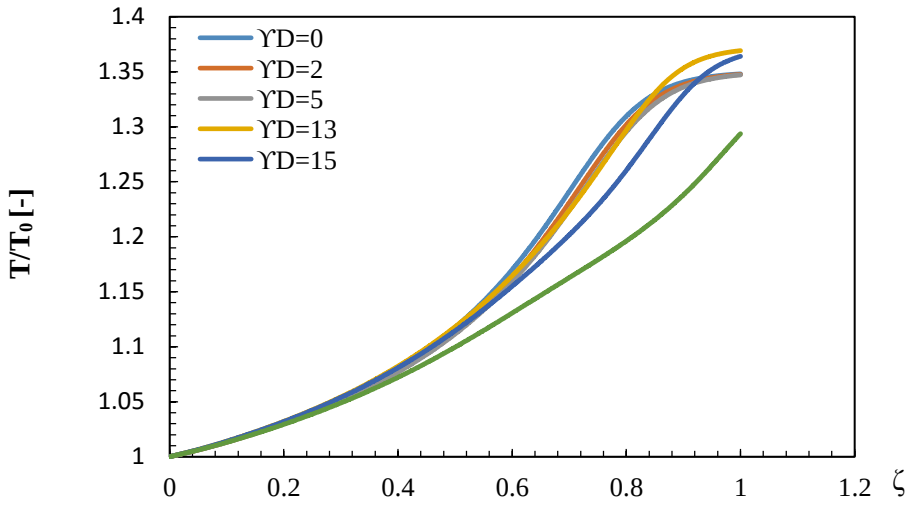

Figure 6.1. Effect of deactivation energy (Υ_D) on the catalytic activity profile by (2D) for AR 3; (a) and (c) by CFD simulation: (b) and (d) are Jaree's results [59]: (e) Temperature by CFD, (Da_D = 4×10^{-6}, P_{e1} = 300, P_{e2} = 40, Da = 0.4, Υ =15 and at τ = 50,000)

The CFD results show a good agreement with those presented by Jaree et al., (2008). [59] In the present simulation, a catalytic activity coefficient for different Υ_D (ranging from 0 to 17) starts from 0.95 with a deviation of 0.03 from starting values of Jaree's. Activity coefficient curves exhibit similar changing trends; (i.e., an increase of the Υ_D moves the deactivation zone forward to the exit of the packed bed). However, at Υ_D = 0, the curve goes up slowly, while it shows a relatively bigger slope in the literature; at Υ_D = 2, the curve keeps constant values of activity till 0.4 ζ(ζ= z/L), length of the packed bed and then rises progressively while it increases straight from the inlet to the outlet in the literature; for Υ_D = 5, both curves go down with drop of 0.006 and 0.015, respectively; at Υ_D = 13, 15 and 17, the deactivation zone appears between 0.6L to 0.8L, while the drop in simulation is much smaller (i.e., 0.15, 0.25 and 0.35) compared with 0.27, 0.40 and 0.57 in Jaree's work (2008) ,this drop increases gradually with the increasing value of Υ_D. [59]

It should be noticed that the rate of deactivation is the fastest at the entrance of the catalytic bed, where the concentration is the highest. This suggests that locating the reaction zone and knowing the deactivation energy may potentially help to minimize the cost of refilling catalyst significantly.

6.3.1.2 Effect of the Damköhler number of deactivation reaction (Da_D)

Figure 6.2 (a) illustrates the catalyst activity coefficient profiles along dimensionless axial position ($\zeta = z/L$) as a function of Damköhler number of deactivation (Da_D), that can be defined as (residence time of the gas in the packed bed to deactivation time).

$$Da_D = \frac{1}{u} A e^{-\left(\frac{E_D}{RT_0}\right)} \qquad (65)$$

The Damköhler number (Da_D) affects the catalyst activity coefficient in the same way as the dimensionless activation energy of deactivation, (Υ_D) does. For high values of Damköhler number (Da_D), catalyst activity decreased, particularly in regions towards the exit, at 0.7ζ-0.8ζ. It is clear, therefore, that local deactivation can be driven to the exit of the packed bed by operating the packed bed at high temperatures or low velocity rates. By comparison between this work with those obtained by jaree et al., (2008) as shown in figure 6.2 (b), a reasonable agreement is demonstrated in the main trend of activity profiles between this work and literature ones. [59] The values of activity coefficients however in Jaree's work reached deeper values than those obtained in our model.

(a)

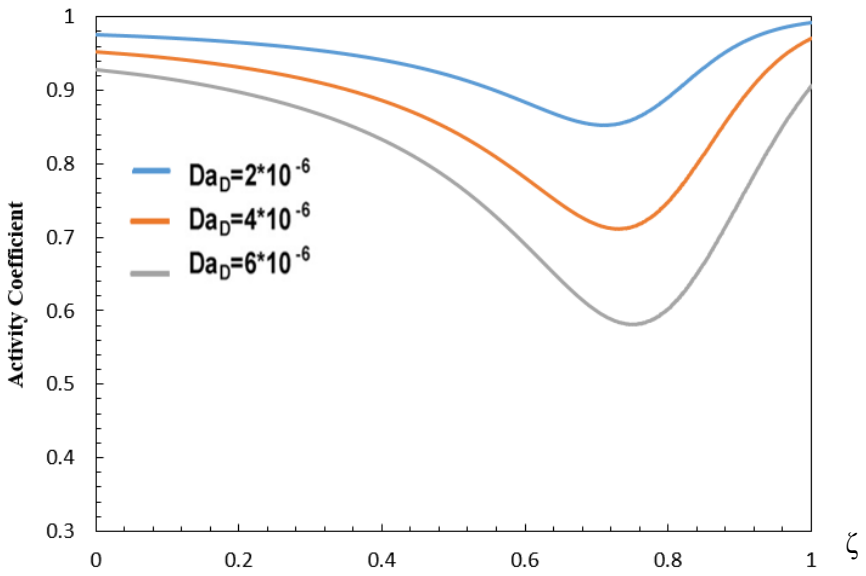

(b)

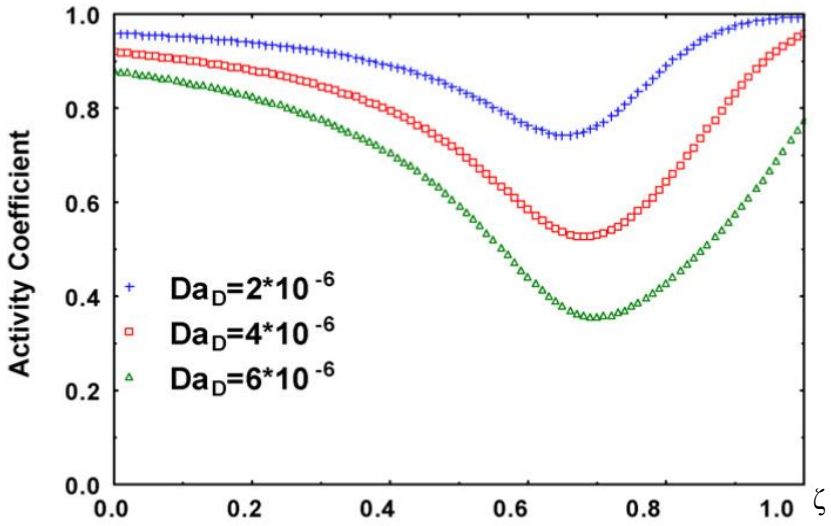

Figure 6.2. Effect of Da_D on the catalytic activity profile (2D) for AR 3; (a) by CFD simulation and (b) Jaree's results [59] :(P_{e1}=300, P_{e2}=40, Da= 0.4, Υ =15, Υ_D =15 and at τ = 50,000)

6.3.1.3 Effect of local deactivation on the temperature runaway " wrong-way behaviour"

Local deactivation was investigated under transient operating conditions. Local deactivation is known to promote higher wrong-way temperature fluctuations (amplifications or extinctions) in packed beds, and therefore, can be predicted if larger wrong way behaviours are observed. [86] Previous section on effect of rate of catalyst deactivation in terms of Damköhler number and activation energy has shown local catalyst profiles which were driven by the differential rates of heat and mass through the packed bed reactor. Temperature runways were not observed at steady-state operations. Local catalyst deactivation was found when adjacent two deactivation rates take place. The lower rate of deactivation accelerated the rate of CO oxidation which in turn released enough thermal energy to dislocate the reaction front of CO oxidation and to propagate through the packed bed. A higher rate of deactivation rate was then generated, driven by the thermal energy, inhibited CO oxidation in the zone adjacent to the reaction zone, generated local concentration of reactant CO travelling through the reactor however, temperature overshoots did not develop temperature runways as shown in Figure 6.1 (e).

In this section, change in inlet temperature is introduced to screen profiles of local deactivation and temperature runaways in packed beds of low AR under conditions of large adjacent deactivation rates. The system was set at steady-state operation, the deactivation was switched on at τ= 1,000 and inlet temperature was decreased from T_0=413 K with a rate of 0.001 K/s at τ= 2,000 as illustrated in Figure 6.3.

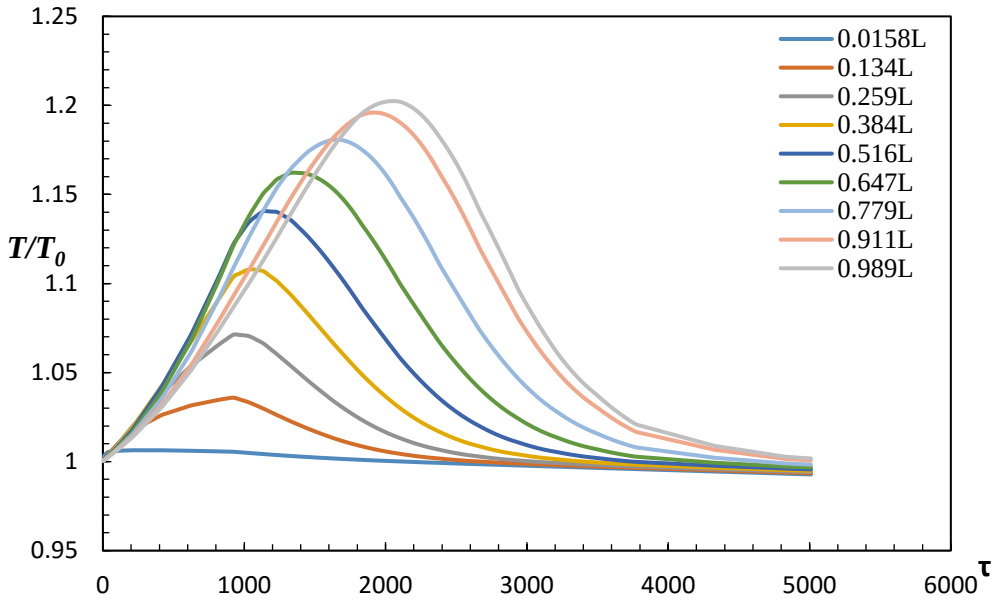

Figure 6.3. Temperature at different axial positions; (Da_D = 4×10^{-6}, Da = 0.4, Υ= 15, Υ_D= 5.5 and τ_{total} = 5000)

Figure 6.3 shows temperature change at different axial positions along the reactor during catalyst deactivation. In the pre-reaction zone (After switching the deactivation at τ= 1,000), temperatures decrease because less CO molecules were converted to product and less heat was released due to catalyst deactivation pushing the wave of un-reacted CO downstream (front of the bed). At the start of deactivation at 1000, the front zone temperature decreased but when the inlet temperature started to decrease at 2000, the entire zone temperature increased instead and went up to a certain maximum value. This wrong way behaviour was more remarkable at the zone near the exit about 0.7L-0.9L. This occurred because when the concentration wave arrived at the reaction front, the auto-catalytic nature of the main reaction took on and released additional heat travelling at significantly higher temperatures than that of the adiabatic value. Overall, the study of the catalysts deactivation was quite satisfactory because the simulation allowed visualization of local deactivation and how it can be promoted under differential heat and mass rates through the bed.

Differential rates for local deactivation and temperature runways were more pronounced under transient operations of inlet temperature.

6.3.2By 3D Model

The simulation by 3D modelling was carried out under similar operating conditions used in the 2D modelling. The only change was on the use of a 3D geometry which implies the 3D flow, mass and heat transfer model. The effect of deactivation rate in terms of dimensionless activation energy, Damköhler number, mass and heat transfers were investigated for AR values of 3 and 4 of the packed bed. The results were compared with those obtained by the 2D modelling.

6.3.2.1Effect of dimensionless activation energy of deactivation (Υ_D)

Figures 6.4 illustrates a cut line inside the packed bed for catalyst activity coefficient along dimensionless axial position (ζ) by 3D modelling with different values of Υ_D, for ARs 3 and 4. It can be seen that for a specific AR, the activity coefficient starts at the same value at any value of Υ_D, and with the increase of Υ_D, the value of activity coefficient decreases with a moving wave towards the front of the packed bed. 3D models have shown similar trends to 2D of deactivation profiles when deactivation rate, mass and heat transfer were varied. The extent of catalyst deactivation in the 3D models was larger than in the 2D models as shown in Figure 6.4 Furthermore, the deactivation waves moved more towards the front of the packed bed in the 3D models. However, modelling by 3D allowed local profiles of deactivation to be observed at packing pore level. The deactivation was quite asymmetrical along axial and radial directions of the particle surface leading to uneven rates of thermal expansion and contraction, which have the potential to break the particle, or to cause local deactivation associated with temperature runaways.

(a)

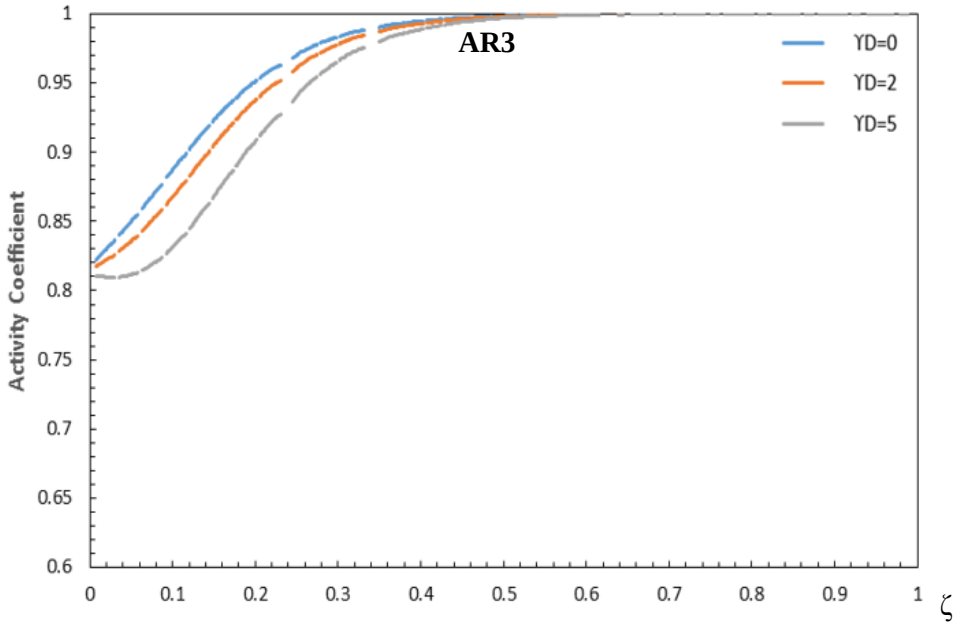
AR3
YD=0
YD=2
YD=5
Activity Coefficient
1
0.95
0.9
0.85
0.8
0.75
0.7
0.65
0.6
0
0.1
0.2
0.3
0.4
0.5
0.6
0.7
0.8
0.9
1
ζ

(b)

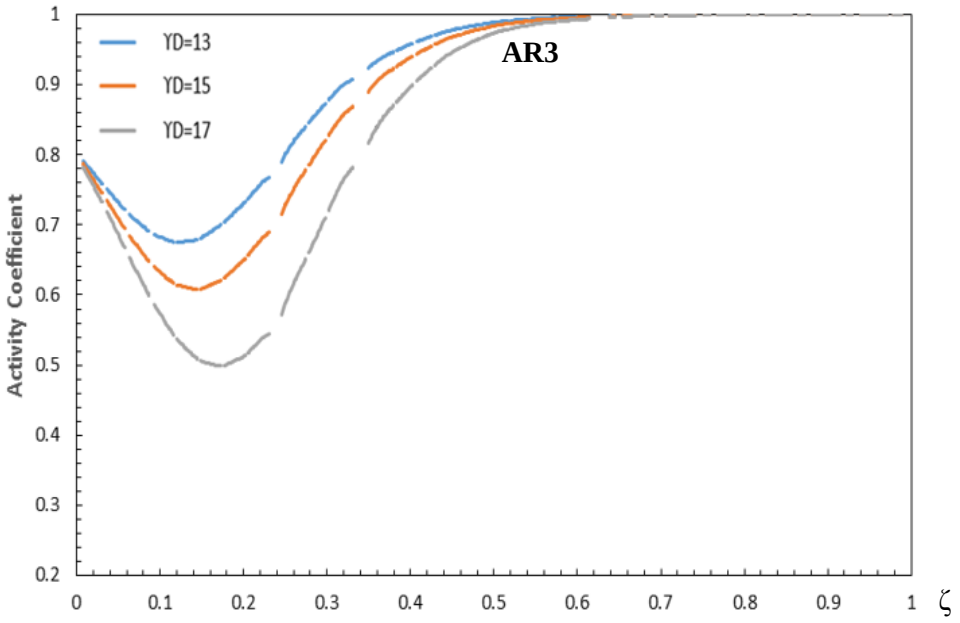
AR3
YD=13
YD=15
YD=17
Activity Coefficient
1
0.9
0.8
0.7
0.6
0.5
0.4
0.3
0.2
0
0.1
0.2
0.3
0.4
0.5
0.6
0.7
0.8
0.9
1
ζ

(c)

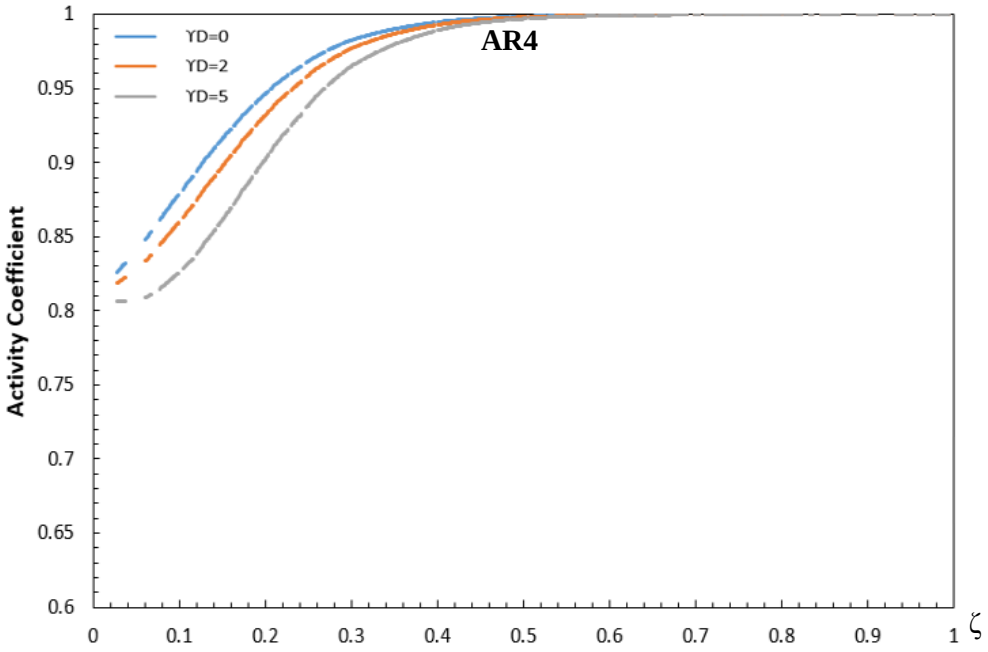

(d)

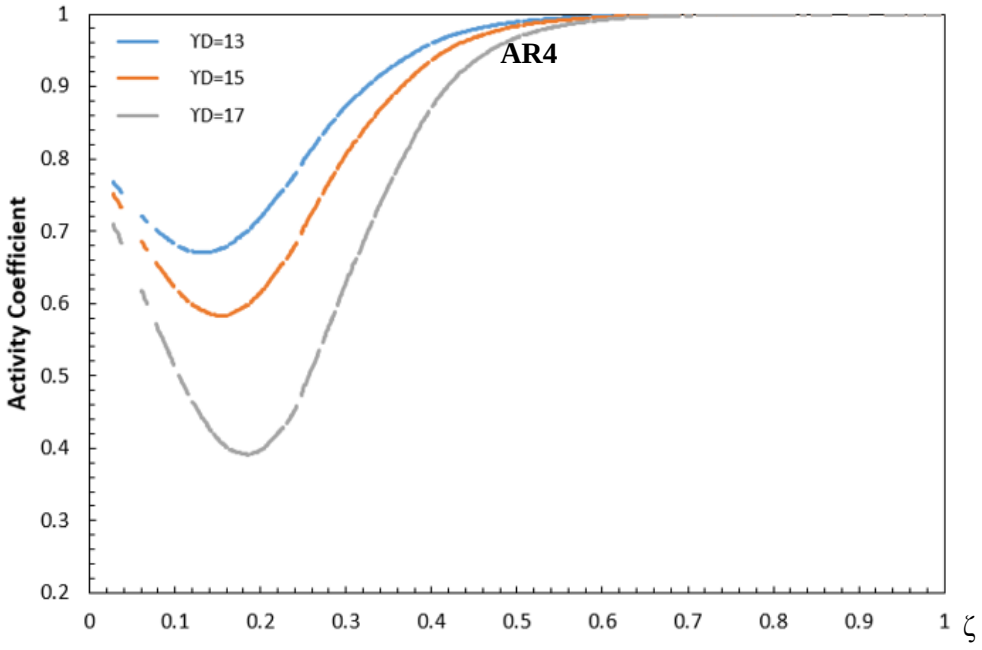

Figure 6.4. Effect of Υ_D on catalyst activity profile by CFD (3D), ($Da_D = 4\times10^{-6}$, $Da = 0.4$, $\Upsilon = 15$ and at $\tau = 50{,}000$)

3D map of activity coefficient along the axial direction under different values of Υ_D (5, 13 and 17) shows the nature of the local deactivation throughout the reactor of AR 3 as demonstrated in Figure 6.5. In fact, the simulation allowed visualization of local deactivation and how it can be promoted under differential heat and mass rates through the bed. Differential rates for local decay and temperature runways were more pronounced under transient operations of inlet temperature. It has to be noticed that several zones of spheres are completely deactivated with increase of time as illustrated in Figure 6.5.

In other words, the 3D modelling allowed observation of local catalyst deactivation at the packing pore level which was not accessible by 2D modelling or by experimental application. Deactivation of catalyst is likely to occur more in regions, where the reaction rates and temperature are highest. However, it was found that local deactivation of the exothermic reactions leads to a slow increase in the average particle temperature, which partially compensate for the decrease in reaction rates.

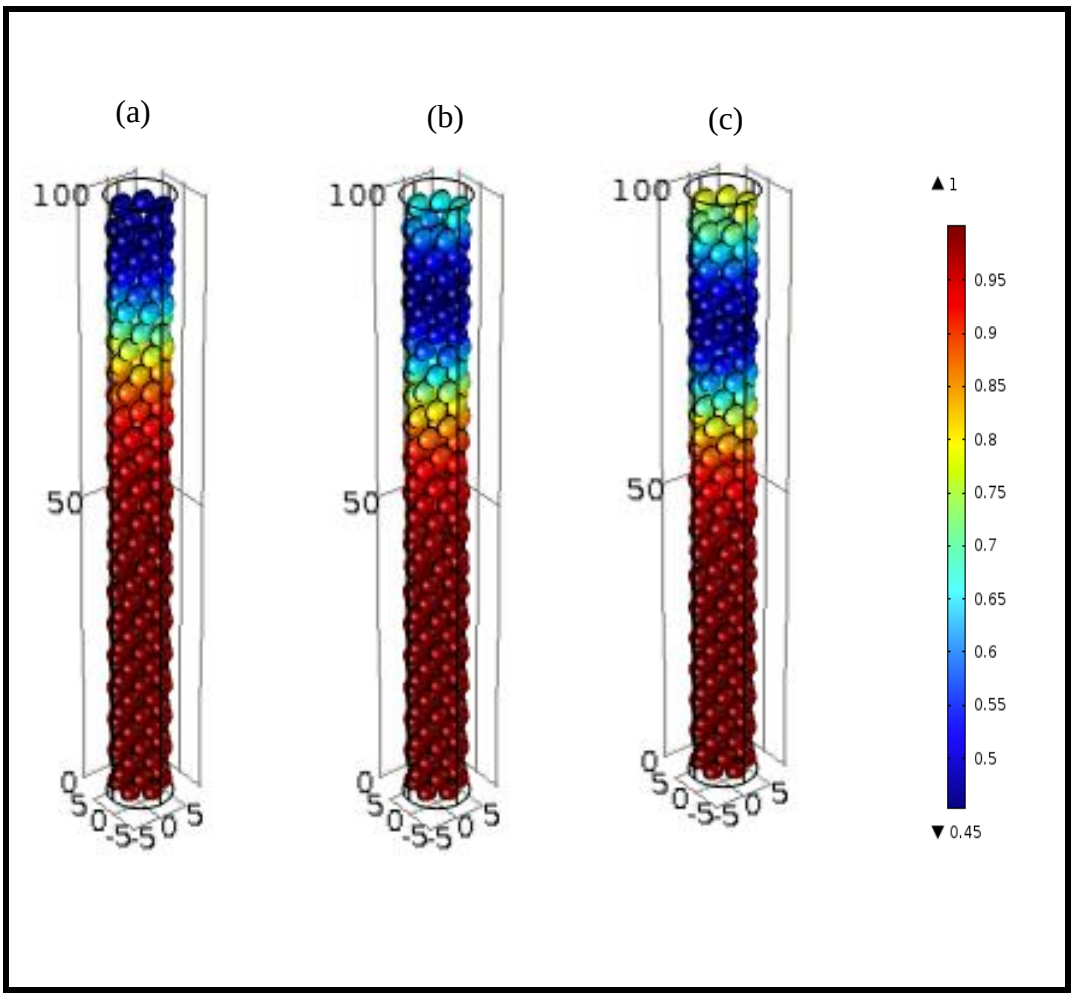

Figure 6.5. 3D Map of activity coefficient under effect of different values of Υ_D for AR3 by 3D CFD; (5, 13 and 17), (a, b and c) respectively.

On the surface of catalyst particles, an understanding of the evolution of the local deactivation can be achieved by examining 2D contour maps on a plane slicing through the bed at Υ_D =17 for ARs 3 and 4 as shown in Figure 6.6. It can be clearly seen that the deactivation on surface of particles appears non-uniform and that could be attributed to the interaction between the packing (solid catalyst) and fluid flow under severe exothermic reaction conditions such as hot spots and wrong behaviour of temperature. Furthermore, at the high deactivation regions, the CO oxidation reaction rate decreases and thus would change from zone to zone based on the value of deactivation.

Because of presence deactivation, the diffusion into the particles decreases, and then as a result, the reaction rate will develop slowly there. Typically, the deactivation must result in higher reactant and lower product mass fractions and this well noticed by the CO reaction rate which becomes more affected by deactivation as time progressed.

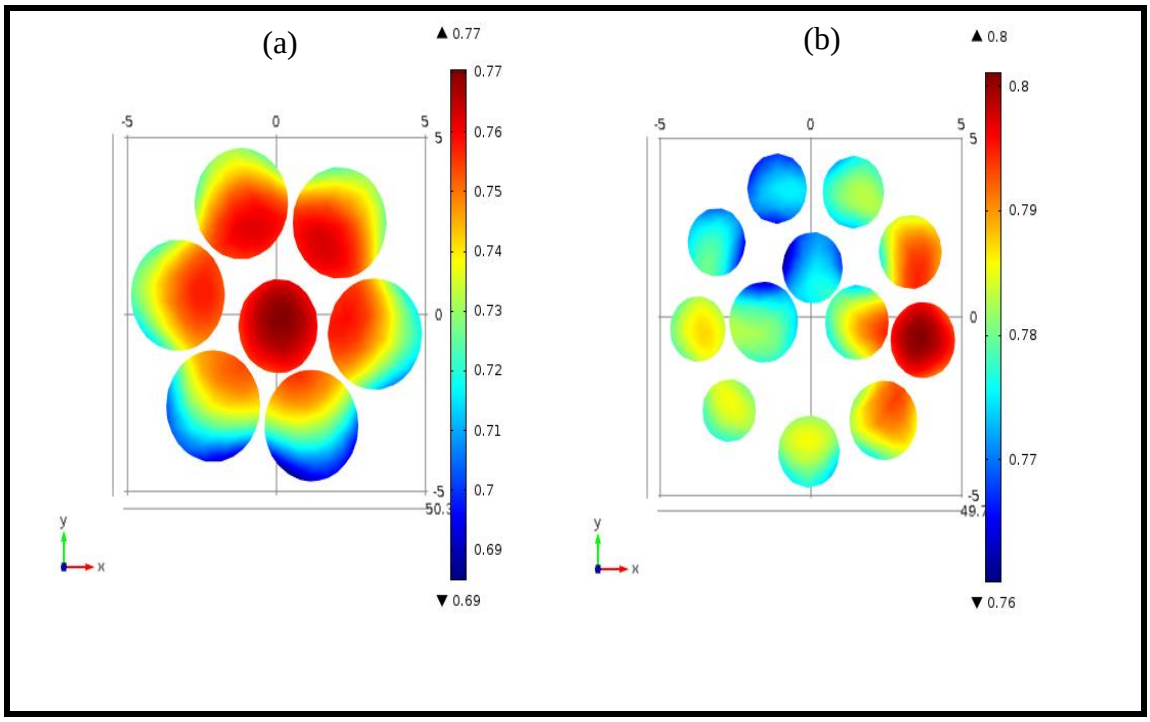

Figure 6.6. 2D Cross- section profiles of deactivation coefficient by CFD ; (a) AR3 and (b) AR 4 at $\Upsilon_D = 17$

By comparing the cross-sectional distribution of deactivation for AR 3 and AR4 in Figure 6.6, it can be clearly seen that the strongest deactivation rates take place in the central zones of the bed for AR3 while they occur at different zones at AR 4 (i.e., herein in the vicinity of the wall for this cross-sectional location), owing to uneven distribution of packing structure, and by inference, associated flow and transports.

6.3.2.2Effect of the Damköhler number (Da_D)

Figure 6.7 shows a cut line inside the bed of catalyst activity coefficient profiles along dimensionless axial position ($\zeta = z/L$) as a function of Damköhler number (Da_D). Again, large values of Da_D promoted local deactivation. Compared with 2D model, the results of simulation by 3D modelling reveal that the activity profile along the entire reactor coordinate shifted more towards the front of the packed bed.

(a)

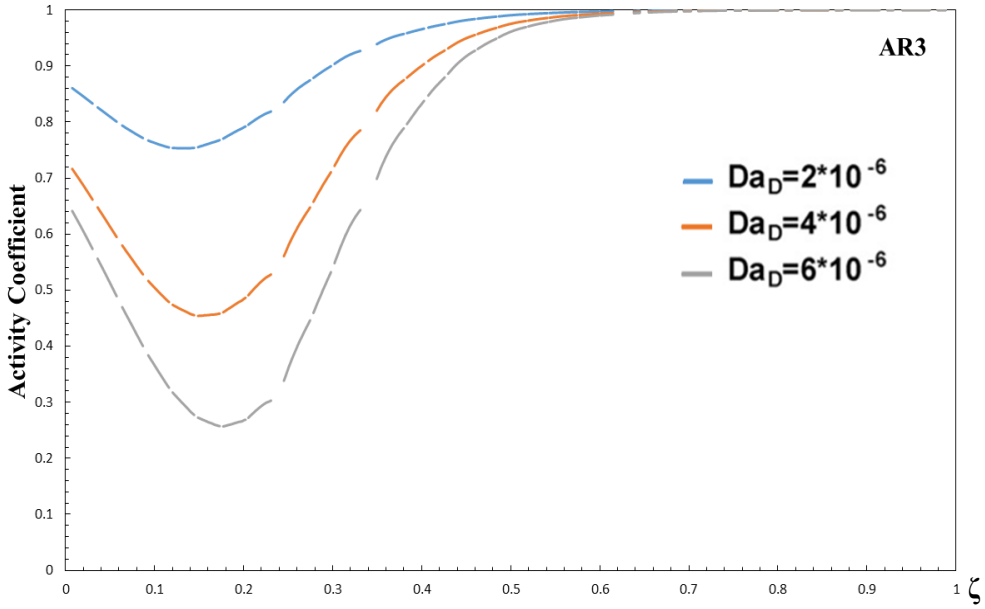

(b)

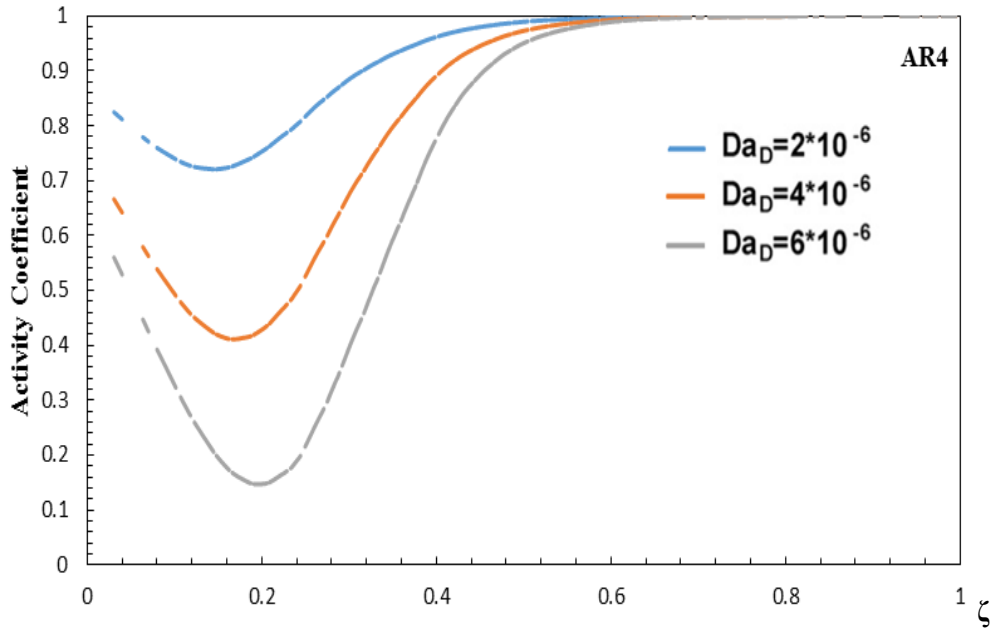

Figure 6.7. Effect of Da_D on the catalytic activity profile by 3D CFD, :(Da = 0.4, Υ=15, Υ_D =15 and at τ = 50,000)

6.3.2.3 Investigation of wrong way behaviour

The wrong-way behaviour was investigated by promoting the differential rate between mass and heat transfer. The system was initially set at steady-state for τ= 10,000, the deactivation was switched on at τ= 10,000, and the inlet temperature (T_0= 413 K) was set to decrease at a rate of 0.001 K/s at τ= 20,000. Figure 6.8 shows the transient temperature change at different axial positions along the reactor during fast catalyst deactivation. In the steady state reaction zone, temperature increased first owing to the release of energy by the exothermic reaction, and then kept constant values even during the activation period (i.e., 10000<τ<20000). When the inlet temperature began to fall at τ= 20,000, it appeared an unexpected rise, and went up to higher values towards the exit of the bed. However, it doesn't show the same behaviour as in the 2D model as shown in Figure 6.3, the temperature's rise did not last for a long time and quickly dropped. This wrong way behaviour becomes very remarkable at the zone that is near the reactor's exit, i.e. 0.75L to 0.90L.

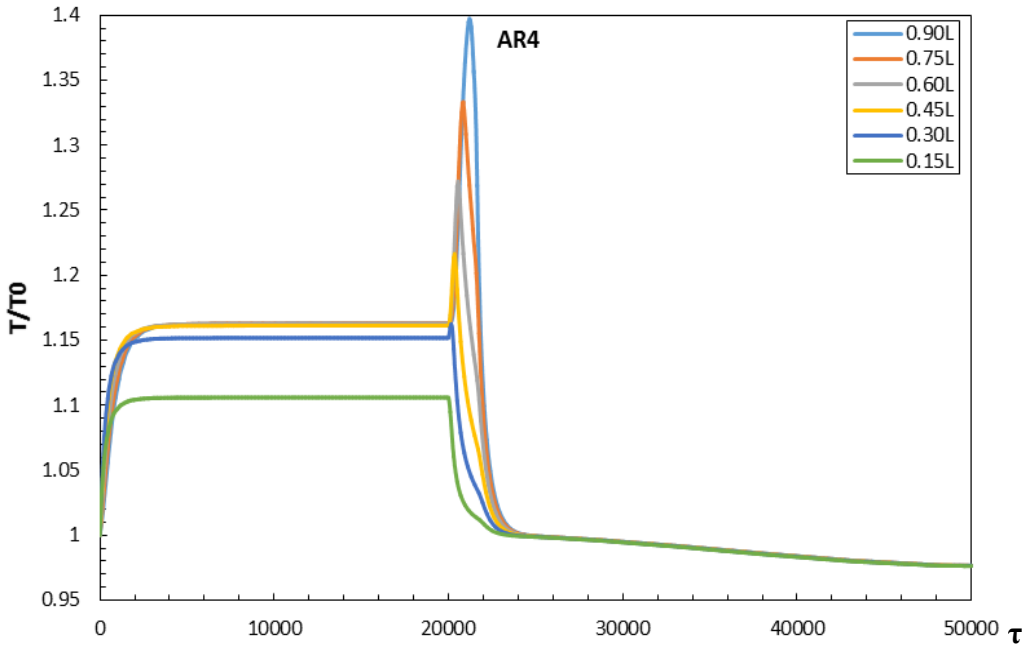

Figure 6.8. History plot of temperature ratio (T/T0) at different axial positions by 3D (Da_D = 4×10^{-6}, Da = 0.4, ϒ= 15, Υ_D= 5.5 and τ_{total}= 50,000)

This behaviour was validated by using similar results from Jaree's (2008) conditions as illustrated in Figure 6.9. [59] For this case, the system was set initially at steady- state and then the deactivation is switched on at time zero. In the pre-reaction zone, temperatures decreased because less CO molecules were converted to products and less heat was released due to catalyst deactivation pushing the wave of un-reacted CO downstream (front of the bed).The front zone temperature decreased but when the inlet temperature started to decrease, the entire zone temperature reached already a certain maximum value. This wrong way behaviour was more noticeable at the zone near the exit about 0.75L-0.9L. This typically occurs when the concentration wave arrives at the reaction front, the auto-catalytic nature of the main reaction takes on and releases additional heat travelling at significantly higher temperatures than that of the adiabatic value. CFD results have shown a reasonable agreement with those obtained by jaree et al., (2008). [59] The temperature profiles were nearly similar but the maximum value (i.e., T/T_0) in present work was 1.14, while in literature was about 1.5.

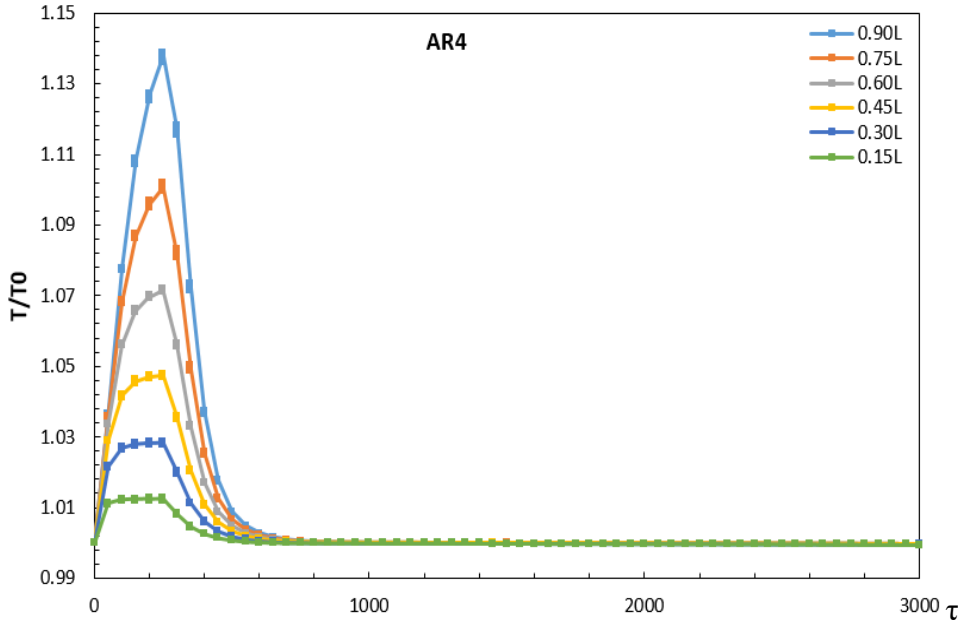

Figure 6.9. History plot of temperature ratio (T/T0) at different axial positions; by CFD (3D) :(Da_D =0.004, Da = 0.4, Υ= 15, Υ_D= 4 and τ_{total}= 3000)

6.3.2.4 Effect of peclet number of axial dispersion (*Pe*)

In general, inside packed beds, dispersion of heat and mass are basically caused via fluid convection and mixing process. In the two flowing sections, the effect of mass and heat dispersions in terms of mass Pe_1 and heat Pe_2 on the activity profiles will be investigated.

6.3.2.4.1Effect of peclet number of mass dispersion (Pe_1)

The effects of mass transfer on deactivation profiles inside the packed bed were investigated by 3D modelling. The Peclet number is a dimensionless number relevant in the study of transport phenomena in fluid flow. It can be defined as the ratio of the rate of advection of a physical quantity by the flow to the rate of diffusion of the same quantity driven by an appropriate gradient. Pe_1 is calculated by equation (66):

$$Pe_1 = \frac{ul}{D} \qquad (66)$$

As the diffusivity of reaction mixture can increase by an order of magnitude if the reaction of oxidation was carried out in helium instead of nitrogen or air (i.e., 5.0 x 10^{-5} to 5.0 x 10^{-4} $m^2 s^{-1}$). [160] Pe_1 was varied from 50 to 500 in the simulation study. Figures 6.10 (a, b) show the trend of catalyst activity coefficient along axial dimensionless position ($\zeta = z/L$) of the packed bed reactor, as a function of Pe_1 for ARs 3 and 4. The value of Pe_1 was varied from 50 to 500 and relevant impact on catalyst activity coefficient was insignificant particularly after Pe_1 = 300. Carrying out this reaction at Pe_1 = 50 instead of Pe_1 = 500 accelerated the deactivation. The result is consistent with Levenspiel's statement [45] where parallel deactivation should be significant in regions of the bed where the concentration of reactants is high such as at the front of isothermal beds, and during catalyst deactivation, the zone of peak activity or deactivation moves down at front of the bed. In general, with increasing the mass transfer, there will be more chance and more time for the reaction to occur and then another chance to the deactivation.

(a)

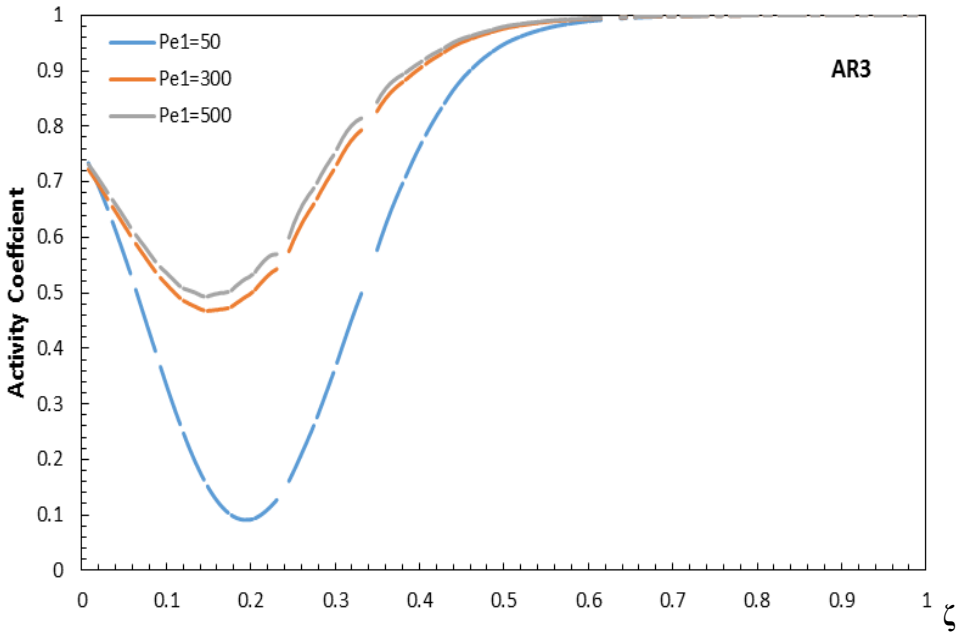

(b)

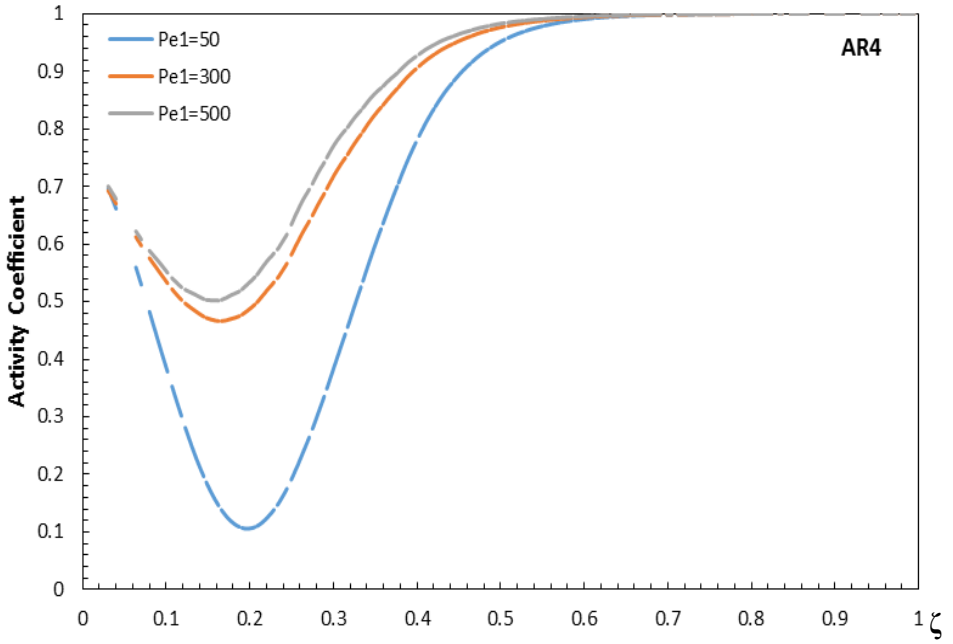

Figure 6.10. Effect of Pe_1 on the catalytic activity profile (3D CFD); (Υ= 15, Υ_D = 15, Da_D =4×10^{-6}, Da = 0.4 and at τ= 50,000)

6.3.2.4.2Effect of peclet number of heat dispersion (Pe_2)

In the context of the transport of heat, effect of Peclet number of heat dispersion (Pe_2) on the deactivation profiles was examined, Pe_2 is defined by equation (67):

$$Pe_2 = \frac{\rho_g C_{pg} u l}{k} \qquad (67)$$

Figures 6.11 (a, b) illustrate tendency of catalyst activity coefficient along axial dimensionless coordinate (ζ) as a function of Pe_2 for ARs of 3 and 4, respectively. High values of Pe_2 promoted more deactivation without a moving wave along the bed length. Values of Pe_2 were varied from 10 to 70. High heat conductivity values of the flowing gas promoted the deactivation owing to higher thermal rates released compared with the mass rates which accelerated the deactivation reaction in the neighbouring front zones. At ζ=0.3 of the bed, it can be seen that, by increasing the value of Pe_2 ,the deactivation became limited due to strong competition between the mass transfer and heat transfer inside the packed bed, leading to hot spots on catalyst and large temperature differences on catalyst particles.

(a)

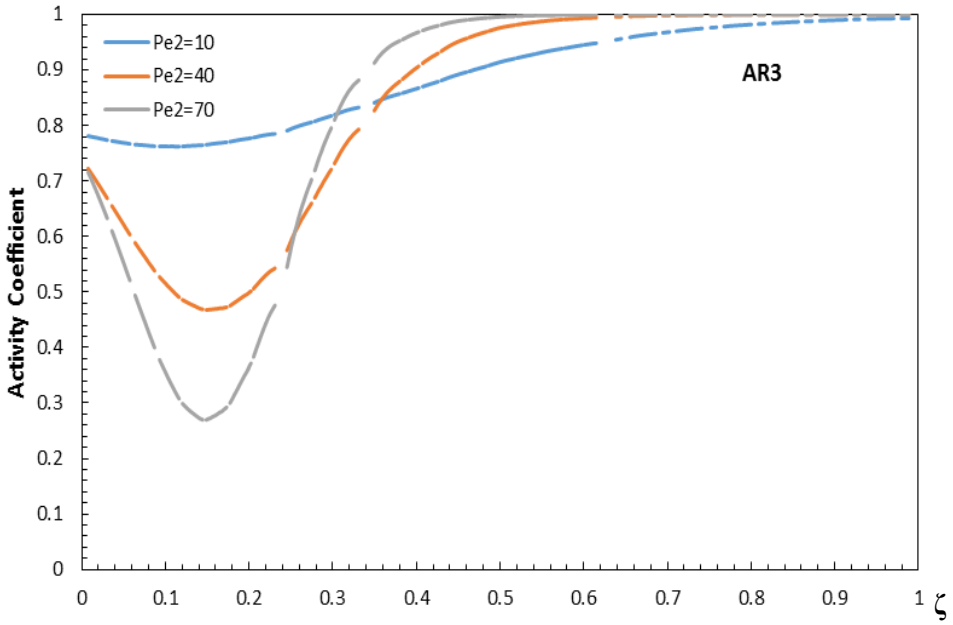

(b)

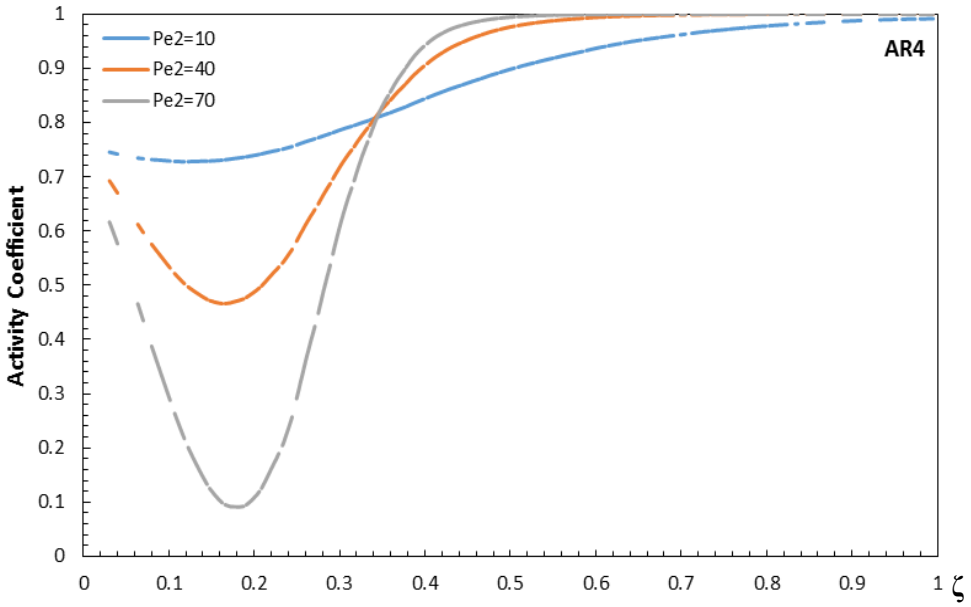

Figure 6.11. Effect of Pe_2 on the catalytic activity profile (3D CFD) ;(Υ = 15, Υ_D = 15, Da_D =4×10^{-6}, Da = 0.4 and at τ= 50,000)

6.3.2.5 Effect of internal mass transfer coefficient on deactivation profiles

The effect of mass transfer inside the solid catalyst on deactivation profiles was investigated as shown in Figures 6.12 and 6.13. The diffusion coefficient in the solid phase or effective internal diffusivity (D_{eff}) was varied from 0.1D and 0.25D (D is the diffusivity in the fluid phase). These two figures clearly show that internal mass transfer doesn't affect the trends of particle deactivation but has a noticeable influence on local deactivation at catalyst pore level. Deactivation affects more the surrounding shell of particles when high deviations exist between diffusivities in the solid and the gas phases. This result is in agreement with Levenspiel's statement [45], where parallel deactivation tends to occur close to the pellet exterior and moves inwards as the catalyst deactivates. Figures 6.12 and 6.13 reveal distinguished regions between the same or different catalyst particles and gas diffusivity. This phenomenon just precisely explains why more deactivation takes place in regions close to the wall and regions surrounding particles where high velocities exit, leading to high convective rates and reducing external mass transfer resistances.

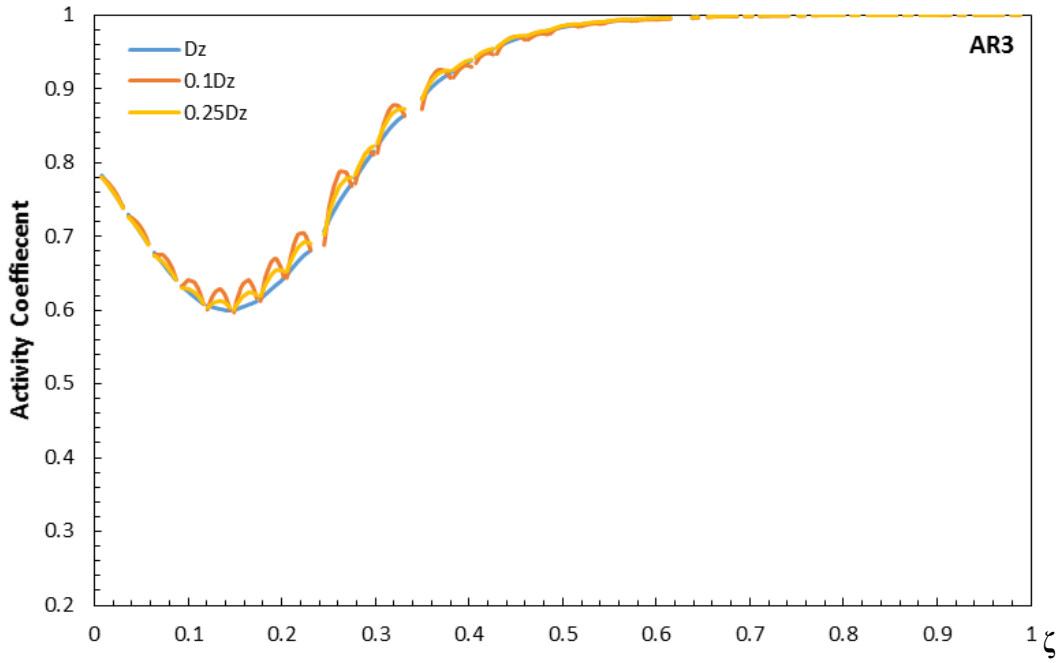

Figure 6.12. Plot of internal mass transfer effect (3D CFD); (Da_D =4×10^{-6}, Da = 0.4, Υ= 15, Υ_D = 15 and at τ= 50,000)

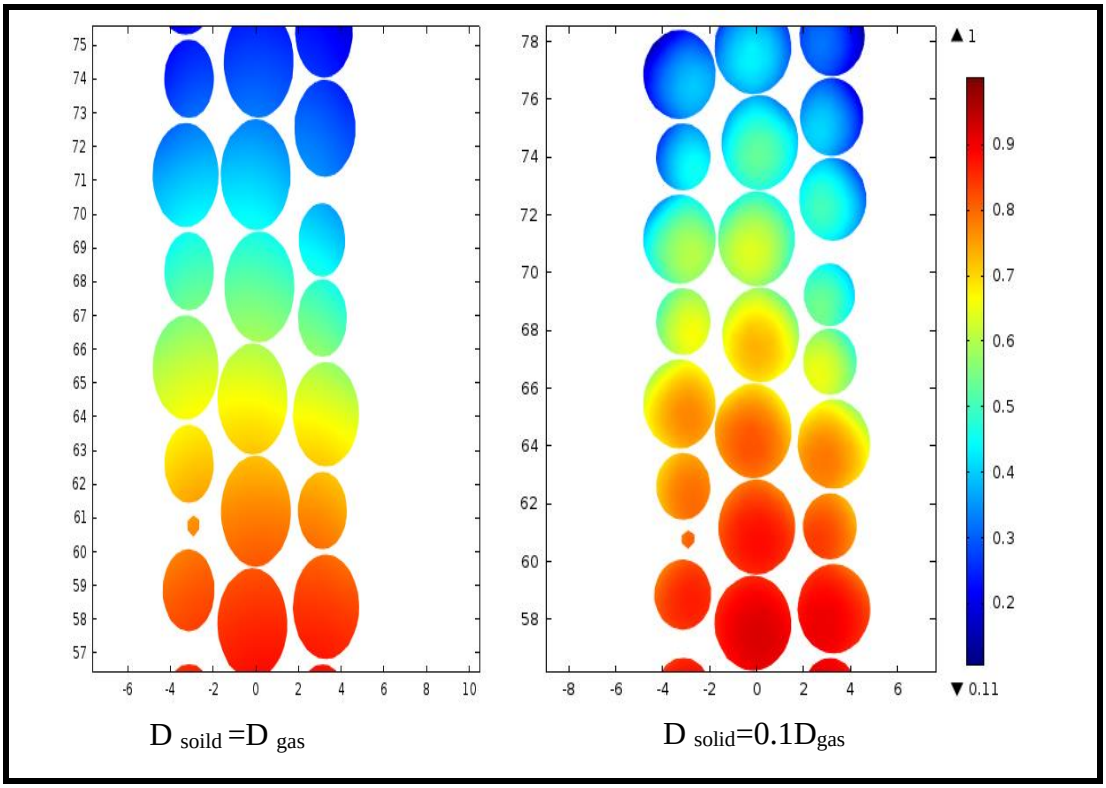

Figure 6.13. Axially cross-sectional profiles of activity coefficient for AR 3.

6.3.2.6 The effect of thermal inertia of the solid catalytic phase

The thermal inertia is a thermal parameter that may affect the heat rates in the packed bed. The heat capacity was varied from the value of Cp_s=900 J $kg^{-1}K^{-1}$ to Cp_s=503 J $kg^{-1}K^{-1}$ for ARs 3 and 4 as shown in Figure 6.14. Lower heat capacity of catalyst particles led to a stronger deactivation with a moving wave along the length coordinate. Lower heat capacity allowed less sink of the energy released leading to more acceleration of the deactivation reaction.

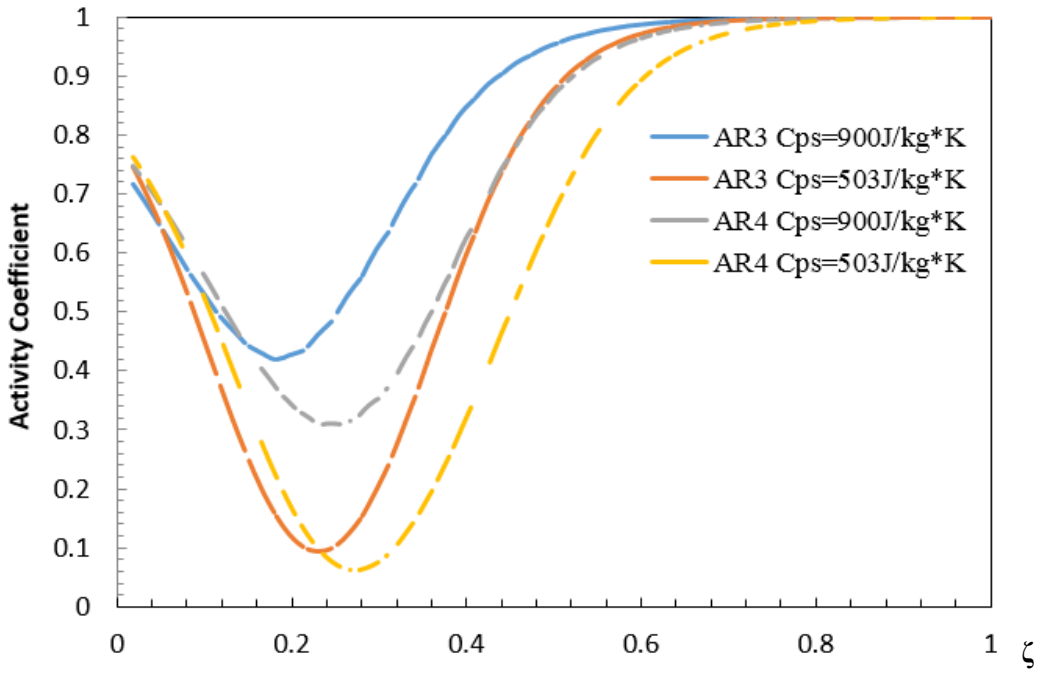

Figure 6.14. Effect of Cp_s on the catalytic activity profile by 3D CFD.

6.3.3 Comparison of Υ_D and Da_D profiles obtained by 2D and 3D modelling

Deactivation profiles by 2D and 3D were compared as demonstrated in Figure 6.15 (a, b and c). Catalyst deactivation by 3D model has a larger extent than the 2D model. The 2D and 3D models have shown similar trends of deactivation profiles when deactivation rate, mass and heat transfer were varied. Moreover, in 3D model the deactivation wave moves more towards the front of the packed bed and allowed local profiles of deactivation to be observed at packing pore level but the starting point of the deactivation was higher by the 2D model. The deactivation was quite asymmetrical along axial and radial directions of the particle surface leading to uneven rates of

thermal expansion and contraction, which have the potential to break the particle or to cause local deactivation associated with temperature runaways.

(a)

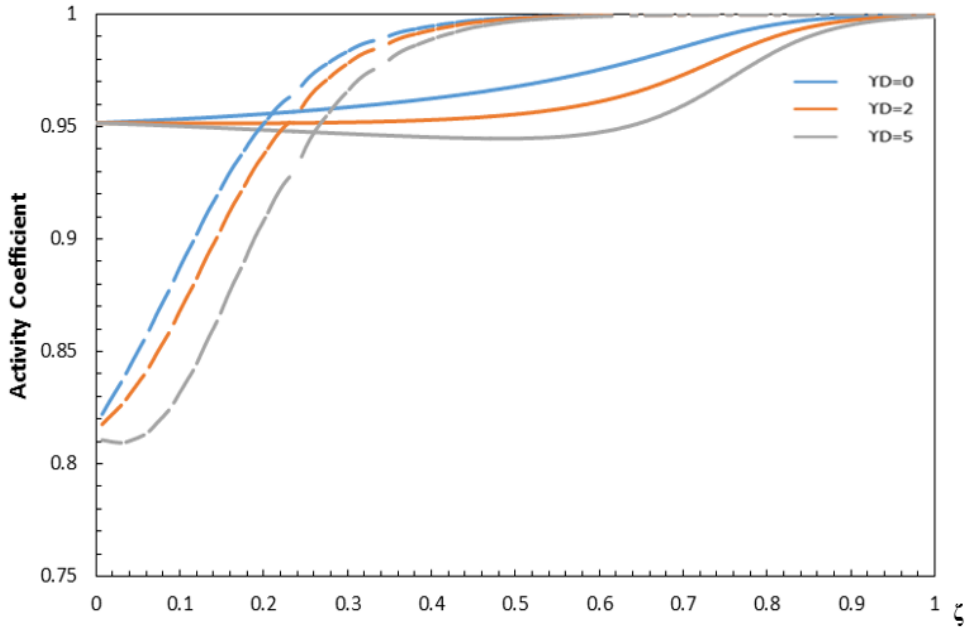

(b)

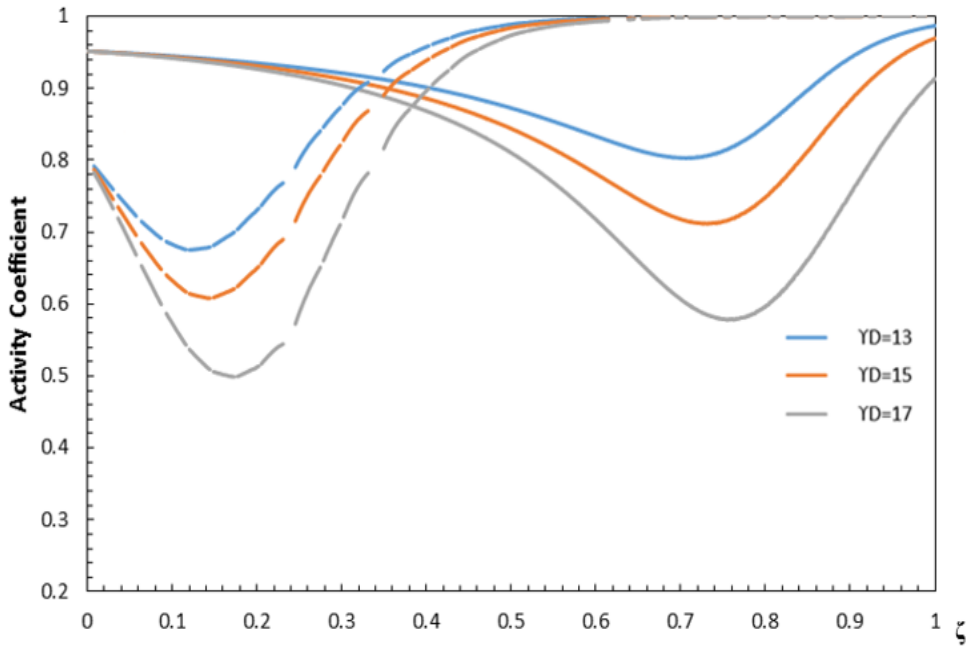

(c)

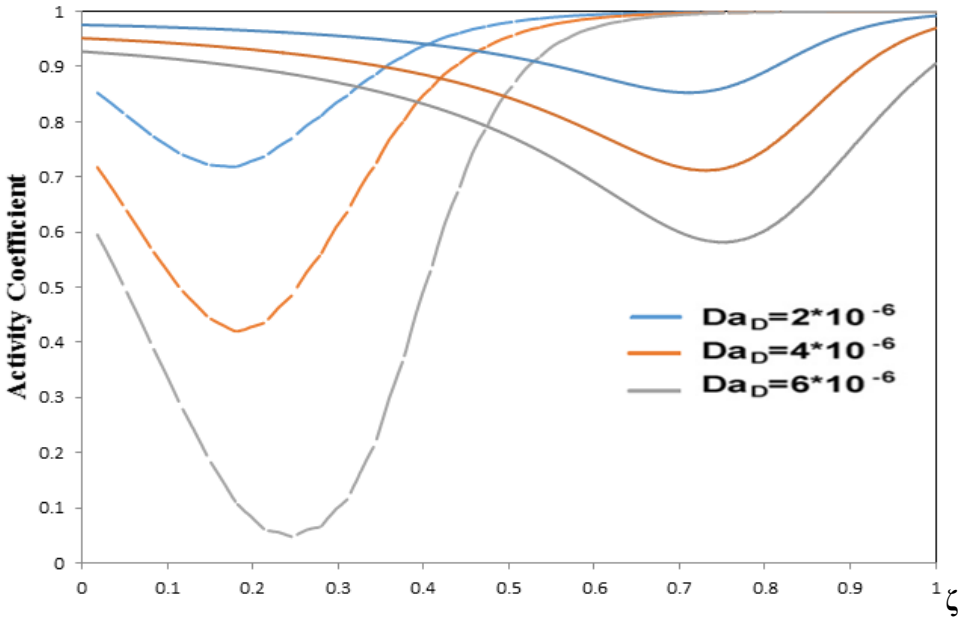

Figure 6.15. Plot of Υ_D (a, b) and Da_D (c) effects on the catalytic activity by 2D (solid line) and 3D (dotted line) modelling for AR 3.

6.3.4 Summary of the chapter

The non-uniform (local) deactivation was investigated in packed bed reactors of low ARs (i.e., 3 and 4) under steady-state and dynamic operations. Both 2D and 3D models were investigated in order to get a comprehensive investigation of detailed catalyst deactivation in packed bed reactors. An increase in the activation energy of deactivation, $\Upsilon_{D,}$ will promote the deactivation. Increasing Υ_D accelerated the reaction rate of CO oxidation, releasing thermal energy, and in turn accelerated the deactivation rate. The Damköhler number (Da_D) affected on deactivation profiles in same way of $\Upsilon_{D.}$

Moreover, Instability of the reactor owing to catalyst deactivation was demonstrated by the wrong-way behaviour of temperature under transient operations (inlet temperature decrease). The study of the catalysts deactivation was a quite satisfactory because the simulation allowed visualization of local deactivation and how it can be promoted under differential heat and mass rates through the

bed. Differential rates for local deactivation and temperature runways were more pronounced under transient operations of inlet temperature.

The extent of catalyst deactivation in the 3D models was larger than those obtained by 2D models and the 3D approach allowed to observe local catalyst deactivation at packing pore level. Peclet Numbers of mass and heat dispersion (Pe_1 and Pe_2) were investigated and found that at higher values of Pe_2 promoted more deactivation without a moving wave along the bed length as it was observed with the Peclet Number of mass dispersion (Pe_1), particularly with AR of 4. Furthermore, the deactivation waves moved more towards the front of the packed bed in the 3D models.

Chapter 7

7. Conclusions and Recommendations

7.1 Conclusions

This work used the 3D CFD modelling to investigate non uniform (local) deactivation in packed bed reactors of low AR under steady-state and dynamic operations. In order to explore the effects of conditions of instability on local deactivation, detailed knowledge of flow dynamics (i.e., local structure of the packed bed, pressure drops and interstitial flow in the void space), heat and mass rate distributions were examined. Simulation by 3D CFD modelling included: (1) generation of representative bed geometries and comparison of the bed structure property such as average porosity and spatial distribution of porosity with literature models, (2) pressure drops and velocity distributions and comparison with experimental data and literature models, and (3) formulation of 3D gas-solid model of fluid flow, mass and heat transfers, including the chemical reaction and the catalytic deactivation under steady-state and dynamic operations and comparison with relevant 2D pseudo-homogeneous models and literature results.

For the generation of an irregular packing configuration of spherical particles, DEM method was employed. The porosity profiles from the CFD simulation results were in a good agreement with the semi-analytical models such as Mueller's expression [104], especially, in the vicinity of the wall. Similar oscillation trends with damping profiles towards the centre of the packed beds were observed. The discrepancies in regions towards the centre were potentially due to the loose structure of the generated packing. In addition, the averaged porosity achieved by CFD simulation was in a good agreement with the models of Zou and Yu [97] where the porosity increased at low AR due to high porosity near the wall in narrow packed beds.

The simulation results had to be validated using at least one experimental parameter. Pressure drop was selected as it necessitated a simple setup. The results of pressure drops by CFD simulation fit well the models predicted by Zhavoronkov, Reichelt and Ergun at high Reynolds numbers, but showed disagreements with the Carman model, which is typically suitable for packed beds of large AR. CFD simulations are proven to be useful for identification of the drawbacks of simplified semi-empirical modelling approaches and for their further improvement by developing better empirical

correlations. The developed CFD based approach provided knowledge that often is difficult to obtain experimentally and could contribute to improving the design of low AR packed beds. The results of 2D model were in a good agreement compared to 3D modelling, confirming the benefit of using the porosity distribution from 3D maps to access insights into industrial packed beds of large computation time and hardware power.

Flow heterogeneity, and particularly in the zone close to the wall, was also characterised by mass dispersion by using a Lagrangian approach. Particles were released at the centre of the packed bed and their propagation along the radial and axial directions was examined. The results have shown changes in axial and radial dispersions and confirmed the impact of the wall on global hydrodynamics inside low AR packed beds. Some discrepancies for radial dispersion coefficients were observed due to the very short domain length, particularly for small values of AR. Unlike radial dispersion, axial dispersion showed agreements with CFD results and literature models.

In addition, mass and heat transfers were simulated by 3D modelling in cylindrical packed beds of spherical catalyst particles of gas/solid reactive system for different ARs. Since strongly exothermic reactions such as catalytic CO oxidation, are carried out in a heated narrow reactor tubes, this work successfully validated uneven flow of heat and mass inside these packed beds. The kinetics of the CO oxidation on alumina catalysts have been shown to be well described by 3D simulation. The conversion of CO oxidation was strongly dependent on reaction temperature and the feed compositions. Flow rates and size of particles played significant roles in the catalytic oxidation reaction. The trends of temperature profiles before and after the light-off by 3D CFD modelling were found in a reasonable agreement with those obtained from the different published works.

CFD, as a modelling tool, could give a clear vision of behaviour of underlying phenomena of fluid flow, mass and heat transfers inside the gas/solid packed bed reactor which would not possible to capture experimentally. The 3D CFD modelling provided detailed information of temperature distribution in the interior of the bed and the temperature difference between solid and gas phases. It allowed analysis of heat transfer phenomena which were validated qualitatively and quantitatively with published data. Radial temperature distributions and also Nusselt number Nu were examined by 3D. Contour maps also showed the temperatures propagation with time evolution throughout the bed and revealed that there is a strong effect for uneven heat transfer particularly at low ARs.

Both 2D and 3D modelling were used in order to get a comprehensive investigation of detailed catalyst deactivation in packed bed reactors. Computational fluid dynamics was used to investigate non-uniform deactivation in packed bed reactors of low aspect ratios under steady-state and

dynamic operations. The effects of parameters such as dimensionless activation energy of deactivation, Damköhler number, Péclet numbers of mass and heat transfers, internal (intra-particle) mass transfer and thermal capacity of the packing on local deactivation profiles were investigated. An increase in the activation energy of deactivation of CO oxidation promoted the deactivation by accelerating the reaction rate, releasing additional thermal energy, which in turn accelerated the deactivation.

Instability of the reactor owing to catalyst deactivation was demonstrated by the wrong-way behaviour of temperature under transient operations (i.e., temperature decrease at the inlet). At the start of deactivation, the front zone temperature decreased but when the inlet temperature started to decrease, the entire zone temperature increased instead and went up to a certain maximum value. This occurred because when the concentration wave arrived at the reaction front, the auto-catalytic nature of the main reaction took on and released additional heat travelling at significantly higher temperatures than that of the adiabatic value. Overall, the study of the catalysts deactivation was quite satisfactory because the simulation allowed visualization of local deactivation and how it can be promoted under differential heat and mass rates through the bed. Differential rates for local deactivation and temperature runways were more pronounced under transient operations of inlet temperature.

The 3D modelling allowed observing local catalyst deactivation at packing pore level. Deactivation occurred more in regions close to the wall and regions surrounding particles (shells) where high velocities exit, leading to high convective rates. Péclet Number of heat dispersion (Pe_2) affected catalytic activity profiles inside the packed bed. Higher values of Pe_2 promoted more deactivation without a moving wave along the bed length as it was observed with the Péclet Number of mass dispersion (Pe_1), particularly with AR of 4. The extent of catalyst deactivation in the 3D models was larger than in the 2D models. Furthermore, the deactivation waves moved more towards the front of the packed bed in the 3D models. The deactivation was quite asymmetrical along axial and radial directions of the particle surface leading to uneven rates of thermal expansion and contraction, which have the potential to break the particle, or to cause local deactivation associated with temperature runaways.

The 3D modelling has shown that catalysts in packed beds with low AR get more deactivation at high dimensionless activation energy of deactivation, high Damköhler number and low Péclet numbers of mass dispersion. Low AR packed beds demonstrated less dispersion along the radial coordinates in the mass transfer, less mixing at low fluid velocity (high Damköhler number) allowing the heat released by CO oxidation to accelerate the deactivation reaction.

7.2 Recommendations

This work allowed for the first time to observe local deactivations in gas/solid packed beds by 3D CFD modelling in porous media that mimic well real structures. It would be worthwhile however to extend this work to:

- Packed beds of larger size to approach conditions of industrially operated packed bed reactors. It is understood that large scales would require additional computation time and power, particularly when simulations are run under transient operations.
- Other deactivation examples that attract more interests from the chemical industry, particularly those associated with other types of deactivations. These types of deactivations however presents non-linear kinetics which would increase complexity of the CFD modelling
- Studies of phenomena of temperature run away (i.e., fires and explosions) which are of primary importance of a number of industries associated with safety measures. Existing 3D modelling approaches are still limited predict such phenomena in absence of associated empirical models.
- Conditions of moving packed beds such as conditions of fuel catalytic cracking (FCC) processes where deactivation and regeneration cycle of acid catalyst is still not accessible with sufficient time and space resolution perspectives.

References

[1] Froment, G.; Bischoff, K. Chemical Reactor Analysis and Design. Wiley, New York. 1979

[2] Ranade,V .Engineering reactors for catalytic reactions. Indian Academy of Sciences 2014, 126, 341-351.

[3] Jafari, A.; Zamankhan, P.; Mousavi, S.M.; Pietarinen, K. Modelling and CFD simulation of flow behaviour and dispersivity through randomly packed bed reactors. Chemical Engineering Science. 2008, 144, 476-482.

[4] Ancheyta, J.; Muñoz, J. A. D.; Macías, M. J. Experimental and theoretical determination of the particle size of hydrotreating catalysts of different shapes. Catalysis Today. 2005, 109, 120-127

[5] Fogler, H. S. Elements of Chemical Reaction Engineering (4th Edition). Prentice Hall. 2005

[6] Wakao, N.; Kaguei, S. Heat and mass transfer in packed beds. McGraw Hill, New York. 1982

[7] Ertan, M.CFD simulation of transort and reaction in cylinderical catalyst particles.. PhD Thesis. Worcester Polytechnic Institute. 2007

[8] Guardo, A.; Coussirat, M.; Recasens, F.; Larray, M.A.; Escaler, X. CFD Study on particle -to-fluid heat transfer in fixed bed reactors: Convective Heat transfer at low and high pressure. Chemical Engineering Science. 2006, 61, 4341- 4353.

[9] Nijemeisland, M.; Dixon, A.; Stitt, E .Catalyst design by CFD for heat transfer and reaction in steam reforming. Chemical Engineering Science. 2004, 59, 5185-5191.

[10] Goodling, J.S.; Vachon, R.I.; Stelpflug, W.S.; YING, S.J. Radial porosity distribution in cylindrical beds packed with spheres. Powder technology. 1983, 35, 23-29.

[11] Guardo, A.; Coussirat, M.; Larryoze, M.; Recasens, F.; Egusquiza, E. CFD flow and heat transfer in nonregular packings of packed bed equipment design .I and EC. 2004, 43, 7049.

[12] Freund, H.; Bauer, J.; Zeiser, T.; Emig, G. Detailed simulation of transport processes in fixed-beds. Industrial Engineering Chemistry Research. 2005, 44, 6423− 6434.

[13] Dixon, A.; Taskin, M.; Nijemeisland, M.; Stitt, E. CFD method to couple three-dimensional transport and reaction inside catalyst particles to the fixed bed flow field. Industrial Engineering Chemistry Research. 2010, 49, 9012−9025.

[14] Vortmeyer, D.; Schuster, J. Evaluation of steady flow profiles in rectangular and circular packed beds by a variational method. Chemical Engineering Science. 1983, 38, 1691−1699.

[15] Govindarao, V. M. H.; Subbanna, M.; Rao, A. V. S.; Ramrao, K. V. S. Voidage profile in packed beds by multi-channel model:effects of curvature of the channels. Chemical Engineering Science. 1990, 45, 362-364.

[16] Dautzenberg, F. M.; Mukherjee, M. Process intensification using multifunctional reactors. Chemical Engineering Science. 2001, 56, 251-267.

[17] Pistocchini, L.; Silvia Garone, S.; Motta, M. Fluid Dynamics Optimization of a Novel Isothermal Adsorption Dehumidification System for Solar Driven Applications. Energy Procedia 2014, 48, 1689-1698.

[18] Alzahrani, F.; Aldehani, M. ; Rusi, H. ; McMaster,M. ; Daniel, F. ; Suttichai ,A. ; Meabh, N. ; Aiouache, F. Gas Flow Visualisation in Low Aspect Ratio Packed Beds by Three-Dimensional Modelling and Near–Infrared Tomography. Industrial & Engineering Chemistry Research. 2015, 54, pp. 12714-12729.

[19] Li, C.H.; Finlayson, B.A. Heat transfer in packed beds - a revaluation. Chemical Engineering Science. 1977, 32, 1055-1066.

[20] Tsotsas, E.; Schlünder, E.-U. Heat transfer in packed beds with fluid flow: remarks on the meaning and the calculation of a heat transfer coefficient at the wall. Chemical Engineering Science.1990, 45, 819-837.

[21] Vortmeyer, D.; Haidegger, E. Discrimination of three approaches to evaluate heat fluxes for wall-cooled fixed bed chemical reactors. Chemical Engineering Science.1991, 46, 2651-2660.

[22] Freiwald, M.G.; Paterson, W.R. Accuracy of model predictions and reliability of experimental data for heat transfer in packed beds. Chemical Engineering Science.1992, 47, 1545-1560.

[23] Behnam, M.; Dixon, A.; Nijemeisland, M.; Stitt, E. A New Approach to Fixed Bed Radial Heat Transfer Modelling Using Velocity Fields from Computational Fluid Dynamics Simulations. Industrial Engineering Chemestry Research. 2013,52,15244-15261.

[24] Behnam, M.; Dixon, A.; Nijemeisland, M.; Stitt, E. Catalyst Deactivation in 3D CFD Resolved Particle Simulations of Propane Dehydrogenation. American Chemical Society , 2010. 49, 10641-10650.

[25] McGreavy, C.; Kam, E.K.T.; Foumeny, E.A.; Guidoum, A.; Ikponmwosa, A.N. A study of flow patterns in packed beds. 2nd International Symposium on Application of Laser Anemometry to Fluid Mechanics Lisbon, July. 1984.

[26] McGreavy, C.; Foumeny, E.A.; Javed, K.H. Characterization of transport properties for fixed bed in terms of local bed structure and flow distribution. Chemical Engineering Science. 1986, 41, 787-797.

[27] Bey, O.; Eigenberger, G. Fluid flow through catalyst filled tubes. Chemical Engineering Science. 1997, 52, 1365-1376.

[28] Thompson, K.E.; Fogler, H.S. (1997) .Modelling flow in disordered packed beds from Pore-scale fluid mechanics. American institute of chemical engineering Journal.1997, 43, 1377-1389.

[29] Cheng, Z.; Yuan, W. Estimating radial velocity of fixed beds with low tub to particle diameter ratios. American institute of chemical engineering Journal.1997, 43, 1319-1324.

[30] De Klerk, A. Voidage variation in packed beds at small column to particle diameter ratio. American institute of chemical engineering Journal.2003, 49, 2022-2029.

[31] Renzo, A.; Di maio, F.P. Comparison of contact-force models for the simulation of collisions in DEM-based granular flow codes. 2004, Chemical engineering science. 59, 525-54.

[32] Winterberg, M.; Tsotsas, E. Impact of tube-to-particle-diameter ratio on pressure drop in packed beds. American institute of chemical engineering Journal. 2000, 46, 1084-1088.

[33] Freund, H.; Zeiser, T.; Huber, F.; Klemm, E.; Brenner, G.; Durst, F.; Emig, G. Numerical simulations of single phase reacting flows in randomly packed fixed bed reactors and experimental validation. Chemical engineering science. 2003, 58:903-910.

[34] Di Felice, R.; Gibilaro, L.G. Wall effects for the pressure drop in fixed beds. Chemical engineering science. 2004, 59, 3037-3040.

[35] Bai, H., Theuerkauf, J.;Gillis, P.A. A Coupled DEM and CFD Simulation of Flow Field and Pressure Drop in Fixed Bed Reactor with Randomly Packed Catalyst Particles. Industrial Engineering Chemistry Research. 2009. 48, 4060-4074.

[36] Baker, M. J.; Young, P. G.; Tabor, G. R. Image based meshing of packed beds of cylinders at low aspect ratios using 3d MRI coupled with computational fluid dynamics. Computers Chemical Engineering. 2011, 35, 1969-1977.

[37] Eppinger, T.; Seidler, K.; Kraume, M. DEM-CFD simulations of fixed bed reactors with small tube to particle diameter ratios. Chemical Engineering Journal. 2011, 166, 324 - 331.

[38] Rong, L. W.; Dong, K. J.; Yu, A. B.Lattice-Boltzmann simulation of fluid flow through packed beds of uniform spheres: Effect of porosity. Chemical Engineering Science.2013, 99, 44-58.

[39] Morrise, D.; Calvin, H. Heterogeneous catalyst deactivation and regeneration: review. Catalysts. 2015, 5,145-269.

[40] Birtill, J. But will it last until the shutdown? Deciphering catalyst decay. Catalysis Today. 2003, 81, 531-545.

[41] Moulijn, J. Catalyst deactivation: is it predictable? What to do? Applied Catalysis. 2001, 212, 3-16.

[42] Pio, F.; Luca, l. Catalyst deactivation. Catalysis Today. 1999, 52,165-181.

[43] Baker, R.T.; Bartholomew, C.H.; Dadyburjor, D.B. Sintering and Redispersion: Mechanisms and Kinetics. In Stability of Supported Catalysts: Sintering and Redispersion; Horsley, J.A., Ed.; Catalytica: Mountain View, CA, USA, 1991, 169-225.

[44] Szépe, S.; Levenspiel, O. Optimal temperature policies for reactors subject to catalyst deactivation—I batch reactor. Chemical Engineering Science. 1968. 23, 881-894.

[45] Szépe, S.; levenspiel, O. Proceedings of the Fourth Europrean Symposium on Chemical Reaction Engineering. Pergamon Press, Brussels. 1971.

[46] Pacheco, A.; Peetersen, E.E.A novel interpretation of temperature versus time curves for deactivating catalyst systems. Journal of Catalyst .1986, 98, 380-385.

[47] Herington, E.F.G.; Rideal, E.K. On the poisoning of metallic catalysts. Transaction of the Faraday Society. 1944, 40, 505-516.

[48] Fuentes, G.A. Catalyst deactivation and steady-state activity: A generalized power-law equation model. Applied Catalyst. 1985, 15, 33-40.

[49] Birtill, J. Measurement and Modelling of the Kinetics of Catalyst Decay in Fixed Beds: The Eurokin Survey. Industrial Engineering Chemistry Research. 2007, 46, 2392-2398.

[50] Yakhnin, V.Z.; Menzinger, M. Convective instability and its suppression in packed-bed- and monolith reactors. Chemical Engineering Science. 1999. 54, 4547- 4557.

[51] Clifford, M.J. .; Roberts, E.P.L. ; Cox, S.M. The influence of segregation on the yield for a series–parallel reaction. Chemical Engineering Science. 53 , 1998 , 1791-1801.

[52] Cote, A.S. ; Delgass, W.N. ; Ramkrishna, D. ; Investigation of spatially patterned catalytic reactors. Chemical Engineering Science. 54 ,1999, 2627-2635.

[53] Aida, T. .; Nijiyama, N. Chromatographic effect along a packed bed reactor for NO–CO reaction over Pt/Al2O3 under periodic operation. Chemical Engineering Science. 2000, in press.

[54] Aida, T. ; Na-Ranong, D.; Kobayashi, R .; Niiyama, H. Effect of diffusion and adsorption–desorption on periodic operation performance of NO–CO reaction over supported noble metal catalysts. Chemical Engineering Science. 54 , 1999, 4449- 4457.

[55] Quina, M.M.J.; Ferreira, R.M.Q.Thermal runaway conditions of a partially diluted catalytic reactor, Ind. Eng. Chem. Res. 38 , 1999 , 4615- 4623.

[56] Menzinger, M.; Yakhnin, V.; Jaree, A.; Silveston, P. L.; Hudgins, R. R. Dynamic responses of packed bed reactors. Chemical Engineering Science. 2004, 59, 4011-4022.

[57] Menzinger, M.; Rovinsky, A. The differential flow instabilities. In R. Kapral & K. Showalter (Eds.). Chemical waves and patterns. Kluwer Publications. 1995.

[58] Rovinsky, A.; Menzinger, M. Chemical instability induced by a differential flow (Part 1: Theory). Physical Review Letters. 1992, 69, 1193- 1196.

[59] Jaree, A.; Boonsomlanjit, B.; and Limtrakul, J . On the dynamical instability of packed-bed reactors in the presence of catalyst deactivation. Computers and Chemical Engineering. 2008, 32, 2897-2902.

[60] Crider, J. ; Foss, A. Computational studies of transients in packed tubular chemical reactors. American institute of chemical engineering Journal. 1966, 12, 514-522.

[61] McGreavy, C.; Naim, H. Reduced dynamic model of a "xed bed reactor. Canadian Journal Chemical Engineering. 1977, 55, 326-332.

[62] Windes, L.; Schwedock, M.; Ray, H. Steady-state and dynamicmodelling of a packedbed reactorfor the partial oxidationof methanol to Formaldehyde. I. Model development. Chemical Engineering Communications.1989, 78, 1-43.

[63] Yakhnin, V. Z.; Menzinger, M. Moving hot spots and resonance in adiabatic packed-bed reactors. American institute of chemical engineering Journal. 1998, 44, 1222-1225.

[64] Jaree, A.; Hudgins, R. R.; Budman, H.; Silveston, P. L.; Yakhnin, V.; Menzinger, M. Application of inlet temperature disturbances in a packed-bed reactor for CO oxidation over Pt/Al_2O_3. Chemical Engineering Science. 2003a, 58, 833- 839.

[65] Durlofsky, L.; Brady, J. F. Analysis of the Brinkman equation as a model for flow in porous media. Physical Fluids. 1987, 30, 3329- 3341.

[66] Jaree, A.; Hudgins, R.; Budman, H.; Silveston, P.; Yakhnin, V.; Menzinger, M. Hysteresis and extinction waves in catalytic CO oxidation caused by reactant concentration perturbations in a packedbed reactor. Ind. Eng. Chem. Res. 2003, 42, 1662-1673

[67] Zhang, W.; Thompson, K.; Reed, A.; Beenken, L. Relationship between packing structure and porosity in fixed beds of equilateral cylindrical particles. Chemical Engineering Science. 2006, 61, 8060- 8074.

[68] Giese, M.; Rottschafer, K.; Vortmeyer, D. Measured and modelled superficial flow profiles in packed beds with liquid flow. American institute of chemical engineering Journal. 1998, 44, 484-490.

[69] Aiouache, F.; tSaoir, M. N.; Kitagawa, K. Screening wall effects of a thin fluidized bed by near-infrared imaging. Chemical Engineering Journal. 2011, 167, 288-296.

[70] Winterberg, W.; Tsotsas, E.; Krischke, A.; Vortmeyer, D. A. Simple and coherent set of coefficients for modelling of heat and mass transport with and without chemical reaction in tubes filled with spheres. Chemical Engineering Science. 2000, 55, 967- 979.

[71] Gladden, L.; Akpa, B.; Anadon, L.; Heras, J.; Holland, D.; Mantle, M.; Matthews, S.; Mueller, C.; Sains, M.; Sederman, A. Dynamic MR Imaging of single- and two-phase flows. Chemical Engineering Research Design. 2006, 84, 272-281.

[72] Theuerkauf, J.; Witt, P.; Schwesig, D. Analysis of particle porosity distribution in fixed beds using the discrete element method. Powder Technol. 2006, 165, 92-99.

[73] Kwapinski,W.;Winterberg,M.;Tsotsa,E.;Mewes,D. Modeling of the Wall Effect in Packed Bed Adsorption. Chemical Engineering & Technology. 2004. 27 , 1179-1186.

[74] Vortmeyer, D .; Michael, K. The effect of non-uniform flow distribution on concentration profiles and breakthrough curves of fixed bed adsorbers. Chemical Engineering Science. 1985. 40, 2135-2138.

[75] Yang, R.T. Gas Separation by Adsorption Processes. Imperial College, UK. 1997.

[76] Tobiś, J.;Vortmeyer, D . The near-wall channelling effect on isothermal constant-pattern adsorption. Chemical Engineering Science. 1988, 43, 1363-1369.

[77] Bode, J. Computational fluid dynamics applications in the chemical industry. Computers & Chemical Engineering. 1994, 18 SUPPL, S247-S251.

[78] Dalman, M.T.; Merkin, J.H.; McGreavy, C. Fluid flow and heat transfer past two spheres in a cylindrical tube. Computers & Fluids. 1986, 14, 267-281.

[79] Petersen, E.E., Catalyst deactivation: Opportunity amidst woe. Studies in Surface Science and Catalysis.1997, 111, 87-98.

[80] Jaree, A.; Budman, H.; Hudgins,R.R.; Silverston, P.L.;Yakhnin, V.; Menzinger, M. Temperature excursions in packed bed reactors with an axial variation of catalyst activity. Catalysis Today. 2001, 69, 137-146.

[81] Romkes, S.J.P.; Dautzenberg, F.M.; Bleek,C.M.;Calis, H.P.A. CFD modelling and experimental validation of particle-to-fluid mass and heat transfer in a packed bed at very low channel to particle diameter ratio. Chemical Engineering Journal. 2003, 96 , 3-13.

[82] Ahmadi Motlagh, A.H.; Hashemabadi, S.H. CFD based evaluation of heat transfer coefficient from cylindrical particles. International Communications in Heat and Mass Transfer. 2008, 35, 674-680.

[83] Mirhashemi, F.S.; Hashemabadi, S.H.; Noroozi, S. CFD simulation and experimental validation for wall effects on heat transfer of finite cylindrical catalyst. International Communications in Heat and Mass Transfer. 2011, 38, 1148-1155.

[84] Calis, H.; Nijenhuis, A.; Paikert, B.; Dautz, F.; Van, C. CFD modelling and experimental validation of pressure drop and flow profile in a novel structured catalytic reactor packing. Chemical Engineering Science. 2001, 56 ,1713-1720.

[85] Zeiser, T.; Steven, M.; Freund,H.; Lammers,P.; Brenner,G.; Durst,F.; Bernsdorf, J . Analysis of the flow field and pressure drop in fixed-bed reactors with the help of lattice Boltzmann simulations. PHILOSOPHICAL TRANSACTIONS OF THE ROYAL SOCIETY OF LONDON SERIES A-MATHEMATICAL PHYSICAL AND ENGINEERING SCIENCES. 2002, 360 (1972) , 507-520.

[86] HAO, R. Local fluid flow and transports inside a thin packed reactor. MPhil Thesis. Queen's University of Belfast: U.K. 2012

[87] Michiel, N. Influence of catalyst particles geometry on fixed bed reactor near –wall heat transfer using CFD.Ph.D thesis. University of Twente to Worcester Polytechnic Institute: Netherlands. 2003.

[88] Cundall, P.A.; Strack, O.D.L. A discrete numerical model for granular assemblies. Géotechnique. 1979, 29 , 47-65.

[89] Khanal, M.; Schubert, W.; Tomas, J. Discrete element method simulation of bed comminution. Minerals Engineering. 2007, 20 , 179-187.

[90] Radeke, C. Statistische und mechanische analyse der kräfte und bruchfestigkeit von dicht gepackten granularen medien unter mechanischer belastung. PhD Thesis,TU Bergakademie Freiburg, Germany. 2006.

[91] Wei, C. Discrete Element Modelling of constant strain rate and creep tests on a graded asphalt mixture . Ph.D Thesis. University of Nottingham: U.K. 2013.

[92] ITASCA . Particle Flow Code in Three Dimensions, Theory and Background., Itasca Consulting Group Inc., Minnesota. 2008.

[93] Single Issue Tools-Complex-PHOENICS. (Online) Available: http://www.esru.strath.ac.uk/Courseware/Design_tools/PHOENICS/phoenics.htm#target1.

[94] Centre for computational Science, University of Kentucky. (Online) Available: https://www.ccs.uky.edu/UserSupport/SoftwareResources/Fluent/; ANSYS Fluent 12.

[95] Rumpf, H. C. H. ; Gupte, A.R. Einflüsse der Porosität und Korngrößenverteilung im Widerstandsgesetz der Porenströmung. Chemie Ingenieur Technik. 1971. 43, 367-375.

[96] Ergun, S. Fluid flow through packed columns. Chemical Engineering Progress. 1953, 48 , 89-94.

[97] Zou, R.P.; Yu, A.B. The packing of spheres in a cylindrical container: the thickness effect. Chemical Engineering Science . 1995, 50 , 1504-1507.

[98] Roblee, L. H. S.; Baird, R. M.; Tierney, J. W. Radial porosity variation in packed beds. American institute of chemical engineering Journal. 1958, 4, 460- 464.

[99] Sederman, A.; Alexander, P.; Gladden, L. Structure of packed beds probed by Magnetic Resonance Imaging. Powder Technol. 2001, 117, 255-269.

[100] Mueller, G. E. Radial void fraction distributions in randomly packed fixed beds of uniformly sized spheres in cylindrical containers. Powder Technol. 1992, 72, 269-275.

[101] Mueller, G. E. Prediction of radial porosity distributions in randomly packed fixed beds of uniformly sized spheres in cylindrical containers. Chemical Engineering Science. 1991, 46, 706-708.

[102] Dixon, A. Correlations for wall and particle shape effects on fixed bed bulk voidage. Canadian Journal Chemical Engineering. 1988, 66, 705-708.

[103] Mariani, N.J.; Mazza,G.D.; Martiniez,O.M.;Barreto,G. The distribution of particles in cylindrical packed beds. TRENDS IN HEAT, MASS AND MOMENTUM TRANSFER. 1998, 4, 95.

[104] Mueller, G.E. Radial porosity in packed beds of spheres. Powder Technology. 2010, 203 , 626-633.

[105] Kozeny, J. Uber kapillare leitung des Wassers im Boden. Sitzungsber. AKAD. Wiss. Wien . 1927, 136, 271-306.

[106] Carman, P. Fluid flow through granular beds. Transactions of the Institution of Chemical Engineers.1997, 75, S32- S48.

[107] Happel, J. Viscous flow in multiparticle systems: Slow motion of fluids relative to beds of spherical particles. American institute of chemical engineering Journal. 1958, 4, 197- 201.

[108] Bertil Anderson, K. E. Pressure drop in ideal fluidization. Chemical Engineering Science. 1961, 15, 276- 297.

[109] Molerus, O. Druckverlustgleichung fur die Durchstromung von Kugelschuttungen im laminaren und im Ubergangsbereich. Chemie Ingenieur Technik. 1977, 49, 675.

[110] Eisfeld, B.; Schnitzlein, K. The influence of confining walls on the pressure drop in packed beds. Chemical Engineering Science. 2001, 56, 4321- 4329.

[111] Moise, A.; Tudose, R. Air isothermal flow through packed beds. Experimental Thermal and Fluid Science. 1998, 18, 134-141.

[112] Ding, Y.; Wang, Z.; Wen, D.; Ghadiri, M.; Fan, X.; Park, D. Solids behaviour in a gas-solid two-phase mixture flowing through a packed particle bed. Chemical Engineering Science. 2005, 60, 5231-5239.

[113] Metha, D.; and Martinc, H. Wall Effects in Packed Columns. Industrial and Engineering Chemistry Process Design and Development. 1969, 8 , 280-282.

[114] Brauer, H., Grundlagen der Einphasen und Mehrphasenströmungen. Aarau. Frankfurt a.M., Sauerländer. 1971.

[115] Tsotsas, E. ; Schlünder, E.U. Some remarks on channelling and on radial dispersion in packed beds. Chemical Engineering Science. 1988, 43, 1200-1203.

[116] Sahimi, M. Flow and Transport in Porous Media and Fractured Rock. VCH: Weinheim. 1995.

[117] Kloeden, P.E.; Platen, E. Numerical Solution of Stochastic Differential Equations. Spring:Berlin,Heidelberg, New York. 1993, 23, 636.

[118] Bauer, J.; Ortsaufgelöste, Simulation von Transport prozessen in porösen Medien zur Untersuchung von Dispersion und Verweilzeitverhalten. Master's thesis, Lehrstuhl für Chemische Reaktionstechnik. Universität Erlangen-Nürnberg. 2004.

[119] Maier, R.S.; Kroll,D.;Bernard, R.; Howington, S.;Peters, J.; Davis, H.T. Pore-scale simulation of dispersion. Physics of Fluids .2000, 12, 2065-2079.

[120] Delenne, J.-Y.; Youssoufi, M.S .; Cherblanc, F.; Benet, J-C. Mechanical behaviour and failure of cohesive granular materials. International Journal for Numerical and Analytical Methods in Geomechanics. 2004, 28, 1577-1594.

[121] Stasa, P.; Kebo, V.; Kodym, O. Effect of mesh density on the accuracy of the calculation using CFD.SGEM conference proceeding: international Scientific Conference on Social Science &Arts .2014, 2, 161-168.

[122] Celik, I. B.; Ghia, U.; Roache, P. J.; Freitas, C. J.; Coleman, H.; Raad, P. E. Procedure for estimation and reporting of uncertainty due to discretization in cfd applications. Fluids Engineerin journal. 2008, 130, 078001.

[123] Spedding, P. L.; Spencer, R. M. Simulation of packing density and liquid flow in fixed beds. Computer Chemical Engineering. 1995, 19, 43 -73.

[124] Reyes, S. C.; Iglesia, E. Monte Carlo simulations of structural properties of packed beds. Chemical Engineering Science. 1991, 46, 1089-1099.

[125] Nolan, G. T.; Kavanagh, P. E. Computer simulation of random packing of hard spheres. Powder Technol. 1992, 72, 149-155.

[126] Nolan, G. T.; Kavanagh, P. E. Octahedral configurations in random close packing. Powder Technol. 1995, 83, 253-258.

[127] Benenati, R. F.; Brosilow, C. B. Void fraction distribution in beds of spheres. American institute of chemical engineering Journal. 1962, 8, 359-361.

[128] Chan, S. K.; Ng, K. M. Geometrical characteristics of the pore space in a random packing of equal spheres. Powder Technol. 1988, 54, 147-155.

[129] Spedding, P. L.; Spencer, R. M. Simulation of packing density and liquid flow fixed beds-II. Voronoi polyhedra studies. Computer Chemical Engineering. 1998, 22, 247-257.

[130] Parse, J.; Wert, J. A geometrical description of particle distributions in materials. Modelling Simulation in Material Science Engineering. 1993, 1, 275-296.

[131] Lindquist, W. B.; Lee, S. M.; Cork, D. A.; Jones, K. W.; Spanne, S. Medial axis analysis of void structure in three-dimensional tomographic images of porous media. Geophysical Research Journal. 1996, 101, 8297-8310.

[132] Zhavoronkov, N.M.; Aerov, M.E. ; Umnik, N.N. Hydraulic resistance and density of packing of a granular bed. The Journal of Physical Chemistry. 1949, 23, 342-361.

[133] Reichelt, W. Zur Berechnung des Druckverlustes einphasig durchströmter Kugel- und Zylinderschüttungen. Chemie Ingenieur Technik. 1972, 44, 1068-1071.

[134] Atmakidis, T.; Kenig, E. Y. CFD-based analysis of the wall effect on the pressure drop in packed beds with moderate tube/particle diameter ratios in the laminar flow regime. Chem. Eng. J. 2009, 155, 404-410.

[135] Augier, F.; Laroche, C.; Brehon, E. Application of computational fluid dynamics to fixed bed adsorption calculations: Effect of hydrodynamics at laboratory and industrial scale. Sep. Purif. Technol. 2008, 63, 466-474.

[136] Delgado, J. M. P. Q. Longitudinal and transverse dispersion in porous media. Chemical Engineering Research Design. 2007, 85, 1245-1252.

[137] Delgado, J. M. P. Q. A critical review of dispersion in packed beds. Heat Mass Transfer. 2006, 42, 279-310.

[138] Augier, F.; Idoux, F.; Delenne, J. Y. Numerical simulations of transfer and transport properties inside packed beds of spherical particles. Chem. Eng. Sci. 2010, 65, 1055−1064.

[139] V.M.H, G.; RAMRAO, K.V.S.; RAO, A.V.S. Structural characteristics of packed beds at low aspect ratio. Chemical engineering science. 1992, 47, 2105-2109.

[140] Resnick, W.; White, R. Mass transfer in system of gas and fluidized solids. Chemical Engineering progress.1949,45,377.

[141] Wen, D.; Ding, Y. Heat transfer of gas flow through a packed .Chemical Engineering Science.2006,61,3532-3542.

[142] Chen, Y.C.; Luss,D.Wrong-way behavior of packed-bed reactors: Influence of interphase transport. American institute of chemical engineering Journal. 1989, 35 ,1148-1156.

[143] Voltz, S.E.; Morgan, C.R.; Liederman, D.; Jacob, S.M. Kinetic Study of Carbon Monoxide and Propylene Oxidation on Platinum Catalysts. industrial & Engineering Chemistry Process Design and Development. 1973, 12 , 294-301.

[144] Amphlett, J.C. ; Mann, R.F. ; Peppley, B.A. On board hydrogen purification for steam reformation/ PEM fuel cell vehicle power plants. International Journal of Hydrogen Energy. 1996, 21, 673-678.

[145] Tieber, W.; Athenstaedt, W.; Leisch, M. SD-Atom-Probe Study of Oxygen-Adsorption on Stepped Platinum Surfaces. Fresenius Journal Analytical chemistry . 1997, 1-2, 116-118.

[146] Elg, A.P.; Eisert, F.; Rosen, A. The Temperature Dependence of the Initial Sticking Probability of Oxygen on Pt(111) Probed with Second Harmonic Generation. Surface Science. 1997, 382, 57- 66.

[147] Depcik, C.; Loya, S.; Srinivasan, A.; Wentworth, T.; Williams .Adaptive Global Carbon Monoxide Kinetic Mechanism over Platinum/Alumina Catalysts. Catalysts. 2013,3,517-542.

[148] Dhar, H. P. ; Christner.; L. G. Kush, A. K. Nature of CO absorption during H, oxidation in relation to modeling CO poisoning of a fuel cell anode, JI. Electrochem. Sot. 1987 , 134, 3021-3026 .

[149] Birdsell, S. A. ;. Vanderborgh, N. E.; Inbody, M. A. Preferential oxidation of methanol and carbon monoxide for gas clean up during methanol fuel processing. ,1993, Proc. of 28th ICEC .

[150] Kahlich, M.J. ; Gasteiger, H.A.; Behm, R.J. Kinetics of the Selective CO Oxidation in H2-Rich Gas on Pt/Al2O3. Journal of Catalysis. 1997 ,171, 93-105.

[151] Dong, K.H. ; Lim, M.S. Kinetics of selective CO oxidation in hydrogen-rich mixtures on Pt/alumina catalysts. Applied Catalysis A: General. 2002 ,224, 27-38.

[152] Yongtaek, Choi. ; Stenger, H. Kinetics, simulation and insights for CO selective oxidation fuel cell applications. Power Sources. 2004,129, 246-254.

[153] Sarp, K.; Erunal, E.; Shaltaf, R.; Ellialtioglu, S.; Uner,D. on the structure sensitivity of CO oxidation on Alumina supported Pd-Pt Bimetallic Catalyst. Turk Journal .2009,33,11-21.

[154] Akkarat, A. Effect of cerium oxide and zirconium oxide to activity of catalyst. Journal science . 2008, 35, 156-162.

[155] Anna, H.; Andersson, B. Mass transfer in monolith catalysts–CO oxidation experiments and simulations. Pergamum .1998, 53, 2285-2298.

[156] Abdel Halim, K.; Khedr, M.; Nasr,M.; El-mansy, A. Factors affecting CO oxidation over nanosized Fe2O3. Materials Research Bulletin. 2007,42,731-741.

[157] Dixon, A.G. The length effect on packed bed effective heat transfer parameters. Chemical Engineering Journal. 1985, 31, 163-173.

[158] Wehinger, G.; Eppinger, T.; Kraume, M. Detailed numerical simulations of catalytic fixed-bed reactors: Heterogeneous dry reforming of methane. Chemical Engineering Science. 2015,122,197-209.

[159] Jensen, K. F.; Ray, W. H. The bifurcation behaviour of tubular reactors. Chemical Engineering Science. 1982, 37, 199- 222.

[160] Fu, R.S.; Zhang, X.; Pasaogullari, U. Heat and Mass Transfer in Polymer Electrolyte Fuel Cells in UltraLow Humidity Operation. ECS Transactions. 2009, 25, 323- 332.